
A HYBRID NEURAL NETWORK - POLYNOMIAL SERIES SCHEME FOR LEARNING INVARIANT MANIFOLDS OF DISCRETE DYNAMICAL SYSTEMS

Dimitrios G. Patsatzis¹, Nikolaos Kazantzis², Ioannis G. Kevrekidis^{3,4,5}, Constantinos Siettos^{6,*}

⁽¹⁾Modelling Engineering Risk and Complexity, *Scuola Superiore Meridionale*, Naples, Italy

⁽²⁾Dept. of Chemical Engineering, *Worcester Polytechnic Institute*, Worcester, USA

⁽³⁾Dept. of Chemical & Biomolecular Engineering, *Johns Hopkins University*, Baltimore, USA

⁽⁴⁾Dept. of Applied Mathematics and Statistics, *Johns Hopkins University*, Baltimore, USA

⁽⁵⁾Medical School, Department of Urology, *Johns Hopkins University*, Baltimore, USA

⁽⁶⁾Dipartimento di Matematica e Applicazioni “Renato Caccioppoli”, *University of Naples Federico II*, Naples, Italy

June 18, 2025

ABSTRACT

We propose a hybrid machine learning scheme to learn—in physics-informed and numerical analysis-informed fashion—invariant manifolds (IM) of discrete maps for constructing reduced-order models (ROMs) for dynamical systems. The proposed scheme combines polynomial series with shallow neural networks, exploiting the complementary strengths of both approaches. Polynomials enable an efficient and accurate modeling of ROMs with guaranteed local exponential convergence rate around the fixed point, where, under certain assumptions, the IM is demonstrated to be analytic. Neural networks provide approximations to more complex structures beyond the reach of the polynomials’ convergence. We evaluate the efficiency of the proposed scheme using three benchmark examples, examining convergence behavior, numerical approximation accuracy, and computational training cost. Additionally, we compare the IM approximations obtained solely with neural networks and with polynomial expansions. We demonstrate that the proposed hybrid scheme outperforms both pure polynomial approximations (power series, Legendre and Chebyshev polynomials) and standalone shallow neural network approximations in terms of numerical approximation accuracy.

Keywords Discrete Dynamical Systems · Invariant Manifolds · Physics-Informed Hybrid Machine Learning · Polynomial Approximation · Reduced Order Models

1 Introduction

Invariant manifolds (IMs) and attendant methods remain powerful, versatile, and insightful tools in the broader nonlinear dynamical systems theory. An invariant manifold is a subset embedded in the system’s state space with the property that any trajectory starting on it remains on it for all time. These manifolds often capture essential features of the dynamics—such as long-term behavior near equilibria or slow evolution in multiscale systems—and provide a natural framework for reducing the dimensionality of complex models. By restricting the dynamics on the manifold, one can reformulate high-dimensional systems in a lower-dimensional setting without losing critical information [1–4]. Therefore, IMs serve as fundamental geometric structures that govern the long-term behavior of dynamical systems, enabling rigorous stability analysis, bifurcation analysis, and model reduction [1, 2]. Furthermore, their accurate approximation is critical for constructing reliable reduced-order models (ROMs) that capture the nonlinear behavior of complex systems across a wide range of disciplines [2, 3, 5].

*Corresponding author, email: constantinos.siettos@unina.it

Over the years different types of IMs have been identified and properly characterized such as stable/unstable and center manifolds (depending on the nature of the eigenspectrum/eigenvectors of the system’s Jacobian matrix), fast and slow manifolds (depending on an underlying time-scale multiplicity associated with a spectral gap in the system’s Jacobian), as well as inertial manifolds in spatially distributed dynamical systems (depending on the presence of “dissipation terms”) [1–4, 6–15]. Beyond questions of existence and uniqueness, substantial effort has been directed toward developing computational methods for approximating these manifolds by solving the corresponding invariance equations.

Recently, growing interest has emerged in integrating IMs with approaches that have been traditionally rooted in nonlinear dynamical systems and control theory. In this setting, IMs provide a unifying framework through which the behavior of input-driven nonlinear systems can be analyzed, particularly via the notion of control flow; a dynamical structure defined on the product space of admissible inputs and system states [16, 17]. In particular, IMs have been used to compute, analyze, and characterize the responses of nonlinear systems to various exogenous stimuli that drive the system dynamics. Such stimuli are outputs generated by an exogenous system (often known as the exosystem) that models dynamic input changes reminiscent of forcing functions, disturbance events, time-varying system parameters, etc. The exosystem dynamics coupled with the original system dynamics conform to an overall structural configuration of a skew-product (or “master-slave”) system [16–21]. One could identify two approaches whereby IMs assume critical importance in the nonlinear feedback control and state estimation design problems. On the feedback controller and/or state estimator synthesis front, IMs can be creatively used as a “design tool” through which desirable dynamic characteristics can be assigned to the feedback-controlled system and/or the state estimator. This perspective has influenced several important areas, including nonlinear regulation [16, 20, 22, 23], stabilization through immersion and invariance [21], transverse feedback linearization [24], invariance-inducing control [25, 26] and nonlinear observer design [27–31]. Conversely, once a controller is synthesized, IMs parameterized by the controller parameters (design degrees of freedom) can be identified and used to analyze the controlled system dynamics. Therefore, the above IM parameterization allows a transparent analysis of the effect of the available controller design parameters on the feedback-controlled system dynamics by retaining the advantages afforded by well-established methods of nonlinear dynamical system theory. Notable research efforts along these lines include applications to nonlinear H_∞ optimal control [32], controlled center dynamics [16, 17], and nonlinear feedback control of Galerkin systems [33].

For continuous-time systems, the theoretical foundations are well-established. Geometric singular perturbation theory (GSPT) [14, 34] and spectral submanifold theory [35, 36] provide rigorous tools for slow/fast systems and normally hyperbolic manifolds. A variety of computational/numerical methods has been developed [37–41] to enable practical computation of IM approximations, leading to successful applications in diverse domains, such as chemical kinetics [42–44], biochemical networks [45, 46], structural dynamics [36], etc. In contrast, discrete dynamical systems, particularly those with external inputs, lack a systematic framework. The absence of infinitesimal generators (e.g., Lie derivatives) prevents direct translation of continuous-time methods, while input-driven dynamics complicate invariance conditions. Existing approaches rely on local expansions near equilibria [18, 47], which struggle with high-dimensional systems due to combinatorial complexity and suffer from poor accuracy far from equilibria due to series divergence.

Recent advances in Scientific Machine Learning (SciML) have introduced data-driven paradigms for black or gray-box ROMs construction, typically including two steps: data dimensionality reduction for embedding the data into low-dimensional subspaces, using manifold learning methods [48–51], including proper orthogonal decomposition [52–54] and Koopman operator techniques [55–57], followed by surrogate ROMs modelling via, for example, artificial neural networks [52, 58–60], or Gaussian Processes [60–62]. Autoencoders often combine both steps [63–65]. Data-driven approaches for learning low-dimensional stable, unstable and center IMs from high-dimensional microscopic simulators/legacy codes within the Equation-free approach [66] for multiscale computations have also been proposed [41, 45, 67–69]. The core of these approach is the construction of a “coarse” discrete map of the emergent dynamics, based on short simulations of microscale simulations. More recently, “next-generation” Equation-free methods, integrating manifold learning with numerical analysis, have been introduced to eliminate the need of ROMs construction and directly perform bifurcation analysis and control design [70–72].

While the above SciML approaches identify low-dimensional subspaces, they often lack explicit geometric interpretation of true underlying IMs. For continuous-time systems, recent work has begun to bridge this gap by combining neural networks (NNs) with dynamical systems theory, in the context of Physics-Informed Machine Learning (PIML) [73–75]. In particular, in [76] a NN-based framework was introduced to parameterize intrinsic coordinates that solve invariance conditions via PIML loss functions. In [77], we have used NNs to solve the partial differential equation (PDE) corresponding to the invariance equation of singular perturbed dynamical systems for the approximation of slow IMs in the context of GSPT. In [78], we have extended this PIML approach for the general class of fast-slow dynamical systems by introducing linear transformations of the state variables into slow and fast variables.

For discrete-time systems, SciML approaches to IM approximation remain underdeveloped. The fundamental challenge lies in solving the nonlinear functional equations (NFEs) governing the manifold invariance for discrete-time dynamical systems. Traditional methods [18, 19, 47, 68, 69] rely on local power series expansions around equilibria, where coefficients are determined through linear algebraic systems. While these approaches yield accurate approximations near equilibria, they become increasingly intractable for high-dimensional systems despite symbolic computation tools, and critically fail to maintain accuracy far from equilibrium or near dynamic singularities. This limitation presents a substantial obstacle for engineering applications requiring reliable IM approximations across the entire operating domain. Another

In this work, we present a hybrid physics-informed/numerical analysis-informed machine learning framework for IM approximations of discrete-time dynamical systems with input-driven dynamics. Building on established existence theory for such manifolds [18, 19], we solve the governing NFEs through an innovative physics-informed (PI) hybrid scheme that strategically combines the local precision of polynomial series expansions with the global approximation capabilities of NNs. Extending our previous work on the development of numerical analysis-informed machine learning approaches for constructing slow IMs of continuous-time systems [77, 78], here we propose an adaptive/hybrid transition between polynomial series within a defined equilibrium neighborhood \mathcal{D} and NNs outside this region. The polynomial component is implemented through a novel shallow NN-like architecture inspired by [79], where each polynomial term operates as an activated neuron. In particular, we treat the polynomial coefficient as an output weight, and the polynomial as, a different for each neuron, activation function, with the degree of the expansion corresponding to the width of the NN. This formulation accommodates various polynomial bases, including power series for their simplicity in representing local dynamics, as well as Legendre and Chebyshev polynomials for their numerical stability via orthogonal properties on bounded domains—though each option presents its own tradeoffs between conditioning, convergence, and computational cost for high-degree terms. By additionally considering shallow NNs operating outside \mathcal{D} , we enable symbolic differentiation across the entire PI hybrid scheme for providing an efficient, accelerated training.

The performance of the proposed PI hybrid scheme is assessed via three illustrative examples; an artificial one where the true IM is known analytically, the example used in [19] for which the IM approximation via power series expansion is known and an example that generalizes the proposed algorithmic implementation in multiple dimensions. Comparative analysis of the IM approximations provided by the hybrid scheme demonstrates high approximation accuracy over those provided by the traditional expansion approach [19]. More importantly, the hybrid scheme outperforms the IM approximations constructed purely by PI polynomial series or PI NNs, particularly far from/near to the region of the equilibrium, respectively. We note however, that this comes with increased parametric complexity, as the hybrid scheme has more parameters to tune than the other PI schemes. A comprehensive analysis of the role of the degree of the polynomial series and the radius of the polydisc \mathcal{D} is provided in the first two illustrative examples.

The manuscript is structured and organized as follows: we first discuss the conditions of IM existence in discrete-time systems in Section 2 and then present the PI hybrid scheme for the IM approximations. For completeness, we also present the standalone PI polynomial series and NNs approximations, and their implementation. In Section 3, we briefly present the three illustrative examples, and then we assess the performance of the hybrid scheme and the other schemes on the basis of the numerical results in Section 4. We finally offer a few concluding remarks focusing on the proposed method’s comparative advantages and limitations in Section 5, providing also directions for future work.

2 Methodology

Let us consider the non-linear discrete-time dynamical system:

$$\mathbf{x}(k+1) = \mathbf{F}(\mathbf{x}(k), \mathbf{y}(k)), \quad \mathbf{y}(k+1) = \mathbf{G}(\mathbf{y}(k)), \quad (1)$$

where the state space of $\mathbf{x} \in \mathbb{R}^N$ is input-driven by the external dynamics of $\mathbf{y} \in \mathbb{R}^M$. Let $\mathbf{x}(k) = [x_1(k), \dots, x_N(k)]^\top$ and $\mathbf{y}(k) = [y_1(k), \dots, y_M(k)]^\top$ denote the state variables at the $k \in \mathbb{N}$ discrete time step, and the functions $\mathbf{F} : \mathbb{R}^N \times \mathbb{R}^M \rightarrow \mathbb{R}^N$ and $\mathbf{G} : \mathbb{R}^M \rightarrow \mathbb{R}^M$ denote the corresponding vector fields. Without loss of generality, we assume that the origin $(\mathbf{x}_0, \mathbf{y}_0) = (\mathbf{0}^N, \mathbf{0}^M)$ is an equilibrium point of the system in Eq. (1). Additionally, we make the following assumption:

Assumption 1. *The matrix $\mathbf{A} = \partial_{\mathbf{y}} \mathbf{G}(\mathbf{y}_0) \in \mathbb{R}^{M \times M}$ has non-zero eigenvalues, denoted by k_i for $i = 1, \dots, M$, all of which lie either strictly inside or outside the unit disc. This assumption ensures that the $\mathbf{G}(\mathbf{y})$ is locally invertible in a neighborhood of \mathbf{y}_0 .*

The system in Eq. (1) can be rewritten in the form:

$$\begin{aligned} \mathbf{x}(k+1) &= \mathbf{B}\mathbf{x}(k) + \mathbf{C}\mathbf{y}(k) + \mathbf{f}(\mathbf{x}(k), \mathbf{y}(k)), \\ \mathbf{y}(k+1) &= \mathbf{A}\mathbf{y}(k) + \mathbf{g}(\mathbf{y}(k)), \end{aligned} \quad (2)$$

where $\mathbf{B} = \partial_{\mathbf{x}}\mathbf{F}(\mathbf{x}_0, \mathbf{y}_0) \in \mathbb{R}^{N \times N}$ and $\mathbf{C} = \partial_{\mathbf{y}}\mathbf{F}(\mathbf{x}_0, \mathbf{y}_0) \in \mathbb{R}^{N \times M}$ are constant matrices derived from the linearization of the system in Eq. (1) around the equilibrium. The non-linear terms $\mathbf{f} : \mathbb{R}^N \times \mathbb{R}^M \rightarrow \mathbb{R}^N$ and $\mathbf{g} : \mathbb{R}^M \rightarrow \mathbb{R}^M$ are real-valued functions satisfying $\mathbf{f}(\mathbf{x}_0, \mathbf{y}_0) = \mathbf{0}^N$ and $\mathbf{g}(\mathbf{y}_0) = \mathbf{0}^M$. Additionally, their linearization at the equilibrium satisfy $\partial_{\mathbf{x}}\mathbf{f}(\mathbf{x}_0, \mathbf{y}_0) = \partial_{\mathbf{y}}\mathbf{f}(\mathbf{x}_0, \mathbf{y}_0) = \partial_{\mathbf{y}}\mathbf{g}(\mathbf{y}_0) = \mathbf{0}$ with consistent zero-matrix dimensions. The system in Eq. (1) exhibits a unique locally *invariant manifold* (IM) under the assumptions of Theorem 1 in [19], which we restate below (for the proof, see [19]):

Theorem 1 (Invariant Manifold existence, [19]). *Consider the non-linear discrete dynamical system in Eq. (1), where Assumption 1 is satisfied. Additionally, assume that the eigenvalues of the matrix $\mathbf{A} = \partial_{\mathbf{y}}\mathbf{G}(\mathbf{y}_0)$, denoted by k_i for $i = 1, \dots, M$ are not related to the eigenvalues of the matrix $\mathbf{B} = \partial_{\mathbf{x}}\mathbf{F}(\mathbf{x}_0, \mathbf{y}_0)$, denoted by λ_j for $j = 1, \dots, N$, through any resonance condition of the form:*

$$\prod_{i=1}^M k_i^{d_i} = \lambda_j, \quad (3)$$

where d_i are non-negative integers satisfying $\sum_{i=1}^M d_i > 0$. Then, there exists a compact neighborhood $\mathcal{V} \subset \mathbb{R}^M$ around the equilibrium \mathbf{y}_0 , and a unique, locally analytic mapping $\pi : \mathcal{V} \rightarrow \mathbb{R}^N$ such that:

$$\mathcal{M} = \{(\mathbf{x}, \mathbf{y}) \in \mathbb{R}^N \times \mathcal{V} : \mathbf{x} = \pi(\mathbf{y}), \pi(\mathbf{y}_0) = \mathbf{x}_0\}, \quad (4)$$

defines an analytic local invariant manifold (IM) of the system in Eq. (1). This manifold passes through the equilibrium point $(\mathbf{x}_0, \mathbf{y}_0) = (\mathbf{0}^N, \mathbf{0}^M)$. Furthermore, the mapping $\pi(\mathbf{y})$ is the unique solution of the system of nonlinear functional equations (NFEs) associated to Eq. (2):

$$\pi(\mathbf{A}\mathbf{y} + \mathbf{g}(\mathbf{y})) = \mathbf{B}\pi(\mathbf{y}) + \mathbf{C}\mathbf{y} + \mathbf{f}(\pi(\mathbf{y}), \mathbf{y}), \quad \text{with} \quad \pi(\mathbf{y}_0) = \mathbf{x}_0. \quad (5)$$

The system of NFEs in Eq. (5) arises from the invariance of the manifold \mathcal{M} in Eq. (4). Specifically, when the solution of the discrete system in Eq. (2) at the k -th step is on the manifold (i.e., when $\mathbf{x}(k) = \pi(\mathbf{y}(k))$), then the invariance of \mathcal{M} ensures that the system remains on the manifold at the next $k + 1$ -th step. This implies $\mathbf{x}(k + 1) = \pi(\mathbf{y}(k + 1))$, which, upon substitution of the system dynamics from Eq. (2), yields Eq. (5).

According to Theorem 1, the functional map $\mathbf{x} = \pi(\mathbf{y})$ of the IM \mathcal{M} in Eq. (4) can be computed through the solution of the system of NFEs in Eq. (5). Due to their implicit and nonlinear nature, exact solutions are generally intractable, necessitating approximate solutions. Traditional methods [18, 19, 47] use local power series expansions (PSE) around $(\mathbf{x}_0, \mathbf{y}_0)$, where the coefficients are determined by solving a linear system of algebraic equations obtained from the NFEs (see Appendix A). While PSE methods are rigorous near equilibria (with exponential convergence for analytic systems) and interpretable (due to their polynomial form), they face two critical limitations: (i) the number of coefficients grows combinatorially with system dimension $N + M$ and expansion degree h , and (ii) the PSEs diverge far from equilibria and close to singularities, resulting to IM approximation with poor accuracy. While alternatives like Koopman linearization [80] or neural networks (NNs) [76] offer complementary insights, they fail to address the core challenge of solving the NFEs for $\pi(\mathbf{y})$, since Koopman methods linearize dynamics without preserving the manifold's functional structure, while pure NNs lack local theoretical guarantees near equilibria.

These challenges also arise in continuous-time fast/slow dynamical systems for the approximation of slow IMs. In such systems, the invariance equation comes in a form of a partial differential equation (PDE), the solution of which may be approximated by asymptotic expansions [81–83], or by advanced numerical methods [40, 41, 84, 85]. In prior work [77, 78], we demonstrated that physics-informed NNs provide very accurate slow IM approximations, especially near the boundaries of the manifold, where the asymptotic series diverge. Motivated by this observation, we propose a *hybrid scheme* for discrete-time systems that combines the strengths of both approaches by coupling (i) polynomial expansions near the equilibria to preserve theoretical guarantees and (ii) NNs far from equilibria to provide high approximation accuracy where polynomial expansions fail. This unified approach, constrained by the NFEs in Eq. (5), generalizes our earlier work while addressing the discrete-time-specific challenges of combinatorial complexity and input-driven dynamics. Below, we detail this coupling and its implementation.

2.1 The hybrid neural network-polynomial series physics-informed scheme

In this section, we present the proposed hybrid neural network-polynomial series physics-informed (PI) scheme for approximating smooth functionals and here IM functionals $\mathbf{x} = \pi(\mathbf{y})$. A schematic of the proposed scheme is shown in Fig. 1. As previously discussed, the hybrid scheme combines polynomial series expansions in a region around the equilibrium point, and a shallow NNs outside this region. Both components serve as universal approximators of continuous functions on compact domains, as guaranteed by the Weierstrass Approximation Theorem [86, 87] for polynomials and the universal approximation theorems for NNs [88, 89]. The rationale for using such a scheme lies in

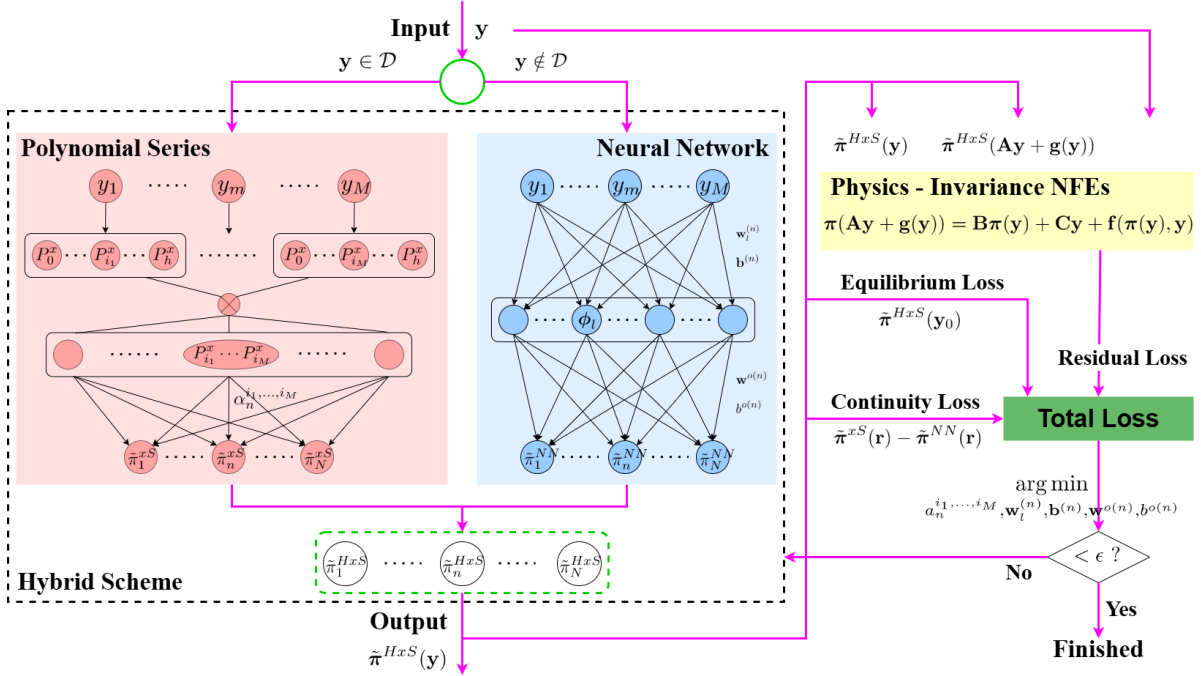


Figure 1: Schematic of the PI hybrid scheme for approximating IM functionals of discrete-time dynamical systems in the form of Eq. (1). The scheme combines polynomial series inside a polydisc \mathcal{D} of radius \mathbf{r} centered at the equilibrium and NNs outside \mathcal{D} . The hybrid IM scheme is trained to minimize a composite loss function that enforces the system of NFEs in Eq. (5), including residuals for manifold invariance, equilibrium constraints and continuity constraints at $\partial\mathcal{D}$. The coefficients of the polynomial series and the parameters of the NN are jointly optimized to minimize the loss.

the continuity properties of the underlying functional to be approximated, the results on the rate of convergence of both approaches, and the complexity in the training process. In particular, if the sought function is analytic around a point, then polynomial approximation (such as Taylor or Chebyshev expansions) offers *geometric/exponential convergence*, meaning that the approximation error decreases exponentially with the degree of the polynomial [90]. In contrast, for standard shallow neural networks for which theoretical approximation results have been derived (see e.g., [91]), the approximation error decays algebraically with the square root of the number of neurons. Thus, while neural networks offer greater flexibility especially in high-dimensions, they may require significantly many neurons to achieve comparable accuracy to low-degree polynomials when approximating smooth functions in a neighborhood of a point. Finally, the training of a neural network (even shallow ones) is known to be an NP-complete problem [92] or even NP-hard in the size of the network and the input dimension [93]. In contrast, fitting a polynomial of fixed degree (e.g., via least squares or Chebyshev projection) reduces to a convex or linear system, which admits a polynomial-time solution.

More specifically, while the polynomial series provide uniform approximations of any analytic function [86, 87, 90], their practical implementation depends on knowing the radius of convergence, which is impossible to determine *a priori* for an unknown function. On the other hand, NNs provide high approximation accuracy throughout a broader domain Ω , but cannot reach the local accuracy of a polynomial series approximation within the region of convergence. To address this challenge for the computation of IM functionals $\mathbf{x} = \pi(\mathbf{y})$, we dynamically define a polydisc $\mathcal{D} = \{\mathbf{y} \in \mathbb{R}^M : |y_m| < r_m, \forall m = 1, \dots, M\}$ of radius $\mathbf{r} = [r_1, \dots, r_M]^\top \in \mathbb{R}^M$ around the equilibrium, within which the polynomial series residuals remain bounded and outside which the NNs provide better approximation accuracy. This avoids reliance on *a priori* radius estimates.

In particular, we approximate the IM functional by the hybrid scheme approximation $\mathbf{x} = \tilde{\pi}^{HxS}(\mathbf{y}, \mathbf{a}, \mathbf{p}; \mathcal{H}_1, \mathcal{H}_2, \mathbf{r}) \in \mathbb{R}^N$, the elements of which for $n = 1, \dots, N$ are expressed as:

$$\tilde{\pi}_n^{HxS}(\mathbf{y}, \mathbf{a}_n, \mathbf{p}_n; \mathcal{H}_1, \mathcal{H}_2, \mathbf{r}) = \tilde{\pi}_n^{xS}(\mathbf{y}, \alpha_n; \mathcal{H}_1)^{H(\mathbf{y}, \mathbf{r})} \cdot \tilde{\pi}_n^{NS}(\mathbf{y}, \mathbf{p}_n; \mathcal{H}_2)^{1-H(\mathbf{y}, \mathbf{r})}, \quad (6)$$

where $\tilde{\pi}_n^{xS}(\mathbf{y}, \alpha_n; \mathcal{H}_1)$ and $\tilde{\pi}_n^{NS}(\mathbf{y}, \mathbf{p}_n; \mathcal{H}_2)$ are the n -th outputs of a polynomial series and a NN, as functions of \mathbf{y} , respectively. These components include the parameters α_n and \mathbf{p}_n and the hyperparameters \mathcal{H}_1 and \mathcal{H}_2 , which will be

discussed next. The function $H : \mathbb{R}^M \times \mathbb{R}^M \rightarrow \mathbb{R}$ in Eq. (6) is a product of Heaviside functions defined as:

$$H(\mathbf{y}, \mathbf{r}) = \prod_{i=1}^M H(r_i^2 - y_i^2) = \begin{cases} 1, & |y_i| < r_i, \quad \forall i = 1, \dots, M, \\ 0, & \text{otherwise.} \end{cases}, \quad (7)$$

which takes the values $H(\mathbf{y}, \mathbf{r}) = 1$ when $\mathbf{y} \in \mathcal{D}$ and $H(\mathbf{y}, \mathbf{r}) = 0$ when $\mathbf{y} \notin \mathcal{D}$. This ensures that the hybrid scheme approximation $\mathbf{x} = \tilde{\pi}^{HxS}(\mathbf{y}, \mathbf{a}, \mathbf{p}; \mathcal{H}_1, \mathcal{H}_2, \mathbf{r})$ in Eq. (6) reduces to a polynomial series (power, Legendre or Chebyshev) approximation within the polydisc \mathcal{D} and a NN approximation outside \mathcal{D} . We hereby note that the hybrid approximation depends also on the radius \mathbf{r} of the polydisc, which is considered in Eq. (6) as an additional hyperparameter.

Polynomial series component The polynomial series component adopts a NN-like architecture inspired by [79] (see Fig. 1). We consider a multivariate polynomial series for the external variables $\mathbf{y} \in \mathbb{R}^M$ of degree h , denoted as $\tilde{\pi}^{xS}(\mathbf{y}, \boldsymbol{\alpha}; \mathcal{H}_1) \in \mathbb{R}^N$, where $\boldsymbol{\alpha}$ contains the polynomial coefficients and \mathcal{H}_1 includes both the degree h and polynomial type x (indicated by superscript xS). Each output dimension n (for $n = 1, \dots, N$) of the vector valued $\tilde{\pi}^{xS}$ is given by:

$$\tilde{\pi}_n^{xS}(\mathbf{y}, \boldsymbol{\alpha}_n; \mathcal{H}_1) = \sum_{i_1, \dots, i_M=0}^h \alpha_n^{i_1, \dots, i_M} P_{i_1}^x(y_1) \cdots P_{i_M}^x(y_M) + \mathcal{O}(\mathbf{P}^x(\mathbf{y})^{h+1}), \quad (8)$$

where $\alpha_n^{i_1, \dots, i_M}$ are the expansion coefficients, $P_{i_j}^x(y_j)$ represents the i_j -th degree polynomial of type x for the variable y_j , and the reminder term $\mathcal{O}(\mathbf{P}^x(\mathbf{y})^{h+1})$ captures higher-order contributions. Although the summation includes terms beyond degree h in its formulation (chosen to mimic a NN-like structure, as shown in Fig. 1), we enforce truncation by setting $\alpha_n^{i_1, \dots, i_M} = 0$ for $i_1 + i_2 + \dots + i_M > h$. The coefficient vector $\boldsymbol{\alpha}_n$ collects all $(\prod_{i=1}^M (h+i))/i!$ coefficients $\alpha_n^{i_1, \dots, i_M}$ up to degree h , with the complete parameter vector $\boldsymbol{\alpha} = [\boldsymbol{\alpha}_1, \dots, \boldsymbol{\alpha}_N]^\top$ in $\tilde{\pi}^{xS}(\mathbf{y}, \boldsymbol{\alpha}; \mathcal{H}_1)$ aggregating all output dimensions $n = 1, \dots, N$.

We implement three polynomial variants in this framework: power series, Legendre and Chebyshev (of the second kind) polynomials, denoted by the superscript $x = P, L, C$ in Eq. (8). The power series polynomials match the traditional PSE approaches [19] with monomials $P_l^P(y_m) = y_m^l$ of degree $l \in \mathbb{N}$ for the variable y_m ($m = 1, \dots, M$). We consider Legendre and Chebyshev polynomials due to their increased accuracy and reduced computational costs in PINN forward problems [79, 94, 95]. Both polynomial types are orthogonal with respect to a weight function $\rho(y_m)$ and are defined on the interval $y_m \in [-1, 1]$ for every $m = 1, \dots, M$. Specifically, any two univariate Legendre/Chebyshev polynomials of degrees $i, j \in \mathbb{N}$ with $i \neq j$ satisfy the orthogonality relation:

$$\langle P_i(y_m), P_j(y_m) \rangle = \int_{-1}^1 P_i(y_m) P_j(y_m) \frac{dy_m}{\rho(y_m)} = 0. \quad (9)$$

For Legendre polynomials with weight function $\rho(y_m) = 1$, the l -th degree monomial is given by the recursive formula:

$$P_0^L(y_m) = 1, \quad P_1^L(y_m) = y_m, \quad P_{l+1}^L(y_m) = \frac{(2l+1)y_m P_l^L(y_m) - l P_{l-1}^L(y_m)}{l+1}, \quad (10)$$

and for Chebyshev polynomials of the second kind with weight function $\rho(y_m) = \sqrt{1-y_m^2}$, the l -th degree polynomial is defined by:

$$P_0^C(y_m) = 1, \quad P_1^C(y_m) = 2y_m, \quad P_{l+1}^C(y_m) = 2y_m P_l^C(y_m) - P_{l-1}^C(y_m). \quad (11)$$

Neural Network component The hybrid scheme (see Fig. 1) further considers a feedforward artificial NN $\tilde{\pi}^{NN}(\mathbf{y}, \mathbf{p}; \mathcal{H}_2) \in \mathbb{R}^N$ with inputs $\mathbf{y} \in \mathbb{R}^M$, where \mathbf{p} is a vector including the parameters of the NN (weights and biases of each layer) and \mathcal{H}_2 includes the NN hyperparameters, such as the number of hidden layers, the type and parameters of activation function, etc.. For simplicity, we assume a single layer feedforward NN (SLFNN) with L neurons in the hidden layer (more expressive architectures were tested and did not show significant numerical accuracy improvement). Each output of the SLFNN, $\tilde{\pi}_n^{NN}(\mathbf{y}, \mathbf{p}_n; \mathcal{H}_2)$ for $n = 1, \dots, N$, is expressed as:

$$\tilde{\pi}_n^{NN}(\mathbf{y}, \mathbf{p}_n; \mathcal{H}_2) = \mathbf{w}^{o(n)\top} \phi(\mathbf{W}^{(n)} \mathbf{y} + \mathbf{b}^{(n)}) + b^{o(n)}, \quad (12)$$

where $\mathbf{p}_n = [\mathbf{w}^{o(n)}, b^{o(n)}, \mathbf{W}^{(n)}, \mathbf{b}^{(n)}]^\top \in \mathbb{R}^{L(M+2)+1}$ includes: (i) the output weights $\mathbf{w}^{o(n)} = [w_1^{o(n)}, \dots, w_L^{o(n)}]^\top \in \mathbb{R}^L$ connecting the hidden to the output layer, (ii) the bias $b^{o(n)} \in \mathbb{R}$ of the output layer, (iii) the internal weights $\mathbf{W}^{(n)} \in \mathbb{R}^{L \times M}$, where each column $\mathbf{w}_l^{(n)} = [w_{l,1}^{(n)}, \dots, w_{l,M}^{(n)}]^\top \in \mathbb{R}^M$ corresponds to the weights between the input neurons and the l -th neuron in the hidden layer, and (iv) the internal

biases $\mathbf{b}^{(n)} = [b_1^{(n)}, \dots, b_L^{(n)}]^\top \in \mathbb{R}^L$ of the neurons in the hidden layer. The outputs of the activated neurons $\phi_l(\mathbf{W}^{(n)}\mathbf{y} + \mathbf{b}^{(n)})$ for $l = 1, \dots, L$ are included in the column vector $\phi(\cdot) \in \mathbb{R}^L$. Here, the logistic sigmoid function is used as the activation function due to its universal approximation properties [88] and its suitability for symbolic differentiation.

Physics-Informed Learning For acquiring an approximation of the IM functional in Eq. (4), the hybrid scheme should provide a solution of the system of NFEs in Eq. (5), according to Theorem 1. Let $\mathbf{y}^{(q)} \in \Omega$ be a set of $q = 1, \dots, Q$ collocation points, selected from the domain Ω where the IM approximation is sought. Further assume a set of $r = 1, \dots, R$ collocation points on the boundary of the polydisc \mathcal{D} of radius r , such that $\mathbf{y}^{(r)} \in \partial\mathcal{D}$. Then, the parameters of $\tilde{\pi}^{HxS}(\mathbf{y}, \mathbf{a}, \mathbf{p}; \mathcal{H}_1, \mathcal{H}_2, r)$, that render it an IM approximation, are computed by the solution of the optimization problem:

$$\begin{aligned} \operatorname{argmin}_{\mathbf{a}, \mathbf{p}} \mathcal{L}(\mathbf{a}, \mathbf{p}; \mathcal{H}_1, \mathcal{H}_2, r) \triangleq & \sum_{q=1}^Q \omega_q \left(\left\| \tilde{\pi}^{HxS}(\mathbf{A}\mathbf{y}^{(q)} + \mathbf{g}(\mathbf{y}^{(q)}), \mathbf{a}, \mathbf{p}; \mathcal{H}_1, \mathcal{H}_2, r) - \right. \right. \\ & \left. \left. - \mathbf{B}\tilde{\pi}^{HxS}(\mathbf{y}^{(q)}, \mathbf{a}, \mathbf{p}; \mathcal{H}_1, \mathcal{H}_2, r) - \mathbf{C}\mathbf{y}^{(q)} - \mathbf{f}(\tilde{\pi}^{HxS}(\mathbf{y}^{(q)}, \mathbf{a}, \mathbf{p}; \mathcal{H}_1, \mathcal{H}_2, r), \mathbf{y}^{(q)}) \right\|^2 \right) + \\ & + \omega_1 \left\| \tilde{\pi}^{HxS}(\mathbf{0}^M, \mathbf{a}, \mathbf{p}; \mathcal{H}_1, \mathcal{H}_2, r) \right\|^2 + \sum_{r=1}^R \omega_2 \left\| \tilde{\pi}_n^{xS}(\mathbf{y}^{(r)}, \boldsymbol{\alpha}_n; \mathcal{H}_1) - \tilde{\pi}_n^{NN}(\mathbf{y}^{(r)}, \mathbf{p}_n; \mathcal{H}_2) \right\|^2. \quad (13) \end{aligned}$$

The first term of the loss function in Eq. (13) is a PI term enforcing the satisfaction of the system of NFEs by $\tilde{\pi}^{HxS}(\cdot)$, while the second term ensures that the $\tilde{\pi}^{HxS}(\cdot)$ passes through the equilibrium (which can be viewed as a loss function at the boundary). Note that the hybrid scheme approximation at the equilibrium consists only of the polynomial series component, since $\mathbf{0}^M \in \mathcal{D}$. The third term is a C^0 continuity in the boundary $\partial\mathcal{D}$ (C^k continuity conditions can be also imposed), as it matches the polynomial series component with the NN component on the boundary collocation points $\mathbf{y}^{(r)} \in \partial\mathcal{D}$. The second and third terms in the loss function serve for pinning the polynomial series and the NN components, respectively, which are further balanced by $\omega_q, \omega_1, \omega_2 \in \mathbb{R}$.

Remark 1. A key feature of the hybrid scheme in Eq. (13) is that the IM approximation $\tilde{\pi}_n^{HxS}(\cdot)$ at $\mathbf{y}^{(q)}$ may be evaluated by the NN, while at $\mathbf{A}\mathbf{y}^{(q)} + \mathbf{g}(\mathbf{y}^{(q)})$ by the polynomial series and vice versa, depending on whether these points lie inside or outside \mathcal{D} . The radius of the polydisc \mathcal{D} is an additional hyperparameter that needs tuning especially in the case of power series polynomials, since when Legendre or Chebyshev polynomials are considered, naturally we choose $r_m = 1$ for $m = 1, \dots, M$.

To solve the optimization problem in Eq. (13), we minimize the non-linear residuals resulting from the loss function, as detailed in Appendix B. Since the optimization problem is solved in $\boldsymbol{\alpha}$ and \mathbf{p} , an overdetermined system requires at least $Q + R = N \left(L(M+2) + \left(\prod_{i=1}^M (h+i) \right) / i! + 1 \right)$ collocation points to form the residuals. For their minimization, we employ the Levenberg-Marquardt (LM) gradient-based optimization algorithm [96], which requires the derivatives of the hybrid scheme w.r.t. to its parameters, as well as the derivatives $\partial_{\mathbf{x}}\mathbf{f}$. The former reduce to the computation of $\partial_{\boldsymbol{\alpha}}\tilde{\pi}^{xS}(\mathbf{y}^{(q)}, \boldsymbol{\alpha}; \mathcal{H}_1)$ and $\partial_{\mathbf{p}}\tilde{\pi}^{NN}(\mathbf{y}^{(q)}, \mathbf{p}; \mathcal{H}_2)$, which can be obtained analytically using symbolic differentiation. $\partial_{\mathbf{x}}\mathbf{f}$ can be also obtained analytically if \mathbf{f} is known explicitly; otherwise, numerical differentiation can be employed.

Finally, we compare the IM approximations provided by the hybrid scheme with those provided by purely using NNs. For completeness, we discuss the optimization problem resulting from NNs in Appendix C. The implementation of the LM algorithm for solving both the hybrid and NN schemes is provided in Appendix D, along with a pseudo-code for minimizing the related non-linear residuals.

Remark 2. We emphasize that the PI optimization problem in Eq. (13) is inherently non-linear, even within the polydisc \mathcal{D} where the polynomial component of the hybrid scheme acts, due to the non-linearity of the NFEs. However, in a regression setting—where the hybrid scheme approximates a function using labeled targets—the polynomial counterpart reduces to a linear residual minimization problem. Unlike non-linear optimization, this problem does not require iterative methods (e.g., the LM algorithm) to determine the polynomial coefficients. Instead, it should be solved directly using linear techniques such as the Moore-Penrose pseudo-inverse, as iterative optimization introduces unnecessary numerical errors in the coefficient estimates; we provide such a polynomial regression example in Appendix E.

Remark 3. Building on Remark 2, one might consider linearizing the PI optimization problem in Eq. (13) by locally approximating the polynomial counterpart via Taylor series expansions around equilibrium, following [18, 19]. However, this would necessitate a two-step procedure for the hybrid scheme; first, solve the linearized problem within \mathcal{D} to obtain the polynomial coefficients and then solve a non-linear optimization problem to train the NN for approximating the IM

outside \mathcal{D} . This approach has several drawbacks: (i) it requires Taylor expansions of the non-linear functions \mathbf{f} and \mathbf{g} in Eq. (2), and as such it does not provide flexibility on the radius of the polydisc \mathcal{D} , since the latter is constrained by the radius of convergence of the Taylor expansions, (ii) it is problem-dependent, as the linearized polynomial series varies for each dynamical system, and (iii) it becomes computationally intractable as the system dimension or polynomial degree increases. In contrast, our method—while sacrificing some accuracy in the polynomial coefficients (see Remark 2)—provides a one-step, plug-and-play solution that avoids these limitations.

2.2 Implementation of the physics-informed approaches for the IM approximation

This section provides all the necessary details for implementing the PI hybrid scheme introduced in Section 2.1, along with the PI NNs scheme. Specifically, we describe the training process and discuss the evaluation of the numerical accuracy of the learned IM approximations. An overview of the training and evaluation process is presented in Algorithm 1, the steps of which are explained in detail in the following paragraphs.

Algorithm 1 Outline of training and evaluation of the IM functionals approximated via the PI hybrid and NN schemes; bold comments denote paragraphs of Section 2.2 where the specific step is discussed.

Require: Discrete system in the form of Eq. (1)

Ensure: Assumptions of Theorem 1 are satisfied around equilibrium $(\mathbf{x}_0, \mathbf{y}_0)$ ▷ $\mathbf{A}, \mathbf{B}, \mathbf{C}, \mathbf{f}(\mathbf{x}, \mathbf{y})$ and $\mathbf{g}(\mathbf{y})$ of Eq. (2)

- 1: Define $\Omega \subset \mathcal{V}$ to approximate the IM functional Eq. (4)
 - 2: Sample collocation points $\mathbf{y}^{(q)} \in \Omega$, ensuring IM functional exists for $q = 1, \dots, Q$ ▷ See *Training data acquisition*
 - 3: Sample testing data points $(\mathbf{x}^{(s)}, \mathbf{y}^{(s)}) \in \mathcal{M}$ on the IM, ensuring $\mathbf{y}^{(s)} \in \Omega$ for $s = 1, \dots, S$ ▷ See *Testing data acquisition*
 - 4: Select type of IM approximation $type \leftarrow HxS$ or NN . ▷ *Hybrid scheme or pure NNs*
 - 5: Select architectures and set hyperparameters $\mathcal{H}_1, \mathcal{H}_2$ and/or \mathbf{r} depending on $type$ ▷ See *Architectures and Hyperparameters*
 - 6: Set collocation points $\mathbf{y}^{(r)} \in \partial\mathcal{D}$ for $r = 1, \dots, R$
 - 7: **for** multiple training realizations **do**
 - 8: Initialize parameters \mathbf{a} and \mathbf{p} ▷ See *Parsimonious initialization of parameters*
 ▷ Solve the related PI optimization problem by using the LM algorithm (see Appendix D for details)
 - 9: **repeat** ▷ LM algorithm iterations
 - 10: Form non-linear residuals of the loss function ▷ Use Eq. (13) for HxS or Eq. (C.1) for NN
 - 11: Form Jacobians of the non-linear residuals with derivatives of loss function w.r.t. the parameters
 - 12: Perform the LM iteration to update the parameters and the damping factor
 - 13: **until** Convergence or maximum epochs reached
 - 14: Compute training metrics with the learned parameters on the collocation points $\mathbf{y}^{(q)}$ ▷ See *Training metrics*
 - 15: Compute evaluation metrics with the learned parameters on the testing set $(\mathbf{x}^{(s)}, \mathbf{y}^{(s)})$ ▷ See *Numerical accuracy metrics*
 - 16: Average over multiple realizations and compute confidence intervals, both on training and evaluation metrics
 - 17: Visualize numerical accuracy based on the parameter set with the best performance on the evaluation metrics
-

2.2.1 Training process

The training process was conducted over 100 training realizations to quantify the uncertainty in training performance. Below, we outline its key components: training data acquisition, the architectures and hyperparameters selected, the initialization of parameters, and the metrics used to evaluate convergence. These components correspond to steps 2, 5, 7, and 13 of Algorithm 1, respectively. The minimization of non-linear residuals via the LM algorithm is presented in Appendix D.

Training data acquisition To learn the IM approximations using the proposed PI hybrid scheme in Section 2.1—or the PI NN scheme in Appendix C—a collection of Q collocation points $\mathbf{y}^{(q)}$ for $q = 1, \dots, Q$ is required. Since the IM \mathcal{M} in Eq. (4) is defined in a local neighborhood $\mathcal{V} \subset \mathbb{R}^M$ around the equilibrium \mathbf{y}_0 (see Theorem 1), the collocation points are collected within a desired domain $\Omega \subset \mathcal{V}$, chosen to avoid singular points.

For the $M = 1$ -dim. case, $\Omega = [a_1, b_1]$ is an interval containing $y_0 = 0$. However, the generalization of Ω in higher dimensions is not straightforward. For example, there is no guarantee that the IM exists for all \mathbf{y} in the hyperrectangle $\Omega = [a_1, b_1] \times [a_2, b_2] \times \dots \times [a_M, b_M]$. To address this, for $M > 1$, we collected collocation points from numerically derived trajectories, following the approach in [77, 78]. Specifically, we selected 200 initial conditions randomly chosen outside a predefined hyperrectangle Ω and generated trajectories of the system in Eq. (1). After discarding a transient of $k = 8$ time steps (to allow the system to approach the IM), we recorded all subsequent time steps until reaching the equilibrium, using a cutoff of 0.001 for each variable (for avoiding oversampling near the equilibrium). After ensuring $\mathbf{y} \in \Omega$ for the recorded points, we randomly selected Q of them and used their \mathbf{y} values to form the training dataset $\mathbf{y}^{(q)}$ for $q = 1, \dots, Q$. For the $M = 1$ -dim. cases, we simply sampled Q uniform points from $\mathcal{U}([a_1, b_1])$.

To enable fair comparison of computational training times between the PI hybrid and NNs schemes, we chose the number of collocation points Q such that the number of residuals is 20 times the number of unknown parameters of the–common between two PI schemes–NN component.

In addition, for the continuity term in the loss function in Eq. (13), it is further required to collect R collocation points on the boundary ∂D . For the $M = 1$ -dim. case, we simply select the two points $\mathbf{y}^{(r)} = \pm \mathbf{r}$. For higher dimensions, we uniformly sample 5^{M-1} points along each hyperplane of $\partial D = \{\mathbf{y} \in \mathbb{R}^2 : |y_m| = r_m, \forall m = 1, \dots, M\}$; e.g., for $M = 2$, we sample $R = 4 \cdot 5 = 20$ points across the four edges of the rectangle ∂D , while for $M = 3$, we sample $R = 6 \cdot 5^2 = 150$ points across the six surfaces of the cube ∂D .

Architectures and Hyperparameters For the polynomial series components of the PI hybrid scheme presented in Eq. (8), we considered power series, Legendre polynomials and Chebyshev polynomials of the second kind. The degree h of the polynomials varied across the examples studied, depending on the desired accuracy. For the NN component, we employed the SLFNN architecture presented in Eq. (12). Increasing the depth to two hidden layers did not yield significant improvements in accuracy, so we used a single hidden layer with $L = 10$ neurons and a logistic sigmoid activation function in all examples.

An important hyperparameter for the PI hybrid scheme is the radius \mathbf{r} of the polydisc \mathcal{D} . Each element r_m of \mathbf{r} is free to vary within the interval $[\min(a_m, b_m), \max(a_m, b_m)]$, where $[a_m, b_m]$ is the range of the y_m variable in the hyperrectangle Ω of the training dataset. For Legendre and Chebyshev polynomials, the restriction $r_m \leq 1$ applies to ensure the polynomials are well-defined. The choice of r_m determines the polydisc \mathcal{D} where the polynomial series counterpart is active. Since no prior information about the underlying IM functional is generally available, r_m requires careful tuning. In all the examples, we tuned r_m starting from values leaving approximately half of the collocation points outside \mathcal{D} . While it is out of the scope of this work, we emphasize that further analysis is needed to determine optimal values of r_m , taking into account the polynomial degree h .

For the optimization problem, we determined the three balancing terms $\omega_q, \omega_1, \omega_2$ in Eq. (13) using residual balancing [97], where the ω_q was set to 1 for the NN residuals; i.e., for $\mathbf{y}^{(q)} \notin \mathcal{D}$. For the implementation of the LM algorithm, we configured the initial damping factor to $\lambda_0 = 10^{-2}$ and the hyperparameters related to the stopping criteria to a maximum number of epochs $k_{max} = 2000$, a relative function tolerance $tol_F = 10^{-8}$ and a relative step tolerance $tol_R = 10^{-4}$; see Appendix D for further details.

Parsimonious initialization of parameters The solution of the optimization problem in Eq. (13) requires an initial guess of the learnable parameters: the coefficients α of the polynomial series counterpart and the parameters \mathbf{p} of the NN one. While a random initial guess can be selected, we observed that such an approach leads to poor convergence for approximately 20% of the training realizations. This behavior arises in high-degree polynomial series, because random initialization can result in high-order terms dominating the loss function, causing the optimizer to converge to suboptimal local minima of the non-linear loss function.

To address this, we employ a parsimonious initialization strategy for the polynomial coefficients α , ensuring that each monomial is $\mathcal{O}(1)$. In particular, we initialize the non-zero coefficients $\alpha_n^{i_1, \dots, i_M}$ in Eq. (8) by sampling random values uniformly distributed in the interval $[-1/c_n^{i_1, \dots, i_M}, 1/c_n^{i_1, \dots, i_M}]$, where

$$c_n^{i_1, \dots, i_M} = \max_{1 \leq q \leq Q} \left\{ \left| P_{i_1}^x(y_1^{(q)}) \cdots P_{i_M}^x(y_M^{(q)}) \right| \right\}, \quad \forall i_1, \dots, i_M = 1, \dots, h, \quad \text{with } i_1 + \dots + i_M \leq h.$$

Here $y_m^{(q)}$ denotes the m -th element of the q -th collocation point $\mathbf{y}^{(q)}$. For the NN parameters \mathbf{p} , we use a uniform Xavier/Glorot initialization [98]. To further avoid numerically exploding or vanishing gradients, we ensure that $\mathbf{W}^{(n)}\mathbf{y} + \mathbf{b}^{(n)} = \mathcal{O}(1)$ by further scaling the Xavier-initialized input weights $w_{l,m}^{(n)}$ by $\max_q(y_m^{(q)}) - \min_q(y_m^{(q)})$. The parameters α and \mathbf{p} , initialized using the above procedure, consistently demonstrated good convergence by improving the conditioning of the optimization problem and enabling the LM algorithm to perform reliably.

Training metrics To evaluate the convergence of the optimization problem in Eqs. (13) and (C.1), we record the values of the respective loss functions at the end of training for each of the 100 realizations of different initial parameters, along with the computational times required for training. The value of each loss function corresponds to the squared l_2 error, $\|\mathcal{F}\|_2$, of the non-linear residuals \mathcal{F} minimized through the LM algorithm. To quantify the uncertainty and assess the consistency of convergence, we compute the mean and 5-95% confidence intervals (CIs) of these training metrics across the 100 realizations.

2.2.2 Evaluation of numerical approximation accuracy

For assessing the numerical approximation accuracy of the IM approximations obtained by the PI hybrid and pure NNs scheme, we compare data points that lie exclusively on the true IM \mathcal{M} in Eq. (4) to their corresponding approximations. Specifically, for a given $\mathbf{y} \in \Omega$, the true IM mapping $\pi(\mathbf{y})$ provides the corresponding \mathbf{x} (i.e., $\mathbf{x} = \pi(\mathbf{y})$), while the IM functional approximation yields the estimate $\tilde{\mathbf{x}} = \tilde{\pi}(\mathbf{y})$. By comparing \mathbf{x} and $\tilde{\mathbf{x}}$, we quantify the accuracy of the IM approximation. In the sequel, we discuss the construction of the testing data sets and the error metrics used for quantifying numerical accuracy.

Testing data acquisition As previously discussed, the construction of the testing data set requires data points that lie exclusively on the underlying IM \mathcal{M} in Eq. (4). However, an explicit expression for the IM mapping is generally unknown for dynamical systems of the form Eq. (1). To address this, we collected testing data from numerically derived trajectories. Following the same procedure as for acquiring the training data, we selected $100N$ random initial conditions outside Ω within example-specific bounds, generated trajectories, discarded a transient of $k = 8$ time steps and finally recorded subsequent time steps until reaching the equilibrium, using a cutoff of 0.001 for each variable. We randomly selected $S = 10,000$ from the recorded points and used both $\mathbf{y}^{(s)}$ and $\mathbf{x}^{(s)}$ to form the testing sets, $(\mathbf{x}^{(s)}, \mathbf{y}^{(s)}) \in \mathcal{M}$, ensuring $\mathbf{y}^{(s)} \in \Omega$ for $s = 1, \dots, S$. This construction procedure was followed for every example, except for the first one, where the IM mapping $\pi(y) = \ln(1 + y)$ was analytically known and used to generate the testing data.

Numerical accuracy metrics To assess the numerical approximation accuracy, we simply evaluated the error between $\mathbf{x}^{(s)}$ and $\tilde{\mathbf{x}}^{(s)} = \tilde{\pi}(\mathbf{y}^{(s)})$ on the testing data set. Specifically, we computed the l_1 , l_2 and l_∞ norms of $\|\mathbf{x}_n^{(s)} - \tilde{\pi}_n(\mathbf{y}^{(s)})\|$ for all $s = 1, \dots, S$, as well as the mean squared error $\text{MSE}(\mathbf{x}_n^{(s)}, \tilde{\pi}_n(\mathbf{y}^{(s)}))$ for all the $n = 1, \dots, N$ components of the IM approximations, and report their mean and 5-95% CIs across the 100 parameter sets learned during training.

For visualization purposes, we selected the parameter set with the best l_2 norm error and displayed the absolute errors $|\mathbf{x}^{(s)} - \tilde{\pi}(\mathbf{y}^{(s)})|$ across all points to highlight regions of high and low numerical approximation accuracy.

3 Illustrative examples

To demonstrate the efficiency of the proposed PI hybrid scheme, we consider three illustrative examples. The first example involves a discrete dynamical system with an exact $N = 1$ -dim. IM functional, providing a known exact mapping to validate our approach. The second example focuses on an enzymatic bioreactor problem studied in [19], for which the power series expansion is known. Finally, the third example generalizes in multiple dimensions, allowing us to explore $N = 1$ and $N = 2$ -dim. IMs, which are functions of $M = 1$, $M = 2$ and $M = 3$ variables. Below, we briefly describe the examples and provide the analytic PSE for the IM approximations, derived by the Taylor expansion approach proposed in [18, 19].

3.1 Example with analytic invariant manifold

We first consider a non-linear discrete dynamical system expressed in the form of Eq. (1) with $N = 1$ and $M = 1$:

$$\begin{aligned} x(k+1) &= \beta x(k) + y(k), \\ y(k+1) &= (1 + y(k))^\beta e^{y(k)} - 1, \end{aligned} \quad (14)$$

where $\beta \neq 0$ and $y \geq -1$. For $\beta < 0$, a singularity occurs at $y = -1$. The equilibrium of the system is $(x_0, y_0) = (0, 0)$ and Assumption 1 is satisfied for $\beta \neq -1$. Under this assumption, we rewrite the system in the form of Eq. (2) as:

$$\begin{aligned} x(k+1) &= \beta x(k) + y(k), \\ y(k+1) &= (1 + \beta)y(k) + (1 + y(k))^\beta e^{y(k)} - (1 + \beta)y(k) - 1, \end{aligned} \quad (15)$$

where all the assumptions regarding the non-linear functions are satisfied at the equilibrium point. According to Theorem 1 and since $\mathbf{A} = 1 + \beta$ and $\mathbf{B} = \beta$, an analytic local IM \mathcal{M} exists, in the form of Eq. (4), around a neighborhood of the equilibrium, provided that the non-resonance condition $(1 + \beta)^d \neq \beta$ holds for any $d \in \mathbb{N}$. It can be shown that the IM mapping π , given by:

$$x = \pi(y) = \ln(1 + y), \quad (16)$$

is the exact analytic solution of the NFEs in Eq. (5) for the system Eq. (15). Here, we set $\beta = -0.4$, ensuring that the equilibrium is stable (trajectories are attracted to it) and the non-resonance condition is satisfied. Note that, as previously mentioned and evident from Eq. (16), a singularity exists at $y = -1$.

Although the exact IM mapping is known for this example, we approximated it analytically using the PSE approach proposed in [18], as described in Appendix A. The resulting PSE for the IM approximation coincides with the well known h -th degree Taylor expansion of the logarithmic function:

$$\tilde{x} = \tilde{\pi}^{PSE}(y) = \sum_{i=1}^h \alpha_{PSE}^i P_i^P(y), \quad \text{where } \alpha_{PSE}^i = (-1)^{i+1}/i, \quad \text{and } P_i^P(y) = y^i. \quad (17)$$

The radius of convergence of this power series is $|y| < r = 1$; Additionally, since the exact IM mapping is available in Eq. (16), we approximated it using Legendre and Chebychev polynomials, yielding:

$$\tilde{x} = \tilde{\pi}^{LSE}(y) = \sum_{i=1}^h \alpha_{LSE}^i P_i^L(y), \quad \text{where } \alpha_{LSE}^i = \frac{2i+1}{2} \int_{-1}^1 \ln(1+y) P_i^L(y) dy, \quad (18)$$

for the Legendre approximation, and

$$\tilde{x} = \tilde{\pi}^{CSE}(y) = \sum_{i=1}^h \alpha_{CSE}^i P_i^C(y), \quad \text{where } \alpha_{CSE}^i = \frac{2}{\pi} \int_{-1}^1 \ln(1+y) P_i^C(y) \frac{dy}{\sqrt{(1-y^2)}}. \quad (19)$$

for the Chebyshev approximation. The Legendre and Chebyshev polynomials, $P_i^L(y)$ and $P_i^C(y)$, are defined by the recursive formulas in Eq. (10) and Eq. (11), respectively.

In this example, we not only have the exact expression of the IM mapping in Eq. (16), but also the analytic expressions of the power, Legendre and Chebyshev polynomial series in Eqs. (17) to (19), computed for degree $h = 20$. The former will be used for evaluating the accuracy of the PI schemes, while the latter will serve as approximations for comparison purposes.

3.2 Enzymatic bioreactor problem

We consider the enzymatic bioreactor problem studied in [19], which models a continuous stirred tank reactor (CSTR) where an enzyme converts a substrate into product via a ping-pong bi-mechanism. The system is described by the following non-linear ODEs for the substrate concentration S and the enzyme concentration E :

$$\begin{aligned} \frac{dS}{dt} &= \frac{k_1 E S}{1 - k_2 S} + v_r (S_0 - S), \\ \frac{dE}{dt} &= -k_{d1} E, \end{aligned} \quad (20)$$

where k_1 , k_2 and k_{d1} are kinetic parameters, v_r is the ratio of the flow rate of substrate to the reactor volume and S_0 is the substrate concentration in the feed stream. We adopt the parameter values $k_1 = 0.082$, $k_2 = 0.59$, $k_{d1} = 0.0034$, $v_r = 2$ and $S_0 = 3.4$, following [19]. To transform the continuous system in Eq. (20) into a discrete one, we use a time-discretization step $\delta = 0.01$, yielding the discrete dynamical system:

$$\begin{aligned} S(k+1) &= (1 - \delta v_r) S(k) + \delta \frac{k_1 E(k) S(k)}{1 - k_2 S(k)} + \delta v_r S_0, \\ E(k+1) &= (1 - \delta k_{d1}) E(k). \end{aligned}$$

With the chosen parameter set, the system exhibits a stable equilibrium $(S^0, E^0) = (S_0, 0)$. Introducing the deviation from equilibrium $x = S - S^0$ and $y = E - E^0$, we obtain a discrete dynamical system in the form of Eq. (1), which can be further cast in the form of Eq. (2) as:

$$\begin{aligned} x(k+1) &= (1 - \delta v_r) x(k) + \frac{\delta k_1 S_0}{1 - k_2 S_0} y(k) + \frac{\delta k_1 y(k) x(k)}{(1 - k_2 S_0)(1 - k_2 S_0 - k_2 x(k))}, \\ y(k+1) &= (1 - \delta k_{d1}) y(k). \end{aligned} \quad (21)$$

The system in Eq. (21) satisfies all the assumptions regarding the non-linear functions at the equilibrium $(x_0, y_0) = (0, 0)$. Additionally, since $\mathbf{A} = 1 - \delta k_{d1}$ and $\mathbf{B} = 1 - \delta v_r$, the assumptions of Theorem 1 are satisfied, as the non-resonance condition $(1 - \delta k_{d1})^d \neq 1 - \delta v_r$ holds for any $d \in \mathbb{N}$. This implies the existence of an analytic $N = 1$ -dim. IM \mathcal{M} in the form of Eq. (4), the mapping of which $\tilde{x} = \tilde{\pi}(y)$ can be approximated by solving the NFEs Eq. (5). Following Appendix A, we obtained the PSE approximation of the IM functional $\tilde{x} = \tilde{\pi}^{PSE}(y)$ in the form of Eq. (A.2). The analytically determined coefficients $\pi^1, \dots, \pi^{1, \dots, 1}$ are in excellent agreement with those reported in [19] for a Taylor expansion of degree $h = 10$.

3.3 Multi-dimensional example

We now consider a discrete dynamical system that can be generalized to multiple dimensions in both \mathbf{x} and \mathbf{y} . Specifically, we examine the system:

$$\begin{aligned}\hat{\mathbf{x}}(k+1) &= \cos(\hat{\mathbf{B}}\hat{\mathbf{x}}(k)) + \hat{\mathbf{C}}\hat{\mathbf{y}}(k), \\ \hat{\mathbf{y}}(k+1) &= \sin(\hat{\mathbf{A}}\hat{\mathbf{y}}(k)),\end{aligned}\quad (22)$$

where $\hat{\mathbf{x}} \in \mathbb{R}^N$, $\hat{\mathbf{y}} \in \mathbb{R}^M$, and $\hat{\mathbf{A}} \in \mathbb{R}^{M \times M}$, $\hat{\mathbf{B}} \in \mathbb{R}^{N \times N}$ and $\hat{\mathbf{C}} \in \mathbb{R}^{N \times M}$. The equilibrium points of this system, say $(\hat{\mathbf{x}}_0, \hat{\mathbf{y}}_0)$, satisfy:

$$\hat{\mathbf{x}}_0 - \cos(\hat{\mathbf{B}}\hat{\mathbf{x}}_0) - \hat{\mathbf{C}}\hat{\mathbf{y}}_0 = \mathbf{0}_N, \quad \hat{\mathbf{y}}_0 - \sin(\hat{\mathbf{A}}\hat{\mathbf{y}}_0) = \mathbf{0}_M.$$

Here, we compute the IM around the origin $\hat{\mathbf{y}}_0 = \mathbf{0}^M$, which implies that $\hat{\mathbf{x}}_0$ satisfies $\hat{\mathbf{x}}_0 - \cos(\hat{\mathbf{B}}\hat{\mathbf{x}}_0) = \mathbf{0}^N$. The Jacobian matrix of the system in Eq. (22) at the equilibrium points $(\hat{\mathbf{x}}_0, \hat{\mathbf{y}}_0)$ is:

$$\mathbf{J}(\hat{\mathbf{x}}_0, \hat{\mathbf{y}}_0) = \begin{bmatrix} -diag(\sin(\hat{\mathbf{B}}\hat{\mathbf{x}}_0)) \hat{\mathbf{B}} & \hat{\mathbf{C}} \\ \mathbf{0}^{M \times N} & diag(\cos(\hat{\mathbf{A}}\hat{\mathbf{y}}_0)) \hat{\mathbf{A}} \end{bmatrix} = \begin{bmatrix} -diag(\mathbf{1}^N - \hat{\mathbf{x}}_0^2)^{1/2} \hat{\mathbf{B}} & \hat{\mathbf{C}} \\ \mathbf{0}^{M \times N} & \hat{\mathbf{A}} \end{bmatrix}, \quad (23)$$

where $\mathbf{0}^{M \times N}$ is the $M \times N$ zero matrix, $\mathbf{1}^N$ is the N -dim. column vector of ones and $\hat{\mathbf{x}}_0^2$ denotes the element-wise square of $\hat{\mathbf{x}}_0$. Equation (23) implies that the stability of the equilibrium points $(\hat{\mathbf{x}}_0, \hat{\mathbf{y}}_0)$ depends on the eigenvalues of $\hat{\mathbf{B}}$ and $\hat{\mathbf{A}}$, since the eigenvalues of $-diag(\mathbf{1}_N - \hat{\mathbf{x}}_0^2)^{1/2}$ are always less than 1.

Next, we introduce deviation variables from the above equilibrium points $\mathbf{x} = \hat{\mathbf{x}} - \hat{\mathbf{x}}_0$ and $\mathbf{y} = \hat{\mathbf{y}}$, rewriting the system in Eq. (22) in the form of Eq. (1) as:

$$\begin{aligned}\mathbf{x}(k+1) &= diag(\hat{\mathbf{x}}_0) \cos(\hat{\mathbf{B}}\mathbf{x}(k)) - diag(\mathbf{1}^N - \hat{\mathbf{x}}_0^2)^{1/2} \sin(\hat{\mathbf{B}}\mathbf{x}(k)) + \hat{\mathbf{C}}\mathbf{y}(k) - \hat{\mathbf{x}}_0, \\ \mathbf{y}(k+1) &= \sin(\hat{\mathbf{A}}\mathbf{y}(k)),\end{aligned}$$

with the equilibrium points now represented by the origin $(\mathbf{x}_0, \mathbf{y}_0) = (\mathbf{0}^N, \mathbf{0}^M)$ in the new state variables. This system can be rewritten in the form of Eq. (2) by setting:

$$\begin{aligned}\mathbf{A} &= \hat{\mathbf{A}}, \quad \mathbf{B} = -diag(\mathbf{1}^N - \hat{\mathbf{x}}_0^2)^{1/2} \hat{\mathbf{B}}, \quad \mathbf{C} = \hat{\mathbf{C}}, \\ \mathbf{f}(\mathbf{x}(k), \mathbf{y}(k)) &= diag(\hat{\mathbf{x}}_0) \left(\cos(\hat{\mathbf{B}}\mathbf{x}(k)) - \mathbf{1}^N \right) + diag(\mathbf{1}^N - \hat{\mathbf{x}}_0^2)^{1/2} \left(\hat{\mathbf{B}}\mathbf{x}(k) - \sin(\hat{\mathbf{B}}\mathbf{x}(k)) \right), \\ \mathbf{g}(\mathbf{x}(k), \mathbf{y}(k)) &= \sin(\hat{\mathbf{A}}\mathbf{y}(k)) - \hat{\mathbf{A}}\mathbf{y}(k).\end{aligned}\quad (24)$$

For any choice of matrices $\hat{\mathbf{A}}$, $\hat{\mathbf{B}}$ and $\hat{\mathbf{C}}$, Eq. (24) implies $\mathbf{f}(\mathbf{x}_0, \mathbf{y}_0) = \mathbf{g}(\mathbf{y}_0) = \mathbf{0}$ and $\partial \mathbf{f} / \partial \mathbf{x}|_{(\mathbf{x}_0, \mathbf{y}_0)} = \partial \mathbf{f} / \partial \mathbf{y}|_{(\mathbf{x}_0, \mathbf{y}_0)} = \partial \mathbf{g} / \partial \mathbf{y}|_{(\mathbf{y}_0)} = \mathbf{0}$ with appropriate dimensionality. However, to satisfy Assumption 1 the matrix $\hat{\mathbf{A}}$ needs to have non-zero eigenvalues.

In the sequel, we consider three cases of different dimensions for the original system in Eq. (22) aligned with the above state space representation Eq. (24). We chose parameters such that the resulting system trajectories are attracted to their equilibrium points and the non-resonance conditions are satisfied, thus ensuring the existence of an IM through Theorem 1. In all cases, we compute the PSE approximations $\tilde{\mathbf{x}} = \tilde{\pi}^{PSE}(\mathbf{y})$ of the IM functionals by determining the coefficients of the Taylor series expansion in Eq. (A.2), as described in Appendix A. The resulting PSE approximations of the IM are used for comparison with the IM approximations provided by the PI schemes.

3.3.1 An example of $N = 1$ and $M = 1$

First, we consider a simple case with $N = 1$ and $M = 1$; i.e., $\mathbf{x} \in \mathbb{R}$ and $\mathbf{y} \in \mathbb{R}$. We select the parameter values $\hat{\mathbf{A}} = 0.99$, $\hat{\mathbf{B}} = 0.8$, $\hat{\mathbf{C}} = 0.5$, which result to $\hat{\mathbf{x}}_0 = 0.8014$. Substituting these values into the expressions in Eq. (24) shows that the resulting system satisfies the non-resonance condition of Theorem 1, since the eigenvalue of $\hat{\mathbf{A}}$, $k_1 = 0.99$, and the eigenvalue of $\hat{\mathbf{B}}$, $\lambda_1 = -0.1196$, are not related by $k_1^d \neq \lambda_1$ for any $d \in \mathbb{N}$. Hence, according to Theorem 1, a $N = 1$ -dim. IM \mathcal{M} exists, with the mapping $\tilde{\mathbf{x}} = \tilde{\pi}(\mathbf{y})$, where $\tilde{\pi} : \mathbb{R} \rightarrow \mathbb{R}$, satisfying the NFES in Eq. (5). Here, the IM develops around a stable fixed point, since $|k_1|, |\lambda_1| < 1$. The PSE approximation of the IM was computed up to degree $h = 5$.

3.3.2 An example of $N = 1$ and $M = 2$

Next, we consider a case where $N = 1$ but the input dynamics is realized by $M = 2$ independent dynamic variables, that is $\mathbf{x} \in \mathbb{R}$ and $\mathbf{y} \in \mathbb{R}^2$. We select the parameter values:

$$\hat{\mathbf{A}} = \begin{bmatrix} 0.99 & 0.8 \\ -0.1 & 0.9 \end{bmatrix}, \quad \hat{\mathbf{B}} = 0.2, \quad \hat{\mathbf{C}} = [0.5 \quad -0.8], \quad (25)$$

which result to $\hat{\mathbf{x}}_0 = 0.9808$. For these parameter values, we obtain by Eq. (24) that the matrix \mathbf{A} has a pair of complex eigenvalues of $k_{1,2} = 0.945 \pm 0.2792i$, while the eigenvalue of $\hat{\mathbf{B}}$ is $\lambda_1 = -0.039$. There is no resonance relation $k_1^{d_1} k_2^{d_2} = \lambda_1$ that holds true for any $d_1, d_2 \in \mathbb{N}$ with $d_1 + d_2 > 0$. Since all the assumptions of Theorem 1 are satisfied, a $N = 1$ -dim. IM \mathcal{M} exists. In this case however, the mapping $\tilde{\mathbf{x}} = \tilde{\boldsymbol{\pi}}(\mathbf{y})$ has two independent input variables, since $M = 2$, i.e., $\boldsymbol{\pi} : \mathbb{R}^2 \rightarrow \mathbb{R}$. Here, the PSE approximation of the IM was computed up to $h = 4$ degree. Another important difference with the IM in Section 3.3.1 is that in this case, the IM is developed around a stable spiral, since $k_{1,2}$ are complex and $|\Re(k_{1,2})|, |\lambda_1| < 1$.

3.3.3 An example of $N = 2$ and $M = 3$

Finally, we consider a case of the system in Eq. (22) where $N = 2$ and $M = 3$. In particular, we select the parameter values:

$$\hat{\mathbf{A}} = \begin{bmatrix} 0.9 & 0.8 & 0 \\ -0.1 & 0.7 & 0.4 \\ 0 & -0.5 & 0.8 \end{bmatrix}, \quad \hat{\mathbf{B}} = \begin{bmatrix} -0.8 & 0.3 \\ 0.7 & -0.9 \end{bmatrix}, \quad \hat{\mathbf{C}} = \begin{bmatrix} 0.2 & -0.4 & 0.7 \\ -0.1 & 0.8 & 0.9 \end{bmatrix}, \quad (26)$$

which result to $\hat{\mathbf{x}}_0 = [0.9072, 0.9715]^\top$. Substituting these parameter values into Eq. (24), implies that the matrix \mathbf{A} has the eigenvalues $k_1 = 0.8727, k_{2,3} = 0.7637 \pm 0.5234i$, while the matrix \mathbf{B} has the eigenvalues $\lambda_1 = 0.4323, \lambda_2 = 0.1177$. As in Section 3.3.2, these eigenvalues imply that the origin is a stable spiral. Since no resonance condition exists for these eigenvalues (that is, there are no $d_1, d_2, d_3 \in \mathbb{N}$ with $d_1 + d_2 + d_3 > 0$, such that $k_1^{d_1} k_2^{d_2} k_3^{d_3} = \lambda_1$ or $k_1^{d_1} k_2^{d_2} k_3^{d_3} = \lambda_2$), all the assumptions of Theorem 1 are satisfied. Hence, a $N = 2$ -dim. IM \mathcal{M} develops around the origin, with the mapping $\tilde{\mathbf{x}} = \tilde{\boldsymbol{\pi}}(\mathbf{y})$, which in this case has $M = 3$ inputs and $N = 2$ outputs, that is $\boldsymbol{\pi} : \mathbb{R}^3 \rightarrow \mathbb{R}^2$. This IM mapping satisfies again the NFEs in Eq. (5) and for its PSE approximation we considered a multi-variate Taylor series expansion of degree $h = 3$.

4 Numerical Results

This section evaluates the efficiency of the proposed PI hybrid scheme in learning IM approximations for the three examples described in Section 3. We examine their convergence, numerical approximation accuracy and the computational training cost. Additionally, we compare the IM approximations provided by the PI hybrid schemes with those obtained by purely using PI NNs and the PSE expansions derived by the symbolic approach proposed in [18, 19].

Training and evaluation of the PI schemes followed the procedures outlined in Sections 2.2.1 and 2.2.2. All simulations were carried out with a CPU Intel(R) Core(TM) CPU i7-13700H @ 2.40GHz, RAM 32.0 GB using MATLAB R2024b.

4.1 Example with analytic invariant manifold

We first consider the discrete dynamical system in Eq. (15), for which the true IM mapping is known in Eq. (16). This allows us to compare the IM approximations with the exact IM.

The system in Eq. (15) is defined for $y \geq 1$ (when $\beta < 0$) and exhibits a singularity at $y = -1$. We approximate the IM in the domain $\Omega = [-0.9, 2]$. For the PI hybrid scheme, we considered polynomials of degree $h = 10$ and $h = 20$, and NNs with $L = 10$ neurons in the hidden layer. The resulting number of parameters to be computed for the NN component is 31. Accordingly, we collected $Q = 31 \times 20 = 620$ collocation points to train the PI hybrid and pure NN schemes, uniformly sampled from Ω .

Using these collocation points in $\Omega = [-0.9, 2]$, we trained the PI hybrid schemes with power, Legendre and Chebyshev polynomials and $r = 1$ (denoted as HPS, HLS and HCS $r = 1$, respectively) and the PI NN scheme. To explore the effect of the radius of convergence, we also trained the PI hybrid scheme with power series using $r = 0.5$ (denoted as PI HPS $r = 0.5$). To examine the impact of polynomial degree, we considered all hybrid schemes with $h = 10$ (baseline) and $h = 20$. The convergence results of all 9 trained PI approximations are shown in Table 1, as obtained over 100 training realizations with different initial parameters; see Section 2.2.1 for details.

PI schemes		loss $\mathcal{L}(\cdot)$		comp. time (in seconds)	
		mean	5-95% CIs	mean	5-95% CIs
$h = 10$	PI HPS, $r=1$	1.66E-04	[3.37E-06-9.31E-04]	4.42E+01	[1.82E+01-4.93E+01]
	PI HPS, $r=0.5$	6.74E-07	[1.04E-07-3.31E-06]	4.47E+01	[1.87E+01-4.96E+01]
	PI HLS, $r=1$	2.00E-04	[4.69E-06-8.96E-04]	4.27E+01	[4.09E+01-4.56E+01]
	PI HCS, $r=1$	1.52E-04	[2.87E-06-7.46E-04]	4.12E+01	[2.08E+01-4.56E+01]
$h = 20$	PI HPS, $r=1$	3.04E-08	[3.59E-09-1.60E-07]	5.51E+01	[3.47E+01-6.18E+01]
	PI HPS, $r=0.5$	5.65E-07	[2.91E-08-2.30E-06]	5.01E+01	[4.17E+01-5.45E+01]
	PI HLS, $r=1$	1.00E-08	[8.32E-10-3.94E-08]	1.18E+01	[3.82E+00-2.26E+01]
	PI HCS, $r=1$	7.06E-09	[9.19E-10-2.63E-08]	1.44E+01	[4.16E+00-2.45E+01]
PI NN		1.95E-07	[1.44E-08-1.28E-06]	6.06E+00	[3.90E+00-8.40E+00]

Table 1: Convergence results of the proposed PI schemes for the example in Section 3.1. Mean values and 5–95% CIs of the loss function $\mathcal{L}(\cdot)$ and computational training times (in seconds) are reported for 100 randomly initialized realizations. Schemes include PI hybrid schemes (HxS: HPS, HLS, HCS) with $x = P, L, C$ denoting power, Legendre, and Chebyshev polynomials and PI NN. Hyperparameters: polynomial degrees $h = 10$ and $h = 20$, radius $r = 1$ and $r = 0.5$ for the HPS schemes and $L = 10$ neurons for the NN and HxS schemes.

The means and 5-95% CIs of the loss functions in Table 1 indicate that the optimization problems for all PI schemes consistently converge to low loss values (less than $2E-4$) over the selected collocation points. As the degree h increases, the convergence improves for all schemes, except for the HPS scheme with $r = 0.5$. Regarding computational training time, the hybrid schemes are more demanding than the NN scheme, since they additionally consider the polynomial coefficients for the optimization. While in the degree $h = 10$ case, all hybrid schemes require the same computational time, we observe that in the degree $h = 20$ case, the hybrid schemes with the Legendre and Chebyshev polynomials are much faster than those with the power series polynomials. This result indicates that the hybrid scheme with high degree orthogonal polynomials is less computationally intensive than either low degree ones, or power series polynomials.

To evaluate the numerical approximation accuracy of the learned IM approximations, we constructed a testing data set based on the true IM mapping in Eq. (16). Specifically, we collected $S = 3,000$ data points $(x^{(s)}, y^{(s)})$ using the IM mapping $x^{(s)} = \pi(y^{(s)}) = \ln(1 + y^{(s)})$, with $y^{(s)}$ uniformly sampled from Ω . We then computed the errors $x^{(s)} - \tilde{\pi}(y^{(s)})$ using the IM approximations $\tilde{\pi}(y)$ of the trained PI schemes. Table 2 reports the means and 5-95% CIs of the l_1 , l_2 and l_∞ norms of these errors, calculated over the 100 parameter sets obtained during training. For comparison, Table 2 also includes the same error metrics for the PSE, LSE and CSE expansions derived from the true IM in Eqs. (17) to (19).

Scheme	$\ x^{(s)} - \tilde{\pi}(y^{(s)})\ _1$		$\ x^{(s)} - \tilde{\pi}(y^{(s)})\ _2$		$\ x^{(s)} - \tilde{\pi}(y^{(s)})\ _\infty$		
	mean	5-95% CIs	mean	5-95% CIs	mean	5-95% CIs	
$h = 10$	PSE	1.20E+04	6.45E+02	6.59E+01			
	LSE	2.22E+06	1.28E+05	1.40E+04			
	CSE	1.14E+06	6.54E+04	7.11E+03			
	PI HPS, $r=1$	1.17E+00	[1.12E+00-1.23E+00]	4.31E-02	[4.22E-02-4.36E-02]	8.35E-03	[8.16E-03-8.44E-03]
	PI HPS, $r=0.5$	7.97E-02	[3.24E-02-1.74E-01]	4.12E-03	[1.63E-03-9.26E-03]	9.86E-04	[3.63E-04-2.18E-03]
	PI HLS, $r=1$	1.17E+00	[1.12E+00-1.24E+00]	4.28E-02	[4.23E-02-4.35E-02]	8.27E-03	[8.16E-03-8.42E-03]
	PI HCS, $r=1$	1.17E+00	[1.12E+00-1.23E+00]	4.28E-02	[4.23E-02-4.36E-02]	8.28E-03	[8.16E-03-8.44E-03]
	PI NN	5.31E-02	[1.37E-02-1.45E-01]	2.33E-03	[6.27E-04-6.02E-03]	5.35E-04	[1.41E-04-1.38E-03]
$h = 20$	PSE	3.35E+06	2.43E+05	3.44E+04			
	LSE	2.29E+11	1.79E+10	2.71E+09			
	CSE	8.81E+10	6.88E+09	1.04E+09			
	PI HPS, $r=1$	7.25E-02	[1.59E-02-1.56E-01]	3.79E-03	[8.52E-04-7.66E-03]	9.06E-04	[2.00E-04-1.77E-03]
	PI HPS, $r=0.5$	2.14E-02	[9.25E-03-4.40E-02]	8.45E-04	[3.80E-04-1.87E-03]	1.64E-04	[6.91E-05-3.83E-04]
	PI HLS, $r=1$	1.15E-02	[9.66E-03-1.56E-02]	3.18E-04	[2.84E-04-4.00E-04]	4.05E-05	[3.99E-05-4.17E-05]
	PI HCS, $r=1$	1.21E-02	[8.48E-03-1.82E-02]	3.36E-04	[2.75E-04-4.79E-04]	4.11E-05	[3.98E-05-4.27E-05]
	PI NN	5.31E-02	[1.37E-02-1.45E-01]	2.33E-03	[6.27E-04-6.02E-03]	5.35E-04	[1.41E-04-1.38E-03]

Table 2: Numerical approximation accuracy of the IM approximations $\tilde{\pi}(y)$ for the example in Section 3.1. Errors (l_1 , l_2 and l_∞ norms) are reported for the expansions (PSE, LSE, CSE) of the true IM in Eq. (16) and the PI schemes (HPS, HLS, HCS, NN); for hyperparameters see Table 1. Mean values and 5–95% CIs are computed over the 100 parameter sets obtained during training for the PI schemes. The testing data errors are evaluated over $S = 3,000$ points

As shown in Table 2, the purely polynomial-based IM approximations (PSE, LSE and CSE ones derived by the approach in [18, 19]) provide inaccurate results. This inaccuracy worsens as h increases, and is attributed to testing data in

$\Omega = [-0.9, 2]$ lying far from the equilibrium. In this example, the neighborhood of the equilibrium is bounded by the radius of convergence $r = 1$ of the true IM polynomial expansions. In contrast, the PI hybrid schemes and the PI NN deliver accurate IM approximations. In particular, for low-degree polynomials, the PI hybrid scheme with power series and $r = 0.5$ (PI HPS $r = 0.5$) and the PI NN. As h increases, the accuracy of all the PI hybrid schemes improves, and outperforms the approximation provided by the PI NN.

We highlight here that the error metrics in Table 2 are *global* over the testing set Ω . To examine *local* accuracy, we visualize the absolute errors $|x^{(s)} - \tilde{\pi}(y^{(s)})|$ in Figure 2, where panels (a,b) display the approximations in Table 2 for $h = 10$ and $h = 20$, respectively. It is evident that the inaccuracy of all the polynomial series expansions (xSE)

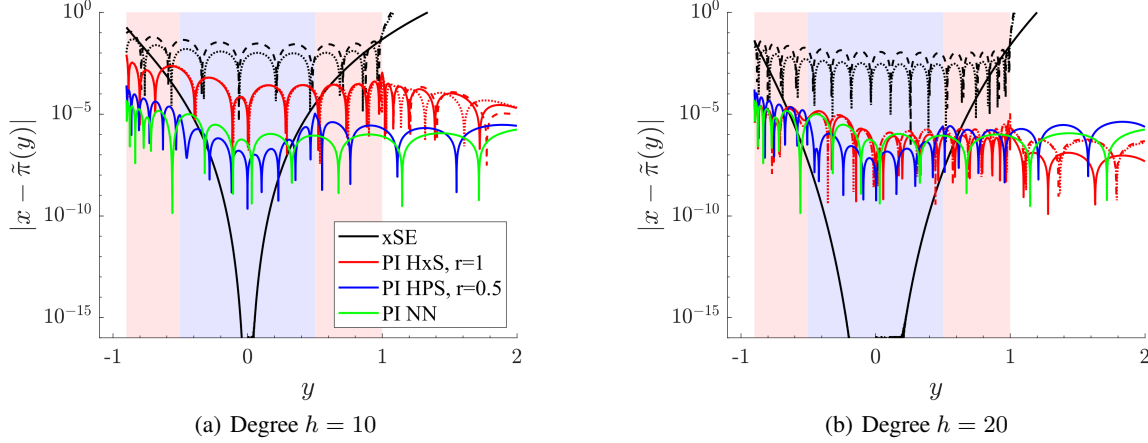


Figure 2: Absolute errors of IM approximations $\tilde{\pi}(y)$ compared to the true IM $x = \ln(1 + y)$ for the example in Section 3.1. Panels show the polynomial series expansions xSE (black), the PI hybrid schemes HxS (red, blue) and the PI NN approximations (green). Power, Legendre, and Chebyshev polynomials ($x = P, L, C$) are distinguished by solid, dashed, and dotted curves, respectively. Red and blue background indicates the radius r of the polydisc \mathcal{D} for the PI hybrid schemes. Panels (a) and (b) correspond to polynomial degrees $h = 10$ and $h = 20$, respectively, and $L = 10$ neurons are used in the NNs.

arises from high errors far from the equilibrium. Figure 2 confirms that the errors of the PI hybrid and PI NN schemes are almost homogeneous in Ω . Interestingly, for $h = 10$, the PI hybrid schemes exhibit lower accuracy than the PI NN scheme, as reflected in Table 2. However, their accuracy improves and matches that of the PI NN schemes, as h increases. It is also shown that the choice of polynomials ($x = P, L, C$) does not affect the approximation accuracy of the hybrid schemes. More importantly, with decreased r , the approximation provided by the PI hybrid schemes is more accurate near the equilibrium than that provided by the PI NN. The next example will demonstrate that the radius r is the most critical hyperparameter for improving the accuracy of the PI hybrid schemes.

4.2 Enzymatic bioreactor problem

We next consider the discrete dynamical system of the enzymatic bioreactor problem in Eq. (21), previously examined in [19], where a PSE of degree $h = 10$ was derived by symbolically solving the NFEs in Eq. (5). Here, we derive IM approximations using the proposed PI hybrid scheme and PI NNs, and compare them with the PSE, focusing on the role of the radius r .

The system in Eq. (21) is biologically plausible for positive concentrations of enzyme $y > 0$, so we approximate the IM in the domain $\Omega = [0, 4]$. We use polynomials of degree $h = 10$ for all schemes and NNs of $L = 10$ neurons in the hidden layer. The number of parameters matches the previous example (Section 4.1), so we collect $Q = 620$ collocation points to train the PI hybrid and NN schemes, uniformly sampled from Ω . All the hyperparameters, except from the radius r , are set as described in Section 2.2.

To explore the role of r , we trained the PI hybrid schemes with power series for $r = 0, 0.5, 1, 2, 4$. The setting with $r = 0$ is equivalent to the PI NN scheme, since the polydisc \mathcal{D} is empty and the NN counterpart is active all over the domain Ω . Conversely, choosing $r = 4$ makes the polydisc \mathcal{D} cover Ω and thus the PI hybrid scheme is equivalent to considering a polynomial series expansion. We also considered Legendre and Chebyshev polynomials with $r = 1$ for the PI hybrid schemes. Below, we present results for the 7 PI approximations, accounting for these equivalences.

The convergence assessment results of the PI hybrid schemes, evaluated over 100 training realizations, are reported in Table 3. The radius r increases from top to bottom with the PI NN scheme being equivalent to the PI HPS hybrid

PI schemes	loss $\mathcal{L}(\cdot)$		comp. time (in seconds)	
	mean	5-95% CIs	mean	5-95% CIs
PI NN (HPS, $r=0$)	3.63E-10	[9.71E-12-7.46E-10]	8.21E+00	[3.72E+00-1.01E+01]
PI HPS, $r=0.5$	3.01E-10	[1.24E-11-3.01E-09]	4.93E+01	[6.30E+00-8.49E+01]
PI HPS, $r=1$	1.37E-09	[1.22E-11-3.00E-09]	2.23E+01	[1.20E+01-7.04E+01]
PI HPS, $r=2$	5.20E-10	[2.52E-11-1.97E-09]	7.17E+01	[1.67E+01-9.44E+01]
PI HPS, $r=4$	3.60E-11	[3.60E-11-3.60E-11]	3.86E-02	[2.17E-02-6.15E-02]
PI HLS, $r=1$	2.31E-10	[1.10E-11-4.24E-09]	8.16E+01	[4.97E+01-9.45E+01]
PI HCS, $r=1$	2.84E-10	[8.35E-12-4.70E-09]	6.60E+01	[1.95E+01-9.36E+01]

Table 3: Convergence results of the proposed PI schemes for the enzymatic bioreactor problem in Section 3.2. Mean values and 5-95% CIs of the loss function $\mathcal{L}(\cdot)$ and computational training times (in seconds) are reported for 100 randomly initialized realizations. Schemes include PI hybrid schemes (HxS: HPS, HLS, HCS) with $x = P, L, C$ denoting power, Legendre, and Chebyshev polynomials and PI NNs. The radii of the PI HPS r vary from 0 to 4 with $r = 0$ being equivalent to the PI NN scheme. Hyperparameters: polynomial degree $h = 10$ and $L = 10$ neurons for the NN and HxS schemes.

schemes for $r = 0$. All the PI schemes consistently converge to very low loss function values (mean loss $\leq 4E-10$). As r increases, the convergence of the PI hybrid schemes remains almost the same, with the $r = 4$ case being lower, as expected since the scheme purely considers polynomial series without the NN counterpart. For this reason, the training times of this particular approximation is negligible. The rest of the PI hybrid schemes are more demanding than the PI NN scheme, since the latter includes less parameters to learn for solving the optimization problem. The Legendre and Chebyshev polynomials show similar convergence to the power series.

For the evaluation of the numerical approximation accuracy of the learned IM approximations, we constructed the testing data set from system trajectories, removing the transients so that the data lie on the IM; see Section 2.2.2. Specifically, we collected $S = 10,000$ data points $(x^{(s)}, y^{(s)})$ in $\Omega = [0, 4]$ by selecting initial conditions for random $x \in [-1, 1]$ and fixed $y = 4.3$. On the basis of the testing set, we computed the errors $x^{(s)} - \tilde{\pi}(y^{(s)})$ for the IM approximations $\tilde{\pi}(y)$ of the trained PI schemes. The means and 5-95% CIs of the l_1 , l_2 and l_∞ norms of these errors, calculated over the 100 parameter sets obtained during training, are reported in Table 4. For comparison, the same metrics are included for the PSE expression derived in [19].

Scheme	$\ x^{(s)} - \tilde{\pi}(y^{(s)})\ _1$		$\ x^{(s)} - \tilde{\pi}(y^{(s)})\ _2$		$\ x^{(s)} - \tilde{\pi}(y^{(s)})\ _\infty$	
	mean	5-95% CIs	mean	5-95% CIs	mean	5-95% CIs
PSE	1.56E+00		1.49E-01		3.10E-02	
PI NN (HPS, $r=0$)	1.01E-01	[1.54E-02-2.28E-01]	3.46E-03	[8.57E-04-4.85E-03]	1.18E-03	[3.86E-04-1.64E-03]
PI HPS, $r=0.5$	5.21E-02	[1.04E-02-1.60E-01]	3.23E-03	[9.23E-04-8.93E-03]	1.19E-03	[4.13E-04-2.93E-03]
PI HPS, $r=1$	9.72E-02	[9.55E-03-1.33E-01]	5.27E-03	[9.21E-04-8.95E-03]	1.55E-03	[4.14E-04-2.97E-03]
PI HPS, $r=2$	5.62E-02	[1.22E-02-1.02E-01]	3.92E-03	[1.18E-03-7.28E-03]	1.37E-03	[5.10E-04-2.47E-03]
PI HPS, $r=4$	8.19E-02	[8.19E-02-8.21E-02]	1.98E-03	[1.98E-03-1.98E-03]	6.88E-04	[6.88E-04-6.88E-04]
PI HLS, $r=1$	4.12E-02	[1.02E-02-1.72E-01]	2.84E-03	[8.66E-04-1.03E-02]	1.05E-03	[3.87E-04-3.33E-03]
PI HCS, $r=1$	4.83E-02	[7.71E-03-1.83E-01]	3.07E-03	[8.09E-04-1.12E-02]	1.11E-03	[3.71E-04-3.63E-03]

Table 4: Numerical approximation accuracy of IM approximations $\tilde{\pi}(y)$ for the enzymatic bioreactor problem in Section 3.2. Errors (l_1 , l_2 and l_∞ norms) are reported for the PSE expansion from [19] and the PI schemes (NN, HPS, HLS, HCS); for hyperparameters see Table 3. Mean values and 5-95% CIs are computed over the 100 parameter sets obtained during training of the PI schemes. Testing data errors are evaluated over $S = 10,000$ points.

Table 4 shows that the PSE approximation, which is based only on power series, provides poor accuracy. On the other hand, the PI hybrid schemes provide higher approximation accuracy with mean l_2 errors at the order of $1E-3$. As r increases, accuracy slightly improves across the testing set. Overall, the PI hybrid schemes achieve slightly higher global accuracy than the PI NN scheme, all of which outperform the PSE approximation.

To evaluate local accuracy, we focus on the absolute errors $|x^{(s)} - \tilde{\pi}(y^{(s)})|$ in the physical space (S, E) in Figure 3, where the PSE approximation derived in [19] and the PI hybrid scheme approximations for different radii r are compared; the PI NN scheme corresponds to $r = 0$ in the hybrid scheme. Figure 3 demonstrates that the PSE provides high accuracy near the equilibrium but exhibits large errors farther away, as reflected in the global accuracy metrics in Table 4. On the other hand, the PI NN scheme generates a homogeneously distributed accuracy profile across the

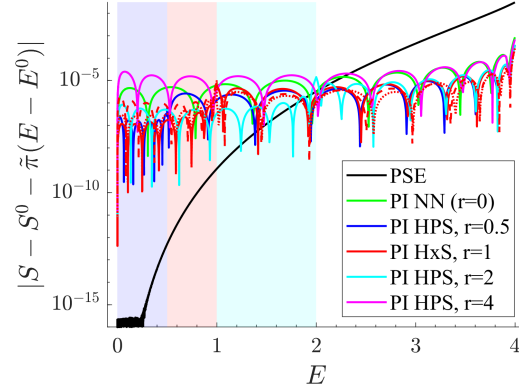


Figure 3: Absolute errors of IM approximations $\tilde{\pi}(y)$ for the enzymatic bioreactor problem in Section 3.2, compared to data on the IM. Errors are projected in the physical space (S, E) . The IM approximations include the power series expansion in [19] (black) and the PI hybrid schemes with different radii r (green, blue, red, cyan), where the one of $r = 0$ is equivalent to the PI NN approximations (green). Power, Legendre, and Chebyshev polynomials are distinguished by solid, dashed, and dotted curves, respectively. Background colors (red, blue, cyan) correspond to the polydiscs \mathcal{D} of each PI hybrid scheme. Polynomial degree is $h = 10$ for all cases, and $L = 10$ neurons are used in the NNs.

entire domain Ω in the order of $1E - 5$. The PI hybrid scheme combines the regions of high accuracy of the above approximations. In particular, as indicated by the highlighted backgrounds in Figure 3, the PI hybrid scheme delivers 1-2 orders higher accuracy than the PI NN within $[0, r]$ (where the polynomial series are active) and comparable (or even higher) accuracy for $E = y > r$. Notably, the accuracy of the PI hybrid schemes improves within $[0, r]$, as r increases. In addition, the Legendre and Chebyshev polynomials provide lower accuracy near the equilibrium than the power polynomials. Similar results were reported for $h = 20$, which are not included for economy of space.

4.3 Multi-dimensional example

In this example, we consider the multi-dimensional system presented in Section 3.3 (see Eq. (22) with definitions in Eq. (24)) and evaluate the performance of the proposed PI hybrid scheme across the three cases $N = 1$ and $M = 1$, $N = 1$ and $M = 2$, and $N = 2$ and $M = 3$, described in Sections 3.3.1 to 3.3.3. For each case, we derived three IM approximations using the proposed PI hybrid schemes (power, Legendre and Chebysen polynomials), one using the PI NNs scheme and the PSE one using the expansion approach proposed in [19]. Unlike the previous examples, which focused on a comprehensive analysis of the role of hyperparameters, here we fix h and r to tuned values for each case considered. This allows us to evaluate the efficiency of hybrid scheme across varying system dimensions.

In the following, we present the results for the three cases together, by summarizing the key findings regarding convergence, computational training time, and global accuracy of the IM approximations. Detailed results for each case, are provided in the Supplements S1 to S3.

Before presenting the results, we provide all relevant details about the training and testing procedures. For the $N = 1$ and $M = 1$ case, we approximate the IM in the domain $\Omega = [-0.6, 0.6]$ tuning the degree of the polynomials to $h = 5$ and the radius to $r = 0.3$ for the PI hybrid scheme. For the $N = 1$ and $M = 2$ case, the domain is $\Omega = [-0.8, 0.8] \times [-0.4, 0.4]$, with $h = 4$, and $\mathbf{r} = [0.2, 0.1]$. For the $N = 2$ and $M = 3$ case, the domain is $\Omega = [-0.7, 0.7] \times [-0.4, 0.4] \times [-0.4, 0.4]$, with $h = 3$ and $\mathbf{r} = [0.2, 0.1, 0.1]$. In all cases, we keep the NNs width to $L = 10$ neurons. To obtain the training data, we collect 20-fold collocation points relative to the number of parameters of the NN counterpart of the hybrid scheme. For the $M = 1$ -dim. case, we uniformly sampled $Q = 620$ points in Ω , while for the other two cases (in which $M > 1$), we generated trajectories randomly initialized for each variable within $[-1, 1]$, as discussed in Section 2.2.1. From the resulting data of \mathbf{y} , we randomly sampled $Q = 820$ and $Q = 2040$ points in Ω to train the hybrid and NN schemes, for the $N = 1$ and $M = 2$, and the $N = 2$ and $M = 3$ cases, respectively. To construct the testing data sets, we followed Section 2.2.2 and generated trajectories by randomly initializing each variable within $[-1, 1]$. After removing the transients, we randomly sampled $S = 10,000$ pairs of data points $(\mathbf{x}^{(s)}, \mathbf{y}^{(s)})$ in the respective Ω for each case.

We hereby highlight the fact that while the degree decreases from $h = 5$ in the $N = 1$ and $M = 1$ case, to $h = 4$ in the $N = 1$ and $M = 2$ case, and then to $h = 3$ in the $N = 2$ and $M = 3$ case, the number of monomials in the PI hybrid scheme is increasing from 6, to 15, and then to 40. This is due to the increase in M and N .

The convergence results of the PI schemes, as evaluated over 100 training realizations with random collocation points and initial parameters, are reported in the Supplement in Table S1.1, S2.1 and S3.1 for the $N = 1$ and $M = 1$, $N = 1$ and $M = 2$, and $N = 2$ and $M = 3$ cases, respectively. Here, we provide a summary over all cases in Table 5, where the mean loss functions values and the mean computational times required for training are reported. As evident by the

PI schemes Case	mean loss $\mathcal{L}(\cdot)$			mean comp. time (in seconds)		
	(1, 1)	(1, 2)	(2, 3)	(1, 1)	(1, 2)	(2, 3)
PI HPS	4.09E-09	2.39E-07	8.59E-04	1.16E+01	5.35E+01	1.47E+02
PI HLS	4.53E-09	2.34E-07	7.07E-04	1.89E+01	9.75E+01	1.60E+02
PI HCS	3.03E-09	3.59E-07	7.03E-04	2.58E+01	1.95E+01	1.43E+02
PI NN	9.83E-09	8.84E-08	8.67E-04	5.69E+00	1.39E+01	1.26E+02

Table 5: Summary of the convergence results of the proposed PI schemes for the three cases $N = 1$ and $M = 1$, $N = 1$ and $M = 2$, and $N = 2$ and $M = 3$ (denoted as (1, 1), (1, 2) and (2, 3)) of the multi-dimensional example in Section 3.3. Mean values of the loss function $\mathcal{L}(\cdot)$ and computational training times (in seconds) are reported for 100 randomly initialized realizations. Schemes include the PI hybrid schemes (HxS: HPS, HLS, HCS), with $x = P, L, C$ denoting power, Legendre, and Chebyshev polynomials and the PI NNs. Detailed results (including CIs) are provided in Table S1.1, S2.1 and S3.1.

low loss function values, all PI schemes converge for all cases considered. Convergence weakens as the dimension of N and M increases. Additionally, the computational time required for training increases with the dimension of the system. As in the previous examples, the training times of the PI hybrid scheme are higher than those required from the PI NN scheme, due to the more parameters included in the PI hybrid scheme. Additionally, the Legendre and Chebyshev polynomials show similar convergence properties to the power series polynomials.

The numerical approximation accuracy of the learned, by the proposed PI schemes, IM approximations was evaluated over data lying on the IM. In particular, we computed the l_1 , l_2 and l_∞ norms of the $\mathbf{x}^{(s)} - \tilde{\pi}(\mathbf{y}^{(s)})$ errors throughout the testing set. We report in the Supplement the means and 5-95% CIs of the above errors, calculated over the 100 parameter sets obtained during training, for all the cases considered; see Table S1.2, S2.2 and S3.2. Here, we present a summary in Table 6, where only the mean values of the l_2 -norm errors are reported for each IM approximation, as derived either with the PSE expansion, or with the trained PI schemes. The PSE approximation provides a fair

Scheme Case	$\ x^{(s)} - \tilde{\pi}(y^{(s)})\ _2$ (1, 1)	$\ x^{(s)} - \tilde{\pi}(\mathbf{y}^{(s)})\ _2$ (1, 2)	$\ x_1^{(s)} - \tilde{\pi}_1(\mathbf{y}^{(s)})\ _2$ (2, 3)	$\ x_2^{(s)} - \tilde{\pi}_2(\mathbf{y}^{(s)})\ _2$ (2, 3)
PSE	1.93E-03	6.17E-02	1.21E-01	7.02E-01
PI HPS	2.00E-04	5.64E-03	9.06E-02	2.70E-01
PI HLS	2.05E-04	5.81E-03	9.01E-02	2.65E-01
PI HCS	1.90E-04	6.88E-03	9.02E-02	2.65E-01
PI NN	2.83E-04	4.11E-03	9.29E-02	2.72E-01

Table 6: Summary of the numerical approximation accuracy results for the IM approximations $\tilde{\pi}(\mathbf{y})$ for the three cases $N = 1$ and $M = 1$, $N = 1$ and $M = 2$, and $N = 2$ and $M = 3$ (denoted as (1, 1), (1, 2) and (2, 3)) of the multi-dimensional example in Section 3.3. l_2 -norm errors are computed for each component ($\pi(y)$, $\pi(\mathbf{y})$ and $[\pi_1(\mathbf{y}), \pi_2(\mathbf{y})]^\top$) of the PSE expansion and the PI schemes (HPS, HLS, HCS, NN). The reported mean values are computed over the 100 parameter sets obtained during training of the PI schemes. Testing data errors are evaluated over $S = 10,000$ points. Detailed results (including l_1 , l_∞ -norm errors and CIs) are provided in Table S1.2, S2.2 and S3.2.

approximation accuracy, which significantly worsens as the dimension M increases. While this trend persists for the PI hybrid and NN schemes, they show a higher global approximation accuracy, which is more pronounced in the $N = 1$ cases. In the $N = 2$ and $M = 3$ case, the IM approximations $\pi(\mathbf{y}) = [\pi_1(\mathbf{y}), \pi_2(\mathbf{y})]^\top$ of the PI hybrid and NN schemes provide slightly higher approximation accuracy than that of the PSE. However, these accuracy results are global, across the testing data set.

To appreciate the accuracy improvement provided by the PI hybrid schemes, we focus on the absolute errors $|\mathbf{x}^{(s)} - \tilde{\pi}(\mathbf{y}^{(s)})|$ for the three cases considered in the physical space $(\hat{\mathbf{x}}, \hat{\mathbf{y}})$ in Figures 4 and 5. Figure 4 displays the absolute errors of the IM approximations for the $N = 1$ and $M = 1$ case, including the PSE scheme. The PSE approximation

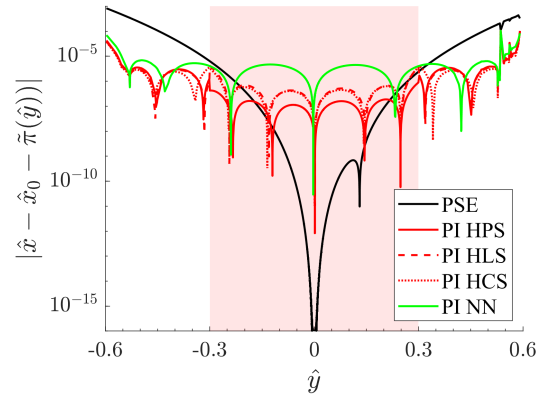


Figure 4: Absolute errors of IM approximations $\tilde{\pi}(y)$ for the case $N = 1$ and $M = 1$ of the multi-dimensional example in Section 3.3.1, compared to data on the IM. Errors are projected in the original state space (\hat{x}, \hat{y}) . The IM approximations include the power series expansion PSE (black), the PI hybrid schemes HxS (red) and the PI NN approximations (green). Power, Legendre, and Chebyshev polynomials ($x = P, L, C$) are distinguished by solid, dashed, and dotted curves, respectively. Red background color indicates the range of the polydisc \mathcal{D} for the PI hybrid schemes. Polynomial degree is $h = 5$ for all cases and $L = 10$ neurons are used in the NNs.

provides very high accuracy near the equilibrium, while deteriorating far from it. On the other hand, the PI NN approximation provides homogeneously distributed high approximation accuracy across the domain. As expected, the PI hybrid schemes improves the accuracy of the PI NN locally, by providing ~ 2 orders higher accuracy within the polydisc \mathcal{D} (denoted by red background), where the polynomial component operates. Additionally, outside \mathcal{D} , the PI hybrid schemes provide slightly better accuracy than the PI NN approximation.

Similar results are derived for the $N = 1$ and $M = 2$, and the $N = 2$ and $M = 3$ cases. The absolute errors $|\mathbf{x}^{(s)} - \tilde{\pi}(\mathbf{y}^{(s)})|$ for all IM approximations are shown in the Supplement in Figures S2.1 and S3.1, while here we focus on the PSE, PI hybrid scheme with power series and the PI NN approximations in Figure 5 (top/bottom row for the $N = 1$ and $M = 2/N = 2$ and $M = 3$ case). Again, the PI hybrid scheme shows very high approximation accuracy within the polydisc \mathcal{D} (denoted by black squares and cubes in Figure 5b,e) where the polynomial counterpart is activated to approximate the IM. Outside \mathcal{D} , the hybrid scheme achieves similarly high approximation accuracy levels to the PI NN approximation. These results demonstrate that the PI hybrid scheme combines the high approximation accuracy provided locally by the polynomial series, while avoiding poor accuracy far from the equilibrium.

5 Conclusions

We present a hybrid physics-informed machine learning scheme for learning (smooth) invariant manifolds (IM) of nonlinear discrete-time dynamical systems. The proposed scheme exploits the interplay and synergistic advantages of polynomial series approximations of solutions to the associated invariance equations representing the IM-map around a fixed point, and those of neural networks. Indeed, polynomial series approximations and neural networks display their own relative pros and cons when used to approximate nonlinear multivariate functions. Polynomials—via Taylor or Chebyshev expansions—offer geometric (exponential) convergence rates around a point, delivering extremely rapid error decay as the degree/truncation order increases; however, they only converge within an (often unknown) radius of convergence, which can be difficult to determine a priori for complex, physics-informed functionals. In contrast, neural networks generally achieve algebraic convergence (approximately proportional to the square root of the number of neurons) but can provide uniform approximations over broader domains, where a polynomial series might diverge. The downside of networks is that their training is an NP-hard problem in general, even for simple problems. Consequently, finding a global minimum of the loss function is not guaranteed, and practical performance depends heavily on initialization, architecture, and training data. Polynomial series approximations also suffer from the curse of dimensionality. While univariate Chebyshev polynomials are well studied, for their multivariate extensions (e.g. tensor-product Chebyshev bases) the number of coefficients explodes combinatorially with the number of variables, while generalizing their alternance and convergence properties for larger numbers of variables and higher polynomial degrees is not an easy task either [99]. In practice, one must truncate the multivariate series expansion by selecting a subset of multi-indices—yet deciding which terms to keep is not trivial, thus neglecting high-order cross terms ad-hoc can significantly degrade accuracy. On the other hand, large multivariate expansions are numerically sensitive:

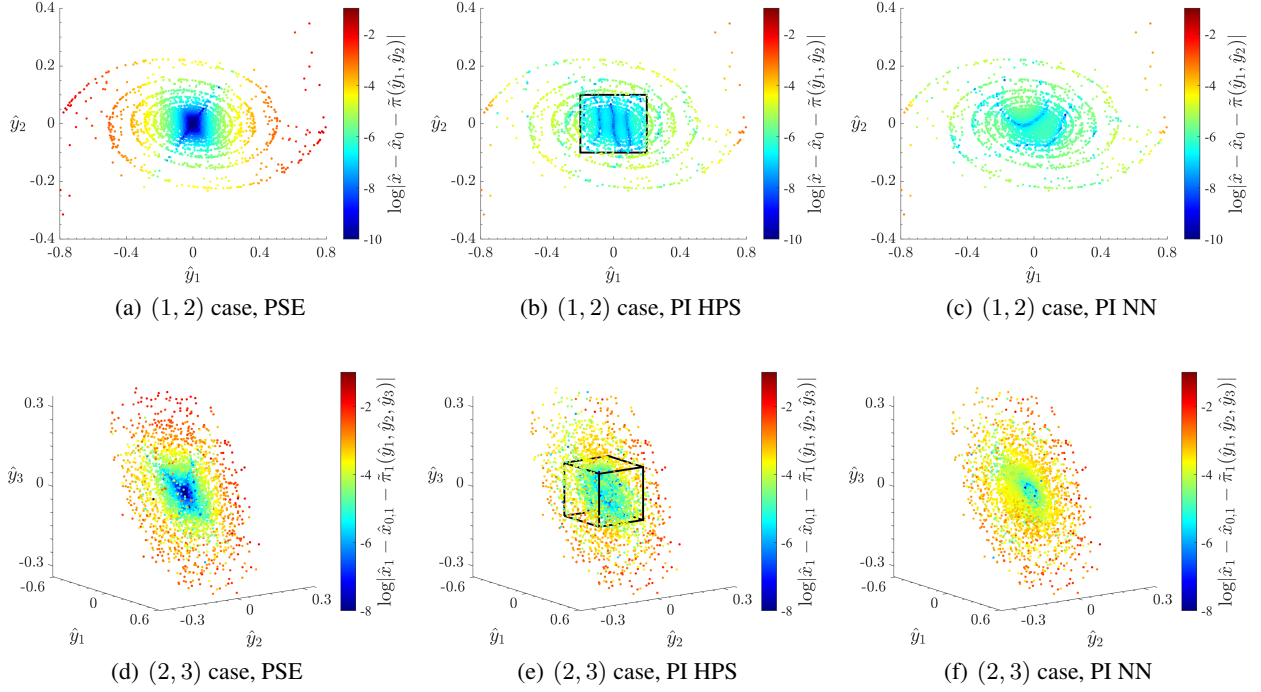


Figure 5: Absolute errors (in logarithmic scale) of IM approximations $\tilde{\pi}(\mathbf{y})$ compared to data on the IM for the $N = 1$ and $M = 2$ case of the multi-dimensional example in Section 3.3.2, denoted as (1, 2) in the top row, and for the $N = 2$ and $M = 3$ case in Section 3.3.3, denoted as (2, 3) in the bottom row. Errors are projected in the original state space $(\hat{\mathbf{x}}, \hat{\mathbf{y}})$ and are shown only for the first component \hat{x}_1 in the (2, 3) case, where $\hat{\mathbf{x}} = [\hat{x}_1, \hat{x}_2]^\top$. Panels show (a,d) the polynomial series expansions, (b,e) the PI hybrid scheme approximations with power polynomials, and (c,f) the PI NN approximations. The black rectangle/cube in panels (b,e) denote the polydiscs \mathcal{D} of the PI hybrid schemes. Polynomial degree is $h = 4$ for the (1, 2) case and $h = 3$ for the (2, 3) case, and $L = 10$ neurons are used in the NNs. Full figures are provided in Figures S2.1 and S3.1.

small errors in the estimation of the coefficients, especially of the higher-degree terms, can lead to large deviations and oscillations in the reconstructed function, especially near the radius of convergence of the domain. As a result, although multivariate Chebyshev constructions exist, their training and evaluation become prohibitively costly as the dimensionality increases. In ongoing and future research work, we plan to rigorously analyze the convergence properties of such a hybrid scheme. Another aspect is that of the incorporation of “parsimonious” tensor-product Chebyshev polynomials for multivariate manifolds, and that of treating the associated radius of convergence as a tunable hyperparameter.

References

- [1] Stephen Wiggins. *Introduction to Applied Nonlinear Dynamical Systems and Chaos*, volume 2 of *Texts in Applied Mathematics*. Springer, 2003.
- [2] John Guckenheimer and Philip Holmes. *Nonlinear oscillations, dynamical systems, and bifurcations of vector fields*, volume 42. Springer Science & Business Media, 2013.
- [3] Vladimir Iгореvich Arnold. *Geometrical methods in the theory of ordinary differential equations*, volume 250. Springer Science & Business Media, 2012.
- [4] Jack Carr. *Applications of centre manifold theory*, volume 35. Springer Science & Business Media, 2012.
- [5] Aleksandr Nikolaevich Gorban and Ilya V Karlin. *Invariant manifolds for physical and chemical kinetics*, volume 660. Springer, 2005.
- [6] Peter Constantin, Ciprian Foias, Basil Nicolaenko, and Roger Témam. Spectral barriers and inertial manifolds for dissipative partial differential equations. *Journal of Dynamics and Differential Equations*, 1:45–73, 1989.

- [7] Antony J Roberts. The utility of an invariant manifold description of the evolution of a dynamical system. *SIAM Journal on Mathematical Analysis*, 20(6):1447–1458, 1989.
- [8] Geoffrey N Mercer and Anthony J Roberts. A centre manifold description of contaminant dispersion in channels with varying flow properties. *SIAM Journal on Applied Mathematics*, 50(6):1547–1565, 1990.
- [9] Peter Constantin, Ciprian Foias, Basil Nicolaenko, and Roger Temam. *Integral manifolds and inertial manifolds for dissipative partial differential equations*, volume 70. Springer Science & Business Media, 2012.
- [10] Xingye Kan, Jinqiao Duan, Ioannis G Kevrekidis, and Anthony J Roberts. Simulating stochastic inertial manifolds by a backward-forward approach. *SIAM Journal on Applied Dynamical Systems*, 12(1):487–514, 2013.
- [11] Panagiotis D Christofides. *Nonlinear and Robust Control of PDE Systems: Methods and Applications to Transport-Reaction Processes*. Systems & Control: Foundations & Applications. Birkhäuser Boston, 2001.
- [12] Roger Temam. *Infinite-dimensional dynamical systems in mechanics and physics*, volume 68. Springer Science & Business Media, 2012.
- [13] Saber N Elaydi. *An Introduction to Difference Equations*, volume 3. Springer, 2010.
- [14] Neil Fenichel. Geometric singular perturbation theory for ordinary differential equations. *Journal of Differential Equations*, 31(1):53–98, 1979.
- [15] Michael S Jolly, Ioannis G Kevrekidis, and Edriss S Titi. Approximate inertial manifolds for the kuramoto-sivashinsky equation: analysis and computations. *Physica D: Nonlinear Phenomena*, 44(1-2):38–60, 1990.
- [16] Fritz Colonius and Wolfgang Kliemann. *The dynamics of control*. Springer Science & Business Media, 2012.
- [17] Boumediene Hamzi, Wei Kang, and Arthur J Krener. The controlled center dynamics. *Multiscale Modeling & Simulation*, 3(4):838–852, 2005.
- [18] Nikolaos Kazantzis. On invariant manifolds of nonlinear discrete-time input-driven dynamical systems. *Physics Letters A*, 292(1-2):107–114, 2001.
- [19] Nikolaos Kazantzis, Nguyen Huynh, and Theresa A Good. A model-based characterization of the long-term asymptotic behavior of nonlinear discrete-time processes using invariance functional equations. *Computers & Chemical Engineering*, 29(11-12):2346–2354, 2005.
- [20] Christopher I Byrnes, Francesco Delli Priscoli, and Alberto Isidori. *Output Regulation of Uncertain Nonlinear Systems*, volume 1. Birkhauser, 1997.
- [21] Alessandro Astolfi and Romeo Ortega. Immersion and invariance: A new tool for stabilization and adaptive control of nonlinear systems. *IEEE Transactions on Automatic Control*, 48(4):590–606, 2003.
- [22] Wei Lin and Christopher I Byrnes. Design of discrete-time nonlinear control systems via smooth feedback. *IEEE Transactions on Automatic Control*, 39(11):2340–2346, 1994.
- [23] B Castillo, Stefano Di Gennaro, Salvatore Monaco, and D Normand-Cyrot. Nonlinear regulation for a class of discrete-time systems. *Systems & Control Letters*, 20(1):57–65, 1993.
- [24] Andrzej Banaszuk and John Hauser. Feedback linearization of transverse dynamics for periodic orbits. *Systems & Control Letters*, 26(2):95–105, 1995.
- [25] Nikolaos Kazantzis. Invariance inducing control of nonlinear discrete-time dynamical systems. *Journal of Nonlinear Science*, 13:579–601, 2003.
- [26] Nikolaos Kazantzis and Michael A Demetriou. Singular control-invariance pdes for nonlinear systems. *Multiscale Modeling & Simulation*, 3(4):731–748, 2005.
- [27] Nikolaos Kazantzis and Costas Kravaris. Discrete-time nonlinear observer design using functional equations. *Systems & Control Letters*, 42(2):81–94, 2001.
- [28] Pauline Bernard. *Observer design for nonlinear systems*, volume 479. Springer, 2019.
- [29] Nikolaos Kazantzis. Map invariance and the state reconstruction problem for nonlinear discrete-time systems. *European Journal of Control*, 15:105–119, 2009.
- [30] Vincent Andrieu and Laurent Praly. On the existence of a kazantzis–kravaris/luenberger observer. *SIAM Journal on Control and Optimization*, 45(2):432–456, 2006.
- [31] Hector Vargas Alvarez, Gianluca Fabiani, Nikolaos Kazantzis, Ioannis G Kevrekidis, and Constantinos Siettos. Nonlinear discrete-time observers with physics-informed neural networks. *Chaos, Solitons & Fractals*, 186:115215, 2024.
- [32] Arjan J van der Schaft. On a state space approach to nonlinear H_∞ control. *Systems & Control Letters*, 16(1):1–8, 1991.

- [33] Cosku Kasnakoglu and Andrea Serrani. Attenuation of oscillations in galerkin systems using center-manifold techniques. *European Journal of Control*, 13(5):529, 2007.
- [34] Christopher KRT Jones. Geometric singular perturbation theory. *Dynamical Systems*, pages 44–118, 1995.
- [35] Morris W Hirsch, Charles Chapman Pugh, and Michael Shub. Invariant manifolds. *Bulletin of the American Mathematical Society*, 76(5):1015–1019, 1970.
- [36] George Haller and Sten Ponsioen. Nonlinear normal modes and spectral submanifolds: existence, uniqueness and use in model reduction. *Nonlinear Dynamics*, 86:1493–1534, 2016.
- [37] Sau-Hai Lam and Dimitris A Goussis. Understanding complex chemical kinetics with computational singular perturbation. In *Symposium (International) on Combustion*, volume 22, pages 931–941. Elsevier, 1989.
- [38] Xavier Cabré, Ernest Fontich, and Rafael De la Llave. The parameterization method for invariant manifolds i: manifolds associated to non-resonant subspaces. *Indiana University mathematics journal*, pages 283–328, 2003.
- [39] Michael Dellnitz and Andreas Hohmann. A subdivision algorithm for the computation of unstable manifolds and global attractors. *Numerische Mathematik*, 75:293–317, 1997.
- [40] Ulrich Maas and Stephen B Pope. Simplifying chemical kinetics: intrinsic low-dimensional manifolds in composition space. *Combustion and Flame*, 88(3-4):239–264, 1992.
- [41] C William Gear, Tasso J Kaper, Ioannis G Kevrekidis, and Antonios Zagaris. Projecting to a slow manifold: Singularly perturbed systems and legacy codes. *SIAM Journal on Applied Dynamical Systems*, 4(3):711–732, 2005.
- [42] Dimitris A Goussis and Ulrich Maas. Model reduction for combustion chemistry. In *Turbulent Combustion Modeling*, pages 193–220. Springer, 2011.
- [43] Efstathios-Al Tingas, Zhandong Wang, S Mani Sarathy, Hong G Im, and Dimitris A Goussis. Chemical kinetic insights into the ignition dynamics of n-hexane. *Combustion and Flame*, 188:28–40, 2018.
- [44] Dimitris M Manias, Efstathios Al Tingas, Christos E Frouzakis, Konstantinos Boulouchos, and Dimitris A Goussis. The mechanism by which ch₂o and h₂o₂ additives affect the autoignition of ch₄/air mixtures. *Combustion and Flame*, 164:111–125, 2016.
- [45] Antonios Zagaris, C William Gear, Tasso J Kaper, and Yannis G Kevrekidis. Analysis of the accuracy and convergence of equation-free projection to a slow manifold. *ESAIM: Mathematical Modelling and Numerical Analysis*, 43(4):757–784, 2009.
- [46] Dimitris G Patsatzis, Dimitris T Maris, and Dimitris A Goussis. Asymptotic analysis of a target-mediated drug disposition model: algorithmic and traditional approaches. *Bulletin of Mathematical Biology*, 78:1121–1161, 2016.
- [47] Alex Haro, Marta Canadell, Jordi-Lluís Figueras, Alejandro Luque, and Josep-Maria Mondelo. The parameterization method for invariant manifolds. *Applied Mathematical Sciences*, 195, 2016.
- [48] Erik Bollt. Attractor modeling and empirical nonlinear model reduction of dissipative dynamical systems. *International Journal of Bifurcation and Chaos*, 17(04):1199–1219, 2007.
- [49] Ronald R Coifman, Stephane Lafon, Ann B Lee, Mauro Maggioni, Boaz Nadler, Frederick Warner, and Steven W Zucker. Geometric diffusions as a tool for harmonic analysis and structure definition of data: diffusion maps. *Proceedings of the National Academy of Sciences*, 102(21):7426–7431, 2005.
- [50] Carmeline J Dsilva, Ronen Talmon, C William Gear, Ronald R Coifman, and Ioannis G Kevrekidis. Data-driven reduction for a class of multiscale fast-slow stochastic dynamical systems. *SIAM Journal on Applied Dynamical Systems*, 15(3):1327–1351, 2016.
- [51] Eleni D Koronaki, Nikolaos Evangelou, Cristina P Martin-Linares, Edriss S Titi, and Ioannis G Kevrekidis. Non-linear dimensionality reduction then and now: Aims for dissipative pdes in the ml era. *Journal of Computational Physics*, 506:112910, 2024.
- [52] Wenqian Chen, Qian Wang, Jan S Hesthaven, and Chuhua Zhang. Physics-informed machine learning for reduced-order modeling of nonlinear problems. *Journal of Computational Physics*, 446:110666, 2021.
- [53] Sirod Sirisup, George Em Karniadakis, Dongbin Xiu, and Ioannis G Kevrekidis. Equation-free/galerkin-free pod-assisted computation of incompressible flows. *Journal of Computational Physics*, 207(2):568–587, 2005.
- [54] Alessandro Della Pia, Dimitrios G Patsatzis, Lucia Russo, and Constantinos Siettos. Learning the latent dynamics of fluid flows from high-fidelity numerical simulations using parsimonious diffusion maps. *Physics of Fluids*, 36(10), 2024.

- [55] Erik M Bollt, Qianxiao Li, Felix Dietrich, and Ioannis Kevrekidis. On matching, and even rectifying, dynamical systems through koopman operator eigenfunctions. *SIAM Journal on Applied Dynamical Systems*, 17(2):1925–1960, 2018.
- [56] Bethany Lusch, J Nathan Kutz, and Steven L Brunton. Deep learning for universal linear embeddings of nonlinear dynamics. *Nature Communications*, 9(1):4950, 2018.
- [57] Alexandre Mauroy, Y Susuki, and I Mezić. *Koopman operator in systems and control*. Springer, 2020.
- [58] Gianluca Fabiani, Nikolaos Evangelou, Tianqi Cui, Juan M Bello-Rivas, Cristina P Martin-Linares, Constantinos Siettos, and Ioannis G Kevrekidis. Task-oriented machine learning surrogates for tipping points of agent-based models. *Nature Communications*, 15(1):4117, 2024.
- [59] Evangelos Galaris, Gianluca Fabiani, Ioannis Gallos, Ioannis Kevrekidis, and Constantinos Siettos. Numerical bifurcation analysis of pdes from lattice boltzmann model simulations: a parsimonious machine learning approach. *Journal of Scientific Computing*, 92(2):1–30, 2022.
- [60] Seungjoon Lee, Mahdi Kooshkbaghi, Konstantinos Spiliotis, Constantinos I Siettos, and Ioannis G. Kevrekidis. Coarse-scale pdes from fine-scale observations via machine learning. *Chaos: An Interdisciplinary Journal of Nonlinear Science*, 30(1):013141, 2020.
- [61] Themistoklis P Sapsis and Antoine Blanchard. Optimal criteria and their asymptotic form for data selection in data-driven reduced-order modelling with gaussian process regression. *Philosophical Transactions of the Royal Society A*, 380(2229):20210197, 2022.
- [62] Zhong Yi Wan, Pantelis Vlachas, Petros Koumoutsakos, and Themistoklis Sapsis. Data-assisted reduced-order modeling of extreme events in complex dynamical systems. *PloS One*, 13(5):e0197704, 2018.
- [63] Wei Chen and Andrew L Ferguson. Molecular enhanced sampling with autoencoders: On-the-fly collective variable discovery and accelerated free energy landscape exploration. *Journal of Computational Chemistry*, 39(25):2079–2102, 2018.
- [64] Alberto Solera-Rico, Carlos Sanmiguel Vila, Miguel Gómez-López, Yuning Wang, Abdulrahman Almashjary, Scott TM Dawson, and Ricardo Vinuesa. β -variational autoencoders and transformers for reduced-order modelling of fluid flows. *Nature Communications*, 15(1):1361, 2024.
- [65] Pantelis R Vlachas, Georgios Arampatzis, Caroline Uhler, and Petros Koumoutsakos. Multiscale simulations of complex systems by learning their effective dynamics. *Nature Machine Intelligence*, 4(4):359–366, 2022.
- [66] Ioannis G. Kevrekidis, C. William Gear, James M. Hyman, Panagiotis G. Kevrekidis, Olof Runborg, and Constantinos Theodoropoulos. Equation-free, coarse-grained multiscale computation: Enabling microscopic simulators to perform system-level analysis. *Communications in Mathematical Sciences*, 1(4):715–762, 2003.
- [67] Antonios Zagaris, Hans G Kaper, and Tasso J Kaper. Fast and slow dynamics for the computational singular perturbation method. *Multiscale Modeling & Simulation*, 2(4):613–638, 2004.
- [68] Constantinos Siettos. Equation-free computation of coarse-grained center manifolds of microscopic simulators. *Journal of Computational Dynamics*, 1(2):377–389, 2014.
- [69] Constantinos Siettos and Lucia Russo. A numerical method for the approximation of stable and unstable manifolds of microscopic simulators. *Numerical Algorithms*, 89(3):1335–1368, 2022.
- [70] Tracy Chin, Jacob Ruth, Clayton Sanford, Rebecca Santorella, Paul Carter, and Björn Sandstede. Enabling equation-free modeling via diffusion maps. *Journal of Dynamics and Differential Equations*, pages 1–20, 2022.
- [71] Nikolaos Evangelou, Felix Dietrich, Eliodoro Chiavazzo, Daniel Lehmborg, Marina Meila, and Ioannis G Kevrekidis. Double diffusion maps and their latent harmonics for scientific computations in latent space. *Journal of Computational Physics*, 485:112072, 2023.
- [72] Dimitrios G Patsatzis, Lucia Russo, Ioannis G Kevrekidis, and Constantinos Siettos. Data-driven control of agent-based models: An equation/variable-free machine learning approach. *Journal of Computational Physics*, 478:111953, 2023.
- [73] Isaac E Lagaris, Aristidis Likas, and Dimitrios I Fotiadis. Artificial neural networks for solving ordinary and partial differential equations. *IEEE Transactions on Neural Networks*, 9(5):987–1000, 1998.
- [74] George Em Karniadakis, Ioannis G Kevrekidis, Lu Lu, Paris Perdikaris, Sifan Wang, and Liu Yang. Physics-informed machine learning. *Nature Reviews Physics*, 3(6):422–440, 2021.
- [75] Maziar Raissi, Paris Perdikaris, and George E Karniadakis. Physics-informed neural networks: A deep learning framework for solving forward and inverse problems involving nonlinear partial differential equations. *Journal of Computational Physics*, 378:686–707, 2019.

- [76] Kathleen Champion, Bethany Lusch, J Nathan Kutz, and Steven L Brunton. Data-driven discovery of coordinates and governing equations. *Proceedings of the National Academy of Sciences*, 116(45):22445–22451, 2019.
- [77] Dimitrios Patsatzis, Gianluca Fabiani, Lucia Russo, and Constantinos Siettos. Slow invariant manifolds of singularly perturbed systems via physics-informed machine learning. *SIAM Journal on Scientific Computing*, 46(4):C297–C322, 2024.
- [78] Dimitrios G Patsatzis, Lucia Russo, and Constantinos Siettos. Slow invariant manifolds of fast-slow systems of odes with physics-informed neural networks. *SIAM Journal on Applied Dynamical Systems*, 23(4):3077–3122, 2024.
- [79] Siping Tang, Xinlong Feng, Wei Wu, and Hui Xu. Physics-informed neural networks combined with polynomial interpolation to solve nonlinear partial differential equations. *Computers & Mathematics with Applications*, 132:48–62, 2023.
- [80] Igor Mezić. Spectral properties of dynamical systems, model reduction and decompositions. *Nonlinear Dynamics*, 41:309–325, 2005.
- [81] Christian Kuehn. *Multiple time scale dynamics*, volume 191. Springer, 2015.
- [82] Alexander N Gorban and Iliya V Karlin. Method of invariant manifold for chemical kinetics. *Chemical Engineering Science*, 58(21):4751–4768, 2003.
- [83] Marc R Roussel and Simon J Fraser. On the geometry of transient relaxation. *The Journal of Chemical Physics*, 94(11):7106–7113, 1991.
- [84] Dimitris A Goussis and Mauro Valorani. An efficient iterative algorithm for the approximation of the fast and slow dynamics of stiff systems. *Journal of Computational Physics*, 214(1):316–346, 2006.
- [85] Dimitris A Goussis and Sau-Hai Lam. A study of homogeneous methanol oxidation kinetics using csp. In *Symposium (International) on Combustion*, volume 24, pages 113–120. Elsevier, 1992.
- [86] Karl Weierstrass. Über die analytische darstellbarkeit sogenannter willkürlicher functionen einer reellen veränderlichen. *Sitzungsberichte der Königlich Preußischen Akademie der Wissenschaften zu Berlin*, 2(633-639):364, 1885.
- [87] Walter Rudin et al. *Principles of mathematical analysis*, volume 3. McGraw-hill New York, 1964.
- [88] George Cybenko. Approximation by superpositions of a sigmoidal function. *Mathematics of Control, Signals and Systems*, 2(4):303–314, 1989.
- [89] Kurt Hornik, Maxwell Stinchcombe, and Halbert White. Multilayer feedforward networks are universal approximators. *Neural Networks*, 2(5):359–366, 1989.
- [90] Theodore J Rivlin. *An introduction to the approximation of functions*. Courier Corporation, 1981.
- [91] Andrew R Barron. Universal approximation bounds for superpositions of a sigmoidal function. *IEEE Transactions on Information Theory*, 39(3):930–945, 1993.
- [92] Avrim Blum and Ronald Rivest. Training a 3-node neural network is np-complete. *Advances in Neural Information Processing Systems*, 1, 1988.
- [93] Vincent Froese and Christoph Hertrich. Training neural networks is np-hard in fixed dimension. *Advances in Neural Information Processing Systems*, 36:44039–44049, 2023.
- [94] Yunlei Yang, Muzhou Hou, Hongli Sun, Tianle Zhang, Futian Weng, and Jianshu Luo. Neural network algorithm based on legendre improved extreme learning machine for solving elliptic partial differential equations. *Soft Computing*, 24:1083–1096, 2020.
- [95] Susmita Mall and Snehashish Chakraverty. Single layer chebyshev neural network model for solving elliptic partial differential equations. *Neural Processing Letters*, 45:825–840, 2017.
- [96] Martin T Hagan and Mohammad B Menhaj. Training feedforward networks with the marquardt algorithm. *IEEE Transactions on Neural Networks*, 5(6):989–993, 1994.
- [97] Sifan Wang, Yujun Teng, and Paris Perdikaris. Understanding and mitigating gradient flow pathologies in physics-informed neural networks. *SIAM Journal on Scientific Computing*, 43(5):A3055–A3081, 2021.
- [98] Xavier Glorot and Yoshua Bengio. Understanding the difficulty of training deep feedforward neural networks. In *Proceedings of the thirteenth international conference on artificial intelligence and statistics*, pages 249–256. JMLR Workshop and Conference Proceedings, 2010.
- [99] John C Mason. Near-best multivariate approximation by fourier series, chebyshev series and chebyshev interpolation. *Journal of Approximation Theory*, 28(4):349–358, 1980.

APPENDIX

A Invariant Manifold approximations via Power Series Expansions

We hereby describe the approach proposed by [18, 19] for deriving approximations of the IM mapping in Eq. (4) by approximating the solution of the system of NFEs in Eq. (5) via power series expansions (PSE). We assume that the IM functional $\mathbf{x} = \boldsymbol{\pi}(\mathbf{y}) \in \mathbb{R}^N$ can be locally approximated by a multivariate Taylor series expansion around the equilibrium $(\mathbf{x}_0, \mathbf{y}_0) = (\mathbf{0}^N, \mathbf{0}^M)$ of degree h . The PSE can be compactly written in the form:

$$\tilde{\boldsymbol{\pi}}^{PSE}(\mathbf{y}) = [\tilde{\pi}_1^{PSE}(\mathbf{y}), \dots, \tilde{\pi}_n^{PSE}(\mathbf{y}), \dots, \tilde{\pi}_N^{PSE}(\mathbf{y})]^\top \quad (\text{A.1})$$

where each element for $n = 1, \dots, N$ can be expressed as:

$$\tilde{\pi}_n^{PSE}(\mathbf{y}) = \pi_n^0 + \sum_{i_1=1}^M \pi_n^{i_1} y_{i_1} + \frac{1}{2!} \sum_{i_1, i_2=1}^M \pi_n^{i_1, i_2} y_{i_1} y_{i_2} + \dots + \frac{1}{h!} \sum_{i_1, \dots, i_h=1}^M \pi_n^{i_1, \dots, i_h} y_{i_1} \dots y_{i_h} + \mathcal{O}(\mathbf{y}^{h+1}). \quad (\text{A.2})$$

Each term in the expansion corresponds to the zeroth, first, second, \dots and h -th order approximations with respect to the components of $\mathbf{y} \in \mathbb{R}^M$, while the reminder term $\mathcal{O}(\mathbf{y}^{h+1})$ captures the higher order contributions, including products of the form $y_{i_1} \dots y_{i_h} y_{i_{h+1}}$.

The coefficients $\pi_n^{i_1, \dots, i_h}$ of the PSE in Eq. (A.2) represent the h -th derivatives of the unknown IM functional at $(\mathbf{x}_0, \mathbf{y}_0)$. The zeroth order coefficient is set to $\pi_n^0 = 0$, since the IM approximation passes from the equilibrium; i.e., $\tilde{\boldsymbol{\pi}}^{PSE}(\mathbf{0}^M) = \mathbf{0}^N$. To determine the remaining coefficients $\pi_n^{i_1, \dots, i_h}$, the power series expansion in Eq. (A.2) is substituted into the NFEs in Eq. (5), and the nonlinear functions \mathbf{f} and \mathbf{g} are expanded around the equilibrium. By equating coefficients of the same order on both sides of Eq. (5), the coefficients $\pi_n^{i_1, \dots, i_h}$ can be computed recursively (i.e., the computation of the h -th order coefficients requires knowledge about the $(h-1)$ -th order ones) through a system of linear algebraic equations [18, 19].

This approach bears similarities to the derivation of center and slow invariant manifold approximations for continuous-time dynamical systems [41, 81–83], which also employ (asymptotic) series expansions. Similarly to the continuous case, this approach relies on the availability of the analytical expressions of \mathbf{f} and \mathbf{g} . By leveraging their Taylor expansions (which are accurate sufficiently far from singularities), the coefficients of the PSE in Eq. (A.2) can be determined through the solution of a linear system of algebraic equations [18, 19]. For a tensorial notation of the above approach, see [19]. We hereby note that as the dimension of the system $N + M$, and/or the desired order h of the PSE increases, this approach becomes increasingly challenging to implement, even with the aid of symbolic computation software, due to its combinatorially increasing number of coefficients to determine.

B Residual minimization of the Physics-Informed Hybrid Scheme

Here, we present the formulation of the PI hybrid scheme optimization problem in Eq. (13) as a non-linear residual minimization problem. First, we collect all the components of the hybrid approximation into the N -dim. column vector:

$$\tilde{\boldsymbol{\pi}}^{HxS}(\mathbf{y}, \mathbf{a}, \mathbf{p}) = [\tilde{\pi}_1^{HxS}(\mathbf{y}, \boldsymbol{\alpha}_1, \mathbf{p}_1), \dots, \tilde{\pi}_N^{HxS}(\mathbf{y}, \boldsymbol{\alpha}_N, \mathbf{p}_N)]^\top, \quad (\text{B.1})$$

where each element $\tilde{\pi}_n^{HxS}(\mathbf{y}, \mathbf{a}_n, \mathbf{p}_n)$ is given by Eq. (6) for $n = 1, \dots, N$. In the ensuing text, we drop the dependence on the hyperparameters $\mathcal{H}_1, \mathcal{H}_2$ and the radius of the polydisc \mathbf{r} for conciseness of the presentation. In addition, let us collect all the tunable parameters into the column vector of $N \left(L(M+2) + \left(\prod_{i=1}^M (h+i) \right) / i! + 1 \right)$ dimensions, as:

$$\boldsymbol{\nu} = [\boldsymbol{\nu}_1, \dots, \boldsymbol{\nu}_n, \dots, \boldsymbol{\nu}_N]^\top = [\boldsymbol{\alpha}_1, \mathbf{p}_1, \dots, \boldsymbol{\alpha}_n, \mathbf{p}_n, \dots, \boldsymbol{\alpha}_N, \mathbf{p}_N]^\top, \quad (\text{B.2})$$

where each pair $\boldsymbol{\nu}_n = [\boldsymbol{\alpha}_n, \mathbf{p}_n]$ for $n = 1, \dots, N$ includes the coefficients of the n -th element of the polynomial series in Eq. (8) and the parameters of the n -th output of the NN in Eq. (12), respectively; i.e., all the parameters of the n -th output of the hybrid scheme in Eq. (6).

Next, consider the set of collocation points $\mathbf{y}^{(q)} \in \Omega$ with $q = 1, \dots, Q$ and the ones on the boundary, $\mathbf{y}^{(r)} \in \partial\mathcal{D}$ with $r = 1, \dots, R$. The optimization problem of the loss function in Eq. (13) over the parameters included in the column vector in Eq. (B.2) is achieved by the minimization of the following non-linear residuals; (i) the residuals corresponding to the first term of the loss function in Eq. (13):

$$\mathcal{F}_{q,n}^{HxS} = \omega_q \left(\tilde{\pi}_n^{HxS}(\mathbf{A}\mathbf{y}^{(q)} + \mathbf{g}(\mathbf{y}^{(q)}), \boldsymbol{\nu}_n) - \sum_{i=1}^N B_{n,i} \tilde{\pi}_i^{HxS}(\mathbf{y}^{(q)}, \boldsymbol{\nu}_i) - \sum_{j=1}^M C_{n,j} y_j^{(q)} - f_n(\tilde{\boldsymbol{\pi}}^{HxS}(\mathbf{y}^{(q)}, \boldsymbol{\nu}), \mathbf{y}^{(q)}) \right), \quad (\text{B.3})$$

where $B_{n,i}$ and $C_{n,j}$ are the (n,i) and (n,j) elements of $\mathbf{B} \in \mathbb{R}^{N \times N}$ and $\mathbf{C} \in \mathbb{R}^{N \times M}$, respectively, $y_j^{(q)}$ is the j -th element of $\mathbf{y}^{(q)} = [y_1^{(q)}, \dots, y_M^{(q)}]^\top \in \mathbb{R}^M$, and f_n is the n -th element of $\mathbf{f} = [f_1, \dots, f_N]^\top$; (ii) the residuals corresponding to the second term of the loss function in Eq. (13):

$$\mathcal{F}_{0,n}^{HxS} = \omega_1 \tilde{\pi}_n^{HxS}(\mathbf{0}^M, \boldsymbol{\nu}_n) = \omega_1 \tilde{\pi}_n^{xS}(\mathbf{0}^M, \boldsymbol{\alpha}_n), \quad (\text{B.4})$$

where the latter equality follows from Eq. (6), since at the equilibrium point only the polynomial series is active; and (iii) the residuals corresponding to the third term of the loss function in Eq. (13):

$$\mathcal{F}_{r,n}^{HxS} = \omega_2 \left(\tilde{\pi}_n^{xS}(\mathbf{y}^{(r)}, \boldsymbol{\alpha}_n) - \tilde{\pi}_n^{NN}(\mathbf{y}^{(r)}, \mathbf{p}_n) \right). \quad (\text{B.5})$$

Note that the residuals in Eq. (B.3) are computed on the basis of all, in general, the coefficients in $\boldsymbol{\nu}$, since all components of \mathbf{y} are contributing to the linear and non-linear terms, $B_{n,i} \cdot \tilde{\pi}_i^{xS}(\mathbf{y}^{(q)}, \boldsymbol{\nu}_i)$ and $f_n(\tilde{\pi}^{xS}(\mathbf{y}^{(q)}, \boldsymbol{\nu}), \mathbf{y}^{(q)})$, respectively. Using the expressions of the residuals in Eqs. (B.3) to (B.5), we then collect all the residuals into the $N(Q + R + 1)$ -dim. column vector:

$$\mathcal{F}^{HxS} = [\mathcal{F}_{1,1}^{HxS}, \dots, \mathcal{F}_{Q,1}^{HxS}, \dots, \mathcal{F}_{q,n}^{HxS}, \dots, \mathcal{F}_{1,N}^{HxS}, \dots, \mathcal{F}_{Q,N}^{HxS}, \mathcal{F}_{0,1}^{HxS}, \dots, \mathcal{F}_{0,n}^{HxS}, \dots, \mathcal{F}_{0,N}^{HxS}, \mathcal{F}_{1,1}^{HxS}, \dots, \mathcal{F}_{R,1}^{HxS}, \dots, \mathcal{F}_{r,n}^{HxS}, \dots, \mathcal{F}_{1,N}^{HxS}, \dots, \mathcal{F}_{R,N}^{HxS}]^\top. \quad (\text{B.6})$$

For the minimization of the above residuals, we employ gradient-based optimization via the LM algorithm, for the implementation of which, the Jacobian matrix $\mathbf{J} = \nabla_{\boldsymbol{\nu}} \mathcal{F}^{HxS}$ is computed via symbolic differentiation. To compute the Jacobian, let ν_k denote any coefficient belonging to the vector of coefficients $\boldsymbol{\nu}_k = [\boldsymbol{\alpha}_k, \mathbf{p}_k]$ of the k -th element of $\boldsymbol{\nu}$ in Eq. (B.2) for $k = 1, \dots, N$. Then, the derivatives of the residuals in Eqs. (B.3) to (B.5) w.r.t. ν_k can be computed by:

$$\frac{\partial \mathcal{F}_{q,n}^{HxS}}{\partial \nu_k} = \omega_q \left(\frac{\partial \tilde{\pi}_n^{HxS}(\mathbf{A}\mathbf{y}^{(q)} + \mathbf{g}(\mathbf{y}^{(q)}), \mathbf{a}_n, \mathbf{p}_n)}{\partial \nu_k} \delta_{nk} - \sum_{i=1}^N \left(B_{n,i} + \frac{\partial f_n}{\partial x_i} \right) \frac{\partial \tilde{\pi}_i^{HxS}(\mathbf{y}^{(q)}, \mathbf{a}_i, \mathbf{p}_i)}{\partial \nu_k} \delta_{ik} \right), \quad (\text{B.7})$$

$$\frac{\partial \mathcal{F}_{0,n}^{HxS}}{\partial \nu_k} = \omega_1 \frac{\partial \tilde{\pi}_n^{xS}(\mathbf{0}^M, \boldsymbol{\alpha}_n)}{\partial \nu_k} \delta_{nk}, \quad (\text{B.8})$$

$$\frac{\partial \mathcal{F}_{r,n}^{HxS}}{\partial \nu_k} = \omega_2 \left(\frac{\partial \tilde{\pi}_n^{xS}(\mathbf{y}^{(r)}, \boldsymbol{\alpha}_n)}{\partial \nu_k} - \frac{\partial \tilde{\pi}_n^{NN}(\mathbf{y}^{(r)}, \mathbf{p}_n)}{\partial \nu_k} \right) \delta_{nk}, \quad (\text{B.9})$$

where the last term in Eq. (B.7) includes contributions from all $\tilde{\pi}_i^{HxS}(\cdot)$ outputs for $i = 1, \dots, N$, since, in general, the gradient $\partial f_n / \partial x_i$ of the vector field is considered full.

We highlight here that the derivatives in Eq. (B.7) are computed on the basis of the hybrid scheme $\tilde{\pi}_n^{HxS}(\cdot)$, while the ones in Eqs. (B.8) and (B.9) are computed on the basis of the hybrid scheme's counterparts; i.e., the polynomial series $\tilde{\pi}_n^{xS}(\cdot)$ and the NN $\tilde{\pi}_n^{NN}(\cdot)$, respectively. For computing the derivatives of the hybrid scheme in Eq. (B.7), we exploit the structure of the hybrid scheme in Eq. (6) and decompose the related derivatives as:

$$\frac{\partial \tilde{\pi}_n^{HxS}(\mathbf{A}\mathbf{y}^{(q)} + \mathbf{g}(\mathbf{y}^{(q)}), \mathbf{a}_n, \mathbf{p}_n)}{\partial \nu_k} = \begin{cases} \frac{\partial \tilde{\pi}_n^{xS}(\mathbf{A}\mathbf{y}^{(q)} + \mathbf{g}(\mathbf{y}^{(q)}), \mathbf{a}_n)}{\partial \nu_k}, & \text{when } \mathbf{A}\mathbf{y}^{(q)} + \mathbf{g}(\mathbf{y}^{(q)}) \in \mathcal{D} \\ \frac{\partial \tilde{\pi}_n^{NN}(\mathbf{A}\mathbf{y}^{(q)} + \mathbf{g}(\mathbf{y}^{(q)}), \mathbf{p}_n)}{\partial \nu_k}, & \text{when } \mathbf{A}\mathbf{y}^{(q)} + \mathbf{g}(\mathbf{y}^{(q)}) \notin \mathcal{D} \end{cases} \quad (\text{B.10a})$$

$$\frac{\partial \tilde{\pi}_n^{HxS}(\mathbf{y}^{(q)}, \mathbf{a}_i, \mathbf{p}_i)}{\partial \nu_k} = \begin{cases} \frac{\partial \tilde{\pi}_i^{xS}(\mathbf{y}^{(q)}, \mathbf{a}_i)}{\partial \nu_k}, & \text{when } \mathbf{y}^{(q)} \in \mathcal{D} \\ \frac{\partial \tilde{\pi}_i^{NN}(\mathbf{y}^{(q)}, \mathbf{p}_i)}{\partial \nu_k}, & \text{when } \mathbf{y}^{(q)} \notin \mathcal{D} \end{cases} \quad (\text{B.11a})$$

$$\frac{\partial \tilde{\pi}_i^{HxS}(\mathbf{y}^{(q)}, \mathbf{a}_i, \mathbf{p}_i)}{\partial \nu_k} = \begin{cases} \frac{\partial \tilde{\pi}_i^{xS}(\mathbf{y}^{(q)}, \mathbf{a}_i)}{\partial \nu_k}, & \text{when } \mathbf{y}^{(q)} \in \mathcal{D} \\ \frac{\partial \tilde{\pi}_i^{NN}(\mathbf{y}^{(q)}, \mathbf{p}_i)}{\partial \nu_k}, & \text{when } \mathbf{y}^{(q)} \notin \mathcal{D} \end{cases} \quad (\text{B.11b})$$

where \mathcal{D} is the polydisc of radius \mathbf{r} within which the polynomial series are active and outside of which the NN acts. A detailed derivation of the piecewise expressions in Eqs. (B.10a, B.10b, B.11a, B.11b) is provided at the end of this section.

Given the expressions in Eqs. (B.10a, B.10b, B.11a, B.11b), the computation of the derivatives of the hybrid scheme's residuals in Eqs. (B.7) to (B.9) is simplified by the computation of the derivatives of the polynomial series and the NN w.r.t. any parameter ν_k belonging in $\boldsymbol{\nu}$ of Eq. (B.2). However, $\boldsymbol{\nu}$ includes both the polynomial series coefficients $\boldsymbol{\alpha}_k$ and the NN parameters \mathbf{p}_k . Hence, in the case where:

1. $\nu_k \equiv \alpha_k^{i_1, \dots, i_M} \in \alpha_k$, the derivatives in Eqs. (B.10a, B.11a) for the coefficient $\alpha_k^{i_1, \dots, i_M}$ corresponding to the i_1 -th, \dots , i_M -th multivariate monomial of Eq. (8), are computed as:

$$\frac{\partial \tilde{\pi}_n^{xS}(\mathbf{y}^{(q)}, \mathbf{a}_n)}{\partial \alpha_k^{i_1, \dots, i_M}} = P_{i_1}^x(y_1^{(q)}) \cdots P_{i_M}^x(y_M^{(q)}), \quad (\text{B.12})$$

for $k = n$ and zero otherwise. Since $\nu_k \equiv \alpha_k^{i_1, \dots, i_M} \notin \mathbf{p}_n$, the derivatives in Eqs. (B.10b, B.11b) are also zero. Similarly, the derivatives in Eq. (B.8) are computed by Eq. (B.12), while the ones in Eq. (B.9) are zero.

2. $\nu_k \in \mathbf{p}_k$, the related derivatives are computed via the symbolic differentiation of the NN output, which is detailed in Appendix C.1. In particular, the derivatives in Eqs. (B.10b, B.11b) are computed by Eq. (C.9), while the ones in Eqs. (B.10a, B.11a) are zero, since now $\nu_k \notin \alpha_k$. Similarly, the derivatives in Eq. (B.9) are computed by Eq. (C.9), while the ones in Eq. (B.8) are zero.

In summary, substitution of Eq. (B.12) and Eq. (C.9) into Eqs. (B.10a, B.10b, B.11a, B.11b), and then to Eqs. (B.7) to (B.9) provides all the related derivatives for the formation of the $N(Q + R + 1) \times N \left(L(M + 2) + \left(\prod_{i=1}^M (h + i) \right) / i! + 1 \right)$ Jacobian matrix $\mathbf{J} = \nabla_{\nu} \mathcal{F}^{HxS}$. A detailed presentation of the iterative procedure of the LM algorithm for the minimization of the residuals is provided in Appendix D, along with a detailed pseudocode.

B.1 Derivation of the hybrid scheme's piecewise derivatives in eqs. (B.10a, B.10b, B.11a, B.11b)

For the computation of the derivatives in eqs. (B.10a, B.10b, B.11a, B.11b), we begin with the definition of the hybrid scheme in Eq. (6), in which the hyperparameters \mathcal{H}_1 and \mathcal{H}_2 are omitted for simplicity:

$$\tilde{\pi}_n^{HxS}(\mathbf{y}, \mathbf{a}_n, \mathbf{p}_n; \mathbf{r}) = \tilde{\pi}_n^{xS}(\mathbf{y}, \alpha_n)^{H(\mathbf{y}, \mathbf{r})} \cdot \tilde{\pi}_n^{NN}(\mathbf{y}, \mathbf{p}_n)^{1-H(\mathbf{y}, \mathbf{r})}. \quad (\text{B.13})$$

Next, we consider the absolute values of the above equality, which enables us to consider the natural logarithm, implying:

$$\begin{aligned} |\tilde{\pi}_n^{HxS}(\mathbf{y}, \mathbf{a}_n, \mathbf{p}_n; \mathbf{r})| &= |\tilde{\pi}_n^{xS}(\mathbf{y}, \alpha_n)^{H(\mathbf{y}, \mathbf{r})} \cdot \tilde{\pi}_n^{NN}(\mathbf{y}, \mathbf{p}_n)^{1-H(\mathbf{y}, \mathbf{r})}| \Rightarrow \\ \ln |\tilde{\pi}_n^{HxS}(\mathbf{y}, \mathbf{a}_n, \mathbf{p}_n; \mathbf{r})| &= H(\mathbf{y}, \mathbf{r}) \ln |\tilde{\pi}_n^{xS}(\mathbf{y}, \alpha_n)| + (1 - H(\mathbf{y}, \mathbf{r})) \ln |\tilde{\pi}_n^{NN}(\mathbf{y}, \mathbf{p}_n)^{1-H(\mathbf{y}, \mathbf{r})}|. \end{aligned} \quad (\text{B.14})$$

Differentiation of the expression in Eq. (B.14) w.r.t. a parameter ν_k that belongs in $\nu_k = [\alpha_k, \mathbf{p}_k]$, after some algebraic manipulations, implies:

$$\begin{aligned} \frac{\partial \tilde{\pi}_n^{HxS}(\mathbf{y}, \mathbf{a}_n, \mathbf{p}_n; \mathbf{r})}{\partial \nu_k} &= H(\mathbf{y}, \mathbf{r}) \frac{\tilde{\pi}_n^{HxS}(\mathbf{y}, \mathbf{a}_n, \mathbf{p}_n; \mathbf{r})}{\tilde{\pi}_n^{xS}(\mathbf{y}, \alpha_n)} \frac{\partial \tilde{\pi}_n^{xS}(\mathbf{y}, \alpha_n)}{\partial \nu_k} + \\ &\quad (1 - H(\mathbf{y}, \mathbf{r})) \frac{\tilde{\pi}_n^{HxS}(\mathbf{y}, \mathbf{a}_n, \mathbf{p}_n; \mathbf{r})}{\tilde{\pi}_n^{NN}(\mathbf{y}, \mathbf{p}_n)} \frac{\partial \tilde{\pi}_n^{NN}(\mathbf{y}, \mathbf{p}_n)}{\partial \nu_k}. \end{aligned} \quad (\text{B.15})$$

Then, substitution of the expression in Eq. (B.13) into Eq. (B.15), further implies:

$$\begin{aligned} \frac{\partial \tilde{\pi}_n^{HxS}(\mathbf{y}, \mathbf{a}_n, \mathbf{p}_n; \mathbf{r})}{\partial \nu_k} &= H(\mathbf{y}, \mathbf{r}) \tilde{\pi}_n^{xS}(\mathbf{y}, \alpha_n)^{H(\mathbf{y}, \mathbf{r})-1} \tilde{\pi}_n^{NN}(\mathbf{y}, \mathbf{p}_n)^{1-H(\mathbf{y}, \mathbf{r})} \frac{\partial \tilde{\pi}_n^{xS}(\mathbf{y}, \alpha_n)}{\partial \nu_k} + \\ &\quad + (1 - H(\mathbf{y}, \mathbf{r})) \tilde{\pi}_n^{xS}(\mathbf{y}, \alpha_n)^{H(\mathbf{y}, \mathbf{r})} \tilde{\pi}_n^{NN}(\mathbf{y}, \mathbf{p}_n)^{H(\mathbf{y}, \mathbf{r})} \frac{\partial \tilde{\pi}_n^{NN}(\mathbf{y}, \mathbf{p}_n)}{\partial \nu_k}. \end{aligned} \quad (\text{B.16})$$

Given Eq. (B.16), we now consider the two distinct cases where \mathbf{y} lies within or outside the polydisc \mathcal{D} with radius r .

1. In the case where $\mathbf{y} \in \mathcal{D}$, we obtain $H(\mathbf{y}, \mathbf{r}) = 1$ according to Eq. (7). Then, only the first term in Eq. (B.16) survives, which can be further simplified to:

$$\frac{\partial \tilde{\pi}_n^{HxS}(\mathbf{y}, \mathbf{a}_n, \mathbf{p}_n; \mathbf{r})}{\partial \nu_k} = \frac{\partial \tilde{\pi}_n^{xS}(\mathbf{y}, \alpha_n)}{\partial \nu_k}, \quad \text{when } \mathbf{y} \in \mathcal{D}. \quad (\text{B.17})$$

2. In the case where $\mathbf{y} \notin \mathcal{D}$, we obtain $H(\mathbf{y}, \mathbf{r}) = 0$ according to Eq. (7). Then, only the second term in Eq. (B.16) survives, which can be further simplified to:

$$\frac{\partial \tilde{\pi}_n^{HxS}(\mathbf{y}, \mathbf{a}_n, \mathbf{p}_n; \mathbf{r})}{\partial \nu_k} = \frac{\partial \tilde{\pi}_n^{NN}(\mathbf{y}, \mathbf{p}_n)}{\partial \nu_k}, \quad \text{when } \mathbf{y} \notin \mathcal{D}. \quad (\text{B.18})$$

The above result can be summarized to the following piecewise expression for the derivative of the hybrid scheme:

$$\frac{\partial \tilde{\pi}_n^{HxS}(\mathbf{y}, \mathbf{a}_n, \mathbf{p}_n; \mathbf{r})}{\partial \nu_k} = \begin{cases} \frac{\partial \tilde{\pi}_n^{xS}(\mathbf{y}, \mathbf{a}_n)}{\partial \nu_k}, & \text{when } \mathbf{y} \in \mathcal{D}, \\ \frac{\partial \tilde{\pi}_n^{NN}(\mathbf{y}, \mathbf{p}_n)}{\partial \nu_k}, & \text{when } \mathbf{y} \notin \mathcal{D}, \end{cases} \quad (\text{B.19a})$$

$$(\text{B.19b})$$

which was used for deriving the piecewise expressions in eqs. (B.10a, B.10b, B.11a, B.11b).

C Approximation of the Invariant Manifold via Physics-Informed Neural Networks

Hereby, we present the use of purely NNs for approximating the IM functional in Eq. (4), for comparison with the proposed hybrid approach. NNs are universal approximators of continuous functions [88, 89] and offer a powerful and flexible framework for handling high-dimensional, nonlinear mappings. We hereby leverage physics-informed loss functions to train NNs that satisfy the NFEs in Eq. (5).

Let us consider the single layer feedforward NN (SLFNN) architecture provided in Eq. (12). Given a set of collocation points $\mathbf{y}^{(q)} \in \Omega$ for $q = 1, \dots, Q$, the SLFNN approximation of the IM functional is obtained by requiring $\tilde{\pi}^{NN}(\mathbf{y}^{(q)}, \mathbf{p}; \mathcal{H}_2)$ to satisfy the system of NFEs in Eq. (5). Then, the parameters \mathbf{p} of the SLFNN that render it an IM approximation, are computed through the solution of the optimization problem:

$$\underset{\mathbf{p}}{\operatorname{argmin}} \mathcal{L}(\mathbf{p}; \mathcal{H}_2) \triangleq \sum_{q=1}^Q \left(\left\| \tilde{\pi}^{NN}(\mathbf{A}\mathbf{y}^{(q)} + \mathbf{g}(\mathbf{y}^{(q)}), \mathbf{p}; \mathcal{H}_2) - \mathbf{B}\tilde{\pi}^{NN}(\mathbf{y}^{(q)}, \mathbf{p}; \mathcal{H}_2) - \mathbf{C}\mathbf{y}^{(q)} - \mathbf{f}(\tilde{\pi}^{NN}(\mathbf{y}^{(q)}, \mathbf{p}; \mathcal{H}_2), \mathbf{y}^{(q)}) \right\|^2 \right) + \omega \left\| \tilde{\pi}^{NN}(\mathbf{0}^M, \mathbf{p}; \mathcal{H}_2) \right\|^2. \quad (\text{C.1})$$

Similarly to the physics-informed optimization problem of the hybrid scheme in Eq. (13), the first term in Eq. (C.1) enforces the NFEs and the second term ensures that the IM approximation passes through the equilibrium point; again we balance these terms by $\omega \in \mathbb{R}$.

For solving the optimization problem in Eq. (C.1), we minimize the non-linear residuals resulting from the loss function. To avoid an underdetermined system, we require at least $Q = N(L(M+2) + 1)$ collocation points, that is the dimension of the parameters \mathbf{p} to be determined. Again, we employ the LM gradient-based optimization algorithm, which, in this case, requires the derivatives of the SLFNN w.r.t. its parameters, $\partial \tilde{\pi}^{NN}(\mathbf{y}^{(q)}, \mathbf{p}; \mathcal{H}_2) / \partial \mathbf{p}$. Due to the single hidden layer and the sigmoid activation function, these derivatives are computed analytically using symbolic differentiation. We next present the formulation of the optimization problem in Eq. (C.1) into a non-linear residual minimization problem and provide all the relevant material for the implementation of the LM algorithm, which is detailed in Appendix D.

C.1 Residual minimization of the Physics-Informed NN loss function

To cast the optimization problem in Eq. (C.1) into a non-linear residual minimization problem, we begin by explicitly writing all the components of the SLFNN into the N -dim. column vector:

$$\tilde{\pi}^{NN}(\mathbf{y}, \mathbf{p}) = [\tilde{\pi}_1^{NN}(\mathbf{y}, \mathbf{p}_1), \dots, \tilde{\pi}_N^{NN}(\mathbf{y}, \mathbf{p}_N)]^\top, \quad (\text{C.2})$$

in which the dependence on the hyperparameters \mathcal{H}_2 of the SLFNN is dropped for conciseness, and each element $\tilde{\pi}_n^{NN}(\mathbf{y}^{(q)}, \mathbf{p}_n)$ is provided by Eq. (12) for $n = 1, \dots, N$. As already discussed, the network parameters are collected into a long column vector of $N(L(M+2) + 1)$ dimensions:

$$\mathbf{p} = [\mathbf{p}_1, \dots, \mathbf{p}_n, \dots, \mathbf{p}_N]^\top, \quad (\text{C.3})$$

where each $\mathbf{p}_n = [\mathbf{w}^{o(n)}, b^{o(n)}, \mathbf{W}^{(n)}, \mathbf{b}^{(n)}]^\top$ includes the weights and biases of the hidden and output layers for the n -th element of the SLFNN in Eq. (C.2).

Given the set of collocation points $\mathbf{y}^{(q)}$ with $q = 1, \dots, Q$, the optimization problem in Eq. (C.1) over the parameters \mathbf{p} of Eq. (C.3) is achieved by the minimization of the non-linear residuals:

$$\mathcal{F}_{q,n}^{NN} = \tilde{\pi}_n^{NN}(\mathbf{A}\mathbf{y}^{(q)} + \mathbf{g}(\mathbf{y}^{(q)}), \mathbf{p}_n) - \sum_{i=1}^N B_{n,i} \tilde{\pi}_i^{NN}(\mathbf{y}^{(q)}, \mathbf{p}_i) - \sum_{j=1}^M C_{n,j} y_j^{(q)} - f_n(\tilde{\pi}^{NN}(\mathbf{y}^{(q)}, \mathbf{p}), \mathbf{y}^{(q)}), \quad (\text{C.4})$$

$$\mathcal{F}_{0,n}^{NN} = \omega \tilde{\pi}_n^{NN}(\mathbf{0}^M, \mathbf{p}_n), \quad (\text{C.5})$$

where the notation is inherited by the residuals corresponding to the hybrid scheme in Eqs. (B.3) and (B.5). The residuals in Eq. (C.4) correspond to the first term of the loss function in Eq. (C.1), while those in Eq. (C.5) correspond to the second term of the loss function. We compactly collect all the residuals into the $N(Q+1)$ -dim. column vector:

$$\mathcal{F}^{NN} = [\mathcal{F}_{1,1}^{NN}, \dots, \mathcal{F}_{Q,1}^{NN}, \dots, \mathcal{F}_{q,n}^{NN}, \dots, \mathcal{F}_{1,N}^{NN}, \dots, \mathcal{F}_{Q,N}^{NN}, \mathcal{F}_{0,1}^{NN}, \dots, \mathcal{F}_{0,n}^{NN}, \dots, \mathcal{F}_{0,N}^{NN}]^\top. \quad (\text{C.6})$$

For the computation of the Jacobian matrix $\mathbf{J} = \nabla_{\mathbf{p}} \mathcal{F}^{NN}$, which is required for performing gradient based minimization of the above residuals via the LM algorithm, we again employ symbolic differentiation. In particular, let p_k denote any coefficient belonging to the vector of coefficients \mathbf{p}_k of the k -th element of \mathbf{p} in Eq. (C.3). Then, the derivatives of the residuals in Eqs. (C.4) and (C.5) w.r.t. p_k are given by:

$$\frac{\partial \mathcal{F}_{q,n}^{NN}}{\partial p_k} = \frac{\partial \tilde{\pi}_n^{NN}(\mathbf{A}\mathbf{y}^{(q)} + \mathbf{g}(\mathbf{y}^{(q)}), \mathbf{p}_n)}{\partial p_k} \delta_{nk} - \sum_{i=1}^N \left(B_{n,i} + \frac{\partial f_n}{\partial x_i} \right) \frac{\partial \tilde{\pi}_i^{NN}(\mathbf{y}^{(q)}, \mathbf{p}_i)}{\partial p_k} \delta_{ik}, \quad (\text{C.7})$$

$$\frac{\partial \mathcal{F}_{0,n}^{NN}}{\partial p_k} = \omega \frac{\partial \tilde{\pi}_n^{NN}(\mathbf{0}^M, \mathbf{p}_n)}{\partial p_k} \delta_{nk}, \quad (\text{C.8})$$

where the last term in Eq. (C.7) includes contributions from all the SLFNN outputs, due to, in general, a dense gradient $\partial f_n / \partial x_i$. For the computation of the derivatives of the SLFNN included in Eqs. (C.7) and (C.8), we now exploit the simple structure of the SLFNN in Eq. (12) and the fact that the derivative of the sigmoid activation function is $\phi'(\cdot) = \phi(\cdot)(1 - \phi(\cdot))$. Letting the parameter p_k be (i) the l -th element of the output weight of the k -th SLFNN output, $w_l^{o(k)}$, or (ii) the k -th element of the output bias, $b^{o(k)}$, or (iii) the l -th element of the internal weight of the h -th input corresponding to the k -th SLFNN output, $w_{lh}^{(k)}$, or (iv) the l -th element of the input bias, $b_l^{(k)}$, the related derivatives for $k = n$ (they are zero $k \neq n$) can be computed as:

$$\begin{aligned} \frac{\partial \tilde{\pi}_n^{NN}(\mathbf{y}^{(q)}, \mathbf{p}_n)}{\partial w_l^{o(k)}} &= -\phi_l(\cdot), & \frac{\partial \tilde{\pi}_n^{NN}(\mathbf{y}^{(q)}, \mathbf{p}_n)}{\partial b^{o(k)}} &= -1, \\ \frac{\partial \tilde{\pi}_n^{NN}(\mathbf{y}^{(q)}, \mathbf{p}_n)}{\partial w_{lh}^{(k)}} &= -w_l^{o(k)} y_h^{(q)} \phi_l(\cdot)(1 - \phi_l(\cdot)), & \frac{\partial \tilde{\pi}_n^{NN}(\mathbf{y}^{(q)}, \mathbf{p}_n)}{\partial b_l^{(k)}} &= -w_l^{o(r)} \phi_l(\cdot)(1 - \phi_l(\cdot)), \end{aligned} \quad (\text{C.9})$$

where $\phi_l(\cdot) = \phi_l(\mathbf{w}_l^{(n)\top} \mathbf{y}^{(q)} + b_l^{(n)})$, $y_h^{(q)}$ denotes the h -th element of the q -th collocation point, for $q = 1, \dots, Q$, $n = 1, \dots, N$, $l = 1, \dots, L$ and $h = 1, \dots, M$. Equation (C.9) provides all the necessary derivatives for the computation of the residual derivatives in Eqs. (C.7) and (C.8), which can be then computed for the formation of the $N(Q+1) \times N(L(M+2)+1)$ Jacobian matrix $\mathbf{J} = \nabla_{\mathbf{p}} \mathcal{F}^{NN}$. The iterative procedure of the LM algorithm for the minimization of the above residuals is described in Appendix D.

D The Levenberg-Marquardt algorithm for the non-linear residuals minimization

Here, we briefly present the Levenberg-Marquardt algorithm [96], a gradient-based optimization algorithm, for the solution of non-linear least squares problems. As already discussed, we employ the LM algorithm to solve the optimization problems resulting in the IM approximation as provided by the hybrid scheme and the pure NN scheme in Eqs. (13) and (C.1), respectively.

The aforementioned optimization problems are reformulated in Appendices B and C.1 into non-linear residual minimization problems. The particular form of the latter is used by the LM algorithm to minimize a residual vector $\mathcal{F}(\mathbf{R}) \in \mathbb{R}^\zeta$ w.r.t. to a vector of parameters $\mathbf{R} \in \mathbb{R}^\eta$ using the Jacobian matrix $\mathbf{J}(\mathbf{R}) = \nabla_{\mathbf{R}} \mathcal{F}(\mathbf{R}) \in \mathbb{R}^{\zeta \times \eta}$; hereby, the dependence of the residuals and the Jacobian matrix on the parameters is explicitly denoted. In correspondence to the above unifying notation, we obtain:

- for the hybrid scheme minimization problem in Appendix B, the parameter vector $\mathbf{R} \equiv \boldsymbol{\nu} \in \mathbb{R}^\eta$ in Eq. (B.2) where $\eta = N \left(L(M+2) + \left(\prod_{i=1}^M (h+i) \right) / i! + 1 \right)$, the residual vector $\mathcal{F}(\mathbf{R}) \equiv \mathcal{F}^{HxS}(\boldsymbol{\nu}) \in \mathbb{R}^\zeta$ in Eq. (B.6) where $\zeta = N(Q+R+1)$, and the Jacobian matrix $\mathbf{J}(\mathbf{R}) \equiv \mathbf{J}(\boldsymbol{\nu}) = \nabla_{\boldsymbol{\nu}} \mathcal{F}^{HxS}(\boldsymbol{\nu})$ which can be computed by Eqs. (B.7) to (B.9).
- for the SLFNNs minimization problem in Appendix C.1, the parameter vector $\mathbf{R} \equiv \mathbf{p} \in \mathbb{R}^\eta$ in Eq. (C.3) where $\eta = N(L(M+2)+1)$, the residual vector $\mathcal{F}(\mathbf{R}) \equiv \mathcal{F}^{NN}(\mathbf{p}) \in \mathbb{R}^\zeta$ in Eq. (C.6) where $\zeta = N(Q+1)$, and the Jacobian matrix $\mathbf{J}(\mathbf{R}) \equiv \mathbf{J}(\mathbf{p}) = \nabla_{\mathbf{p}} \mathcal{F}^{NN}(\mathbf{p})$ which can be computed by Eqs. (C.7) and (C.8).

For the implementation of the LM iterative algorithm, an initial guess of parameters, say \mathbf{R}_0 , and an initial damping factor, say λ_0 , are first set; see Section 2.2.1 for the initialization. Then, at the k -th iteration, the residual vector $\mathcal{F}(\mathbf{R}_k)$ and the Jacobian matrix $\mathbf{J}(\mathbf{R}_k)$ are computed on the basis of the parameter values \mathbf{R}_k . Having constructed the Jacobian matrix, the LM algorithm next estimates the Hessian matrix of the k -th iteration by $\mathbf{J}(\mathbf{R}_k)^\top \mathbf{J}(\mathbf{R}_k)$, which is used for determining the search direction $\mathbf{d}_k \in \mathbb{R}^\eta$ from the solution of the damped linear system:

$$(\mathbf{J}(\mathbf{R}_k)^\top \mathbf{J}(\mathbf{R}_k) + \lambda_k \mathbf{I}_\eta) \mathbf{d}_k = -\mathbf{J}(\mathbf{R}_k)^\top \mathcal{F}(\mathbf{R}_k), \quad (\text{D.1})$$

where λ_k is the damping factor of the k -th iteration, and \mathbf{I}_η is the η -dim. unitary matrix. Finally, the parameters \mathbf{R}_{k+1} and the damping factor λ_{k+1} at the next iteration are updated according to the following (success or fail) condition:

- if the parameters to be updated are reducing the residuals, then updated them and decrease the damping factor, that is if $\|\mathcal{F}(\mathbf{R}_k + \mathbf{d}_k)\|_2 < \|\mathcal{F}(\mathbf{R}_k)\|_2$, then $\mathbf{R}_{k+1} = \mathbf{R}_k + \mathbf{d}_k$ and $\lambda_{k+1} = \lambda_k/10$, or
- if the parameters to be updated are not reducing the residuals, then do not update them, but instead increase the damping factor, that is if $\|\mathcal{F}(\mathbf{R}_k + \mathbf{d}_k)\|_2 \geq \|\mathcal{F}(\mathbf{R}_k)\|_2$, then $\mathbf{R}_{k+1} = \mathbf{R}_k$ and $\lambda_{k+1} = 10\lambda_k$.

The stopping criteria for the termination of the LM algorithm are based on relative convergence of the residuals, relative step tolerance and maximum iteration limits; i.e., the LM algorithm stops when either $\|\mathcal{F}(\mathbf{R}_{k+1}) - \mathcal{F}(\mathbf{R}_k)\|_2 < \text{tol}_F(1 + \|\mathcal{F}(\mathbf{R}_k)\|_2)$, or $\|\mathbf{R}_{k+1} - \mathbf{R}_k\|_2 < \text{tol}_R(1 + \|\mathbf{R}_k\|_2)$, or $k \geq k_{max}$. For the selection of tol_F , tol_R and k_{max} , see Section 2.2.1. A detailed pseudocode of the LM iterative algorithm is provided in Algorithm D.1, which is focused on the minimization problems resulting from both the hybrid and the NNs schemes.

Algorithm D.1 Solution of the physics-informed schemes via the LM algorithm

Require: Discrete dynamical system in Eq. (2) satisfying the assumptions of Theorem 1 ▷ $\mathbf{A}, \mathbf{B}, \mathbf{C}, \mathbf{f}(\mathbf{x}, \mathbf{y})$ and $\mathbf{g}(\mathbf{y})$
Ensure: Collocation points $\mathbf{y}^{(q)} \in \Omega$ for $q = 1, \dots, Q$ ▷ Ensure $\Omega \subset \mathcal{V}$ where IM functional of Eq. (4) exists
1: Set type of IM approximation, $\text{type} \leftarrow \text{HxS}$ or NN ▷ Hybrid scheme or NNs
▷ Set up the physics informed loss function for the selected IM functional approximation
2: **if** $\text{type} = \text{HxS}$ **then**
3: Set polynomial type, $\text{polyType} \leftarrow \text{PS}, \text{LS}$ or CS ▷ Power, Legendre or Chebyshev series
4: Set hyperparameters \mathcal{H}_1 ; degree h , polynomial expressions of polyType
5: Set radius r of polydisc \mathcal{D} , and sample collocation points $\mathbf{y}^{(r)} \in \partial\mathcal{D}$ for $r = 1, \dots, R$
6: Parsimoniously initialize the coefficients α_n of the polyType series in Eq. (8) ▷ See Section 2.2.1
7: Set hyperparameters \mathcal{H}_2 ; number of layers L , activation function, etc
8: Initialize the NN parameters \mathbf{p}_n in Eq. (12) ▷ See Section 2.2.1
9: Set ω for balancing the equilibrium terms in the loss function ▷ See Eqs. (13) and (C.1)
▷ Employ the LM algorithm for solving the related physics-informed minimization problems
10: **if** $\text{type} = \text{HxS}$ **then** ▷ Initialization of LM algorithm
11: Construct parameter vector $\boldsymbol{\nu}$ and set $\mathbf{R}_0 \leftarrow \boldsymbol{\nu}$ ▷ Eq. (B.2)
12: **else if** $\text{type} = \text{NN}$ **then**
13: Construct parameter vector \mathbf{p} and set $\mathbf{R}_0 \leftarrow \mathbf{p}$ ▷ Eq. (C.3)
14: Set $k = 0$, initial damping factor λ_0 , tolerances tol_F , tol_R and maximum iterations k_{max}
15: **repeat** ▷ LM algorithm iterations
16: **if** $\text{type} = \text{HxS}$ **then**
17: Form the residual vector $\mathcal{F}(\mathbf{R}_k)$ ▷ $\mathcal{F}^{\text{HxS}}(\boldsymbol{\nu})$ in Eq. (B.6)
18: Form the Jacobian matrix $\mathbf{J}(\mathbf{R}_k)$ ▷ $\nabla_{\boldsymbol{\nu}} \mathcal{F}^{\text{HxS}}(\boldsymbol{\nu})$ computed via Eqs. (B.7) to (B.9)
19: **else if** $\text{type} = \text{NN}$ **then**
20: Form the residual vector $\mathcal{F}(\mathbf{R}_k)$ ▷ $\mathcal{F}^{\text{NN}}(\mathbf{p})$ in Eq. (C.6)
21: Form the Jacobian matrix $\mathbf{J}(\mathbf{R}_k)$ ▷ $\nabla_{\mathbf{p}} \mathcal{F}^{\text{NN}}(\mathbf{p})$ computed via Eqs. (C.7) and (C.8)
22: Estimate Hessian matrix and find search direction \mathbf{d}_k ▷ Solve Eq. (D.1)
▷ Perform the LM algorithm update
23: Compute the residuals at potential next iteration $\mathcal{F}(\mathbf{R}_k + \mathbf{d}_k)$
24: **if** $\|\mathcal{F}(\mathbf{R}_k + \mathbf{d}_k)\|_2 < \|\mathcal{F}(\mathbf{R}_k)\|_2$ **then** ▷ Reducing residuals
25: Set $\mathbf{R}_{k+1} \leftarrow \mathbf{R}_k + \mathbf{d}_k$ and $\lambda_{k+1} \leftarrow \lambda_k/10$
26: **else** ▷ Increasing residuals
27: Set $\mathbf{R}_{k+1} \leftarrow \mathbf{R}_k$ and $\lambda_{k+1} \leftarrow 10\lambda_k$
28: $k \leftarrow k + 1$
29: **until** $\|\mathcal{F}(\mathbf{R}_{k+1}) - \mathcal{F}(\mathbf{R}_k)\|_2 < \text{tol}_F(1 + \|\mathcal{F}(\mathbf{R}_k)\|_2)$, or $\|\mathbf{R}_{k+1} - \mathbf{R}_k\|_2 < \text{tol}_R(1 + \|\mathbf{R}_k\|_2)$, or $k \geq k_{max}$
30: **return** tuned parameters \mathbf{R}_k ($\boldsymbol{\nu}$ for $\text{type} = \text{HxS}$ and \mathbf{p} for $\text{type} = \text{NN}$)

E Polynomial Regression Accuracy: Linear vs. Non-linear Optimization

This example demonstrates how non-linear optimization techniques, such as the LM algorithm, introduce numerical errors in polynomial regression compared to linear least-squares methods like the Moore-Penrose pseudo-inverse, particularly for high-degree approximations. Consider the Gaussian profile:

$$f(x) = 1 - \exp(-10x^2), \quad (\text{E.1})$$

within the region $x \in [-0.3, 0.3]$ around $f(0) = 0$. Therein, we seek a power series approximation of degree h in the form of Eq. (8), expressed as $\pi(x, \boldsymbol{\alpha}; \mathcal{H}_1) = \sum_{i=0}^h \alpha_i x^i$. Here $\boldsymbol{\alpha} = [\alpha_1, \dots, \alpha_h]^\top$ represents the power series coefficients and \mathcal{H}_1 denotes the hyperparameters, including the degree h of the power series.

Given a set of features $x^{(q)} \in [-0.3, 0.3]$ and their corresponding target values $y^{(q)} = f(x^{(q)})$ for $q = 1, \dots, Q = 200$, we solve the regression optimization problem:

$$\underset{\boldsymbol{\alpha}}{\operatorname{argmin}} \mathcal{L}(\boldsymbol{\alpha}; \mathcal{H}_1) = \sum_{q=1}^Q \|y^{(q)} - \pi(x^{(q)}, \boldsymbol{\alpha}; \mathcal{H}_1)\|^2. \quad (\text{E.2})$$

to determine the coefficients $\boldsymbol{\alpha}$. This least-squares problem can be approached using both non-linear and linear techniques. For the non-linear solution, we employ the LM algorithm, following the iterative procedure described in Appendix D. The residuals \mathcal{F}_q^{PS} and their derivatives w.r.t. the power series coefficients are given by the expressions:

$$\mathcal{F}_q^{PS} = y^{(q)} - \pi(x^{(q)}, \boldsymbol{\alpha}; \mathcal{H}_1), \quad \frac{\partial \mathcal{F}_q^{PS}}{\partial \alpha_i} = -\frac{\pi(x^{(q)}, \boldsymbol{\alpha}; \mathcal{H}_1)}{\partial \alpha_i} = -\left(x^{(q)}\right)^i. \quad (\text{E.3})$$

Alternatively, the problem in Eq. (E.2) can be formulated as a linear system $\mathbf{V}\boldsymbol{\alpha} = \mathbf{y}$, where $\mathbf{V} \in \mathbb{R}^{Q \times h}$ is the so-called Vandermonde matrix and $\mathbf{y} = [y^{(1)}, \dots, y^{(Q)}]^\top$. The solution is then obtained via the Moore-Penrose pseudo-inverse as $\boldsymbol{\alpha} = \mathbf{V}^\dagger \mathbf{y}$.

We solved Eq. (E.2) using both non-linear and linear methods for polynomial degrees $h = 10$ and $h = 20$. Figure E.1 compares the absolute errors of the resulting approximations. For $h = 10$, both methods achieve comparable approximation accuracy. However, at $h = 20$, the non-linear optimization introduces numerical errors, leading to inferior

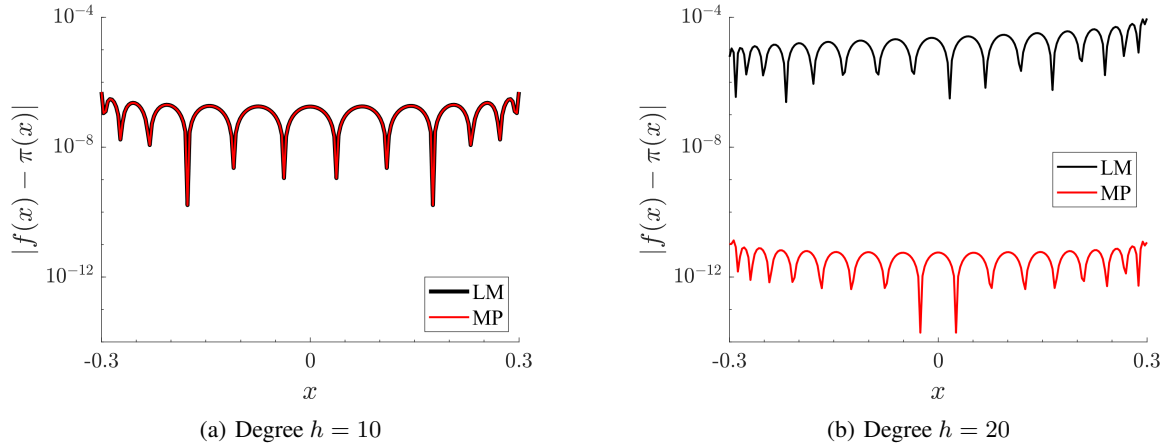


Figure E.1: Absolute errors of the power series approximations $\pi(x)$ of the function $f(x)$ in Eq. (E.1), for polynomials of degree $h = 10$ and $h = 20$. LM and MP denote the use of the Levenberg-Marquardt non-linear optimization algorithm and the Moore-Penrose pseudo-inverse linear least-squares method for obtaining the power series coefficients.

approximation compared to the linear method. This observation aligns with Remark 2, underscoring the advantage of linear techniques for high-degree polynomial regression in our hybrid scheme.

Supplementary Material

A Hybrid Neural Network-Polynomial Series Scheme for Learning Invariant Manifolds of Discrete Dynamical Systems

Dimitrios G. Patsatzis, Nikolaos Kazantzis, Ioannis G. Kevrekidis, Constantinos Siettos

S1 Supplementary Tables for the $N = 1$ and $M = 1$ case of the multi-dimensional example

PI schemes	loss $\mathcal{L}(\cdot)$		comp. time (in seconds)	
	mean	5-95% CIs	mean	5-95% CIs
PI HPS	4.09E-09	[1.99E-09-5.03E-09]	1.16E+01	[3.40E+00-1.74E+01]
PI HLS	4.53E-09	[2.01E-09-4.69E-09]	1.89E+01	[5.49E+00-4.53E+01]
PI HCS	3.03E-09	[2.05E-09-4.25E-09]	2.58E+01	[5.07E+00-4.78E+01]
PI NN	9.83E-09	[1.80E-10-1.18E-08]	5.69E+00	[3.13E+00-1.06E+01]

Table S1.1: Convergence results of the proposed PI schemes for the case $N = 1$ and $M = 1$ of the multi-dimensional example in Section 3.3.1. Mean values and 5–95% CIs of the loss function $\mathcal{L}(\cdot)$ and computational training times (in seconds) are reported for 100 randomly initialized realizations. Schemes include the PI hybrid schemes (HxS: HPS, HLS, HCS), with $x = P, L, C$ denoting power, Legendre, and Chebyshev polynomials and the PI NNs. Hyperparameters: polynomial degree $h = 5$, radius $r = 0.3$ for the HxS schemes, and $L = 10$ neurons for the NN and HxS schemes.

Scheme	$\ x^{(s)} - \tilde{\pi}(y^{(s)})\ _1$		$\ x^{(s)} - \tilde{\pi}(y^{(s)})\ _2$		$\ x^{(s)} - \tilde{\pi}(y^{(s)})\ _\infty$	
	mean	5-95% CIs	mean	5-95% CIs	mean	5-95% CIs
PSE	1.63E-02		1.93E-03		6.08E-04	
PI HPS	3.24E-03	[1.73E-03-4.00E-03]	2.00E-04	[1.79E-04-2.05E-04]	1.10E-04	[1.06E-04-1.07E-04]
PI HLS	3.58E-03	[1.75E-03-3.85E-03]	2.05E-04	[1.78E-04-2.03E-04]	1.11E-04	[1.06E-04-1.08E-04]
PI HCS	3.06E-03	[1.95E-03-3.94E-03]	1.90E-04	[1.79E-04-2.03E-04]	1.07E-04	[1.06E-04-1.08E-04]
PI NN	1.46E-02	[1.51E-03-1.62E-02]	2.83E-04	[1.72E-04-2.98E-04]	1.07E-04	[1.05E-04-1.22E-04]

Table S1.2: Numerical approximation accuracy of IM approximations $\tilde{\pi}(y)$ for the case $N = 1$ and $M = 1$ of the multi-dimensional example in Section 3.3.1. Errors (l_1 , l_2 and l_∞ norms) are reported for the PSE expansion and the PI schemes (HPS, HLS, HCS, NN); for hyperparameters see Table S1.1. Mean values and 5–95% CIs are computed over the 100 parameter sets obtained during training of the PI schemes. Testing data errors are evaluated over $S = 10,000$ points.

S2 Supplementary Tables and Figure for the $N = 1$ and $M = 2$ case of the multi-dimensional example

PI schemes	loss $\mathcal{L}(\cdot)$		comp. time (in seconds)	
	mean	5-95% CIs	mean	5-95% CIs
PI HPS	2.39E-07	[1.48E-08–8.88E-06]	5.35E+01	[1.84E+01–9.79E+01]
PI HLS	2.34E-07	[2.04E-08–9.35E-06]	9.75E+01	[8.82E+01–1.03E+02]
PI HCS	3.59E-07	[3.55E-08–7.65E-06]	1.95E+01	[1.81E+01–2.16E+01]
PI NN	8.84E-08	[3.34E-09–3.19E-07]	1.39E-01	[7.65E-00–1.60E-01]

Table S2.1: Convergence results of the proposed PI schemes for the case $N = 1$ and $M = 2$ of the multi-dimensional example in Section 3.3.2. Mean values and 5–95% CIs of the loss function $\mathcal{L}(\cdot)$ and computational training times (in seconds) are reported for 100 randomly initialized realizations. Schemes include the PI hybrid schemes (HxS: HPS, HLS, HCS), with $x = P, L, C$ denoting power, Legendre, and Chebyshev polynomials and the PI NNs. Hyperparameters: polynomial degree $h = 4$, radius $\mathbf{r} = [0.2, 0.1]$ for the HxS schemes, and $L = 10$ neurons for the NN and HxS schemes.

Scheme	$\ x^{(s)} - \tilde{\pi}(\mathbf{y}^{(s)})\ _1$		$\ x^{(s)} - \tilde{\pi}(\mathbf{y}^{(s)})\ _2$		$\ x^{(s)} - \tilde{\pi}(\mathbf{y}^{(s)})\ _\infty$	
	mean	5-95% CIs	mean	5-95% CIs	mean	5-95% CIs
PSE	6.00E-01		6.17E-02		1.46E-02	
PI HPS	7.19E-02	[1.78E-02–3.26E-01]	5.64E-03	[1.99E-03–2.47E-02]	1.99E-03	[8.29E-04–7.54E-03]
PI HLS	7.24E-02	[1.98E-02–3.44E-01]	5.81E-03	[2.47E-03–2.47E-02]	2.04E-03	[9.22E-04–7.28E-03]
PI HCS	7.65E-02	[2.57E-02–3.34E-01]	6.88E-03	[3.02E-03–2.47E-02]	2.39E-03	[1.14E-03–7.62E-03]
PI NN	5.34E-02	[1.18E-02–9.83E-02]	4.11E-03	[1.31E-03–7.58E-03]	1.61E-03	[6.45E-04–2.80E-03]

Table S2.2: Numerical approximation accuracy of IM approximations $\tilde{\pi}(\mathbf{y}) = \tilde{\pi}(y_1, y_2)$ for the case $N = 1$ and $M = 2$ of the multi-dimensional example in Section 3.3.2. Errors (l_1 , l_2 and l_∞ norms) are reported for the PSE expansion and the PI schemes (HPS, HLS, HCS, NN); for hyperparameters see Table S2.1. Mean values and 5–95% CIs are computed over the 100 parameter sets obtained during training of the PI schemes. Testing data errors are evaluated over $S = 10,000$ points.

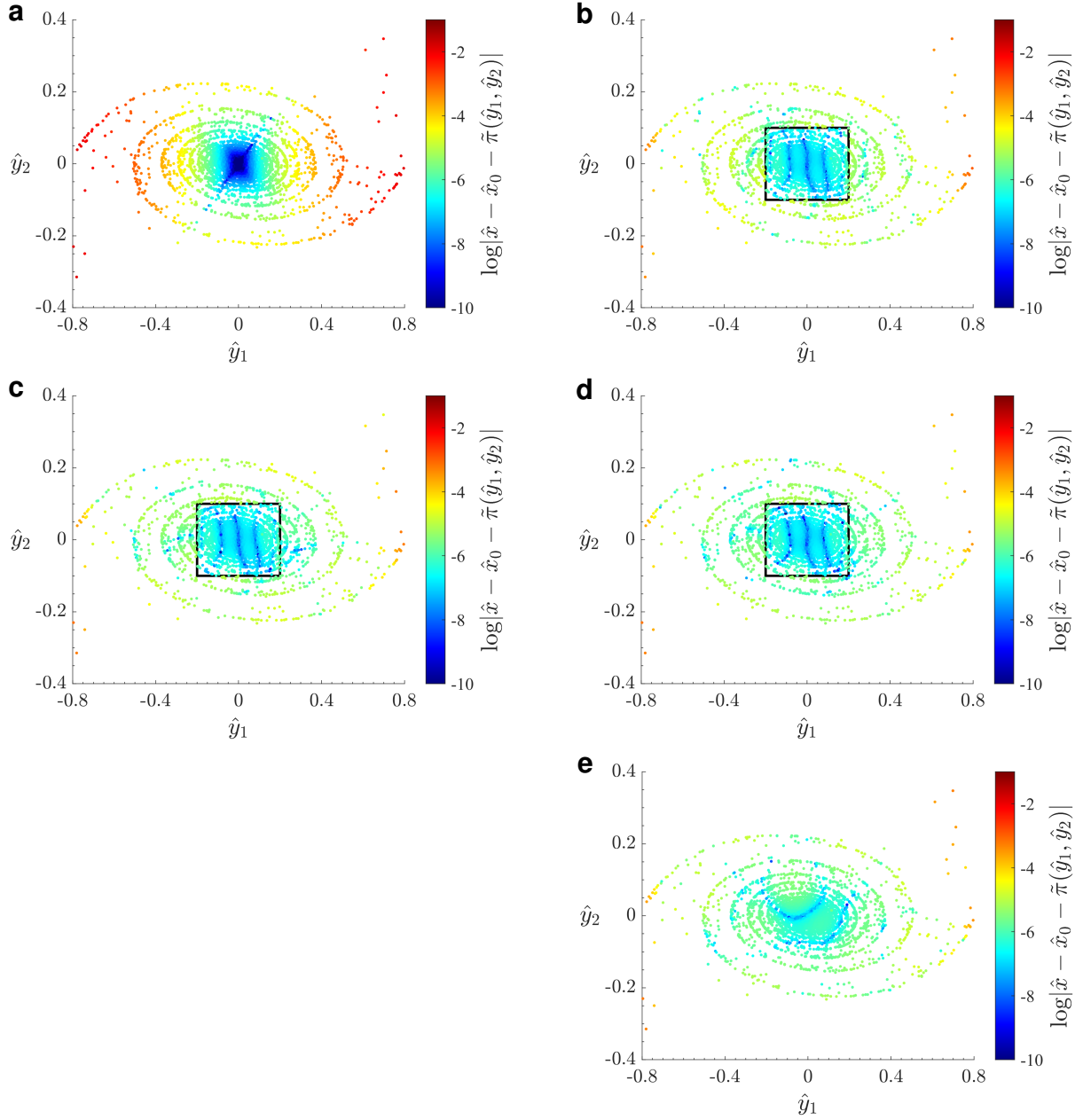


Figure S2.1: Absolute errors (in logarithmic scale) of IM approximations $\tilde{\pi}(y_1, y_2)$ for the case $N = 1$ and $M = 2$ of the multi-dimensional example in Section 3.3.2, compared to data on the IM. Errors are projected in the original state space $(\hat{x}, \hat{y}_1, \hat{y}_2)$. Panels show (a) the polynomial series expansion, (b,c,d) the PI hybrid schemes with Power, Legendre, and Chebyshev polynomials, and (e) the PI NN approximation. The black rectangle in panels (b-d) denotes the polydisc D of the PI hybrid schemes. Polynomial degree is $h = 4$ for all cases and $L = 10$ neurons are used in the NNs.

S3 Supplementary Tables and Figure for the $N = 2$ and $M = 3$ case of the multi-dimensional example

PI schemes	loss $\mathcal{L}(\cdot)$		comp. time (in seconds)	
	mean	5-95% CIs	mean	5-95% CIs
PI HPS	8.59E-04	[5.25E-04-1.49E-03]	1.47E+02	[1.32E+02-2.09E+02]
PI HLS	7.07E-04	[5.01E-04-1.12E-03]	1.60E+02	[1.34E+02-1.74E+02]
PI HCS	7.03E-04	[4.83E-04-1.10E-03]	1.43E+02	[1.32E+02-1.68E+02]
PI NN	8.67E-04	[4.51E-04-3.04E-03]	1.26E+02	[7.29E-01-1.98E-02]

Table S3.1: Convergence results of the proposed PI schemes for the case $N = 2$ and $M = 3$ of the multi-dimensional example in Section 3.3.3. Mean values and 5-95% CIs of the loss function $\mathcal{L}(\cdot)$ and computational training times (in seconds) are reported for 100 randomly initialized realizations. Schemes include the PI hybrid schemes (HxS: HPS, HLS, HCS), with $x = P, L, C$ denoting power, Legendre, and Chebyshev polynomials and the PI NNs. Hyperparameters: polynomial degree $h = 3$, radius $\mathbf{r} = [0.2, 0.1, 0.1]$ for the HxS schemes, and $L = 10$ neurons for the NN and HxS schemes.

Scheme	$\ x_1^{(s)} - \tilde{\pi}_1(\mathbf{y}^{(s)})\ _1$		$\ x_1^{(s)} - \tilde{\pi}_1(\mathbf{y}^{(s)})\ _2$		$\ x_1^{(s)} - \tilde{\pi}_1(\mathbf{y}^{(s)})\ _\infty$	
	mean	5-95% CIs	mean	5-95% CIs	mean	5-95% CIs
PSE	2.26E+00		1.21E-01		3.47E-02	
PI HPS	1.89E+00	[1.53E+00-2.40E+00]	9.06E-02	[8.71E-02-9.50E-02]	3.17E-02	[3.09E-02-3.25E-02]
PI HLS	1.87E+00	[1.58E+00-2.21E+00]	9.01E-02	[8.69E-02-9.37E-02]	3.16E-02	[3.09E-02-3.22E-02]
PI HCS	1.87E+00	[1.53E+00-2.20E+00]	9.02E-02	[8.62E-02-9.47E-02]	3.15E-02	[3.10E-02-3.21E-02]
PI NN	2.09E+00	[1.67E+00-3.49E+00]	9.29E-02	[8.73E-02-1.06E-01]	3.16E-02	[3.09E-02-3.21E-02]
	$\ x_2^{(s)} - \tilde{\pi}_2(\mathbf{y}^{(s)})\ _1$		$\ x_2^{(s)} - \tilde{\pi}_2(\mathbf{y}^{(s)})\ _2$		$\ x_2^{(s)} - \tilde{\pi}_2(\mathbf{y}^{(s)})\ _\infty$	
	mean	5-95% CIs	mean	5-95% CIs	mean	5-95% CIs
PSE	1.17E+01		7.02E-01		2.00E-01	
PI HPS	3.45E+00	[2.87E+00-4.08E+00]	2.70E-01	[2.42E-01-3.02E-01]	1.02E-01	[9.40E-02-1.12E-01]
PI HLS	3.40E+00	[2.95E+00-3.92E+00]	2.65E-01	[2.39E-01-2.93E-01]	1.01E-01	[9.50E-02-1.11E-01]
PI HCS	3.39E+00	[2.90E+00-3.87E+00]	2.65E-01	[2.40E-01-2.92E-01]	1.01E-01	[9.34E-02-1.10E-01]
PI NN	3.57E+00	[2.83E+00-4.56E+00]	2.72E-01	[2.43E-01-3.33E-01]	1.02E-01	[9.45E-02-1.14E-01]

Table S3.2: Numerical approximation accuracy of IM approximations $\tilde{\pi}(\mathbf{y}) = [\tilde{\pi}_1(y_1, y_2, y_3), \tilde{\pi}_2(y_1, y_2, y_3)]^\top$ for the case $N = 2$ and $M = 3$ of the multi-dimensional example in Section 3.3.3; top/bottom rows report the first/second components $\tilde{\pi}_1/\tilde{\pi}_2$. Errors (l_1 , l_2 and l_∞ norms) are reported for the PSE expansion and the PI schemes (HPS, HLS, HCS, NN); for hyperparameters see Table S3.1. Mean values and 5-95% CIs are computed over the 100 parameter sets obtained during training of the PI schemes. Testing data errors are evaluated over $S = 10,000$ points.

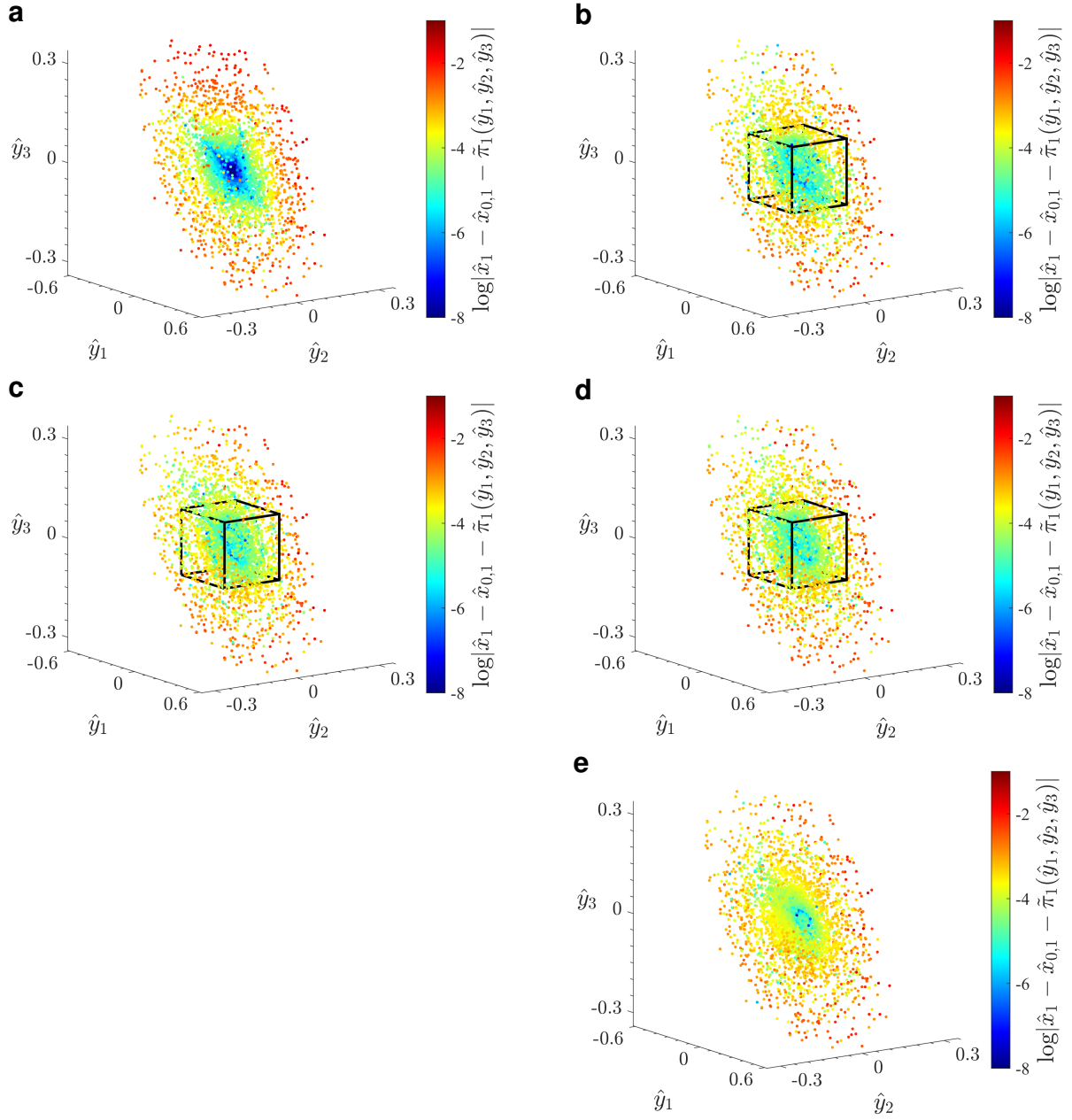


Figure S3.1: Absolute errors (in logarithmic scale) of IM approximations $\tilde{\pi}(y_1, y_2, y_3)$ for the case $N = 2$ and $M = 3$ of the multi-dimensional example in Section 3.3.3, compared to data on the IM. Errors are projected in the original state space $(\hat{x}_1, \hat{x}_2, \hat{y}_1, \hat{y}_2, \hat{y}_3)$ and are shown for the first component \hat{x}_1 . Panels show (a) the polynomial series expansion, (b,c,d) the PI hybrid schemes with Power, Legendre, and Chebyshev polynomials, and (e) the PI NN approximations. The black cube in panels (b-d) denotes the polydisc \mathcal{D} of the PI hybrid schemes. Polynomial degree is $h = 3$ for all cases and $L = 10$ neurons are used in the NNs.